Numerical Modelling of Erosion and Deposition with Cohesive and Non-Cohesive Sediments

Basheer Khalil Ibraheem Al-Hadeethi

Submitted in accordance with the requirements for the degree of Doctor of Philosophy

The University of Leeds

School of Civil Engineering

May, 2018

The candidate confirms that the work submitted is his own and that appropriate credit has been given where reference has been made to the work of others.

This copy has been supplied on the understanding that it is copyright material and that no quotation from the thesis may be published without proper acknowledgement.

The right of ***Basheer Al-Hadeethi*** to be identified as Author of this work has been asserted by him in accordance with the Copyright, Designs and Patents Act 1988.

Acknowledgments

First, all praise to Allah for endowing me with health, knowledge, and strength to overcome all the obstacles to complete this work. Furthermore, I would like to acknowledge my great supervisors, Professor Nigel Wright and Dr Andrew Sleigh for their advice, guidance, and patience through the four years of my PhD period. I would like to thank them for their great support and precise notes and comments and for keeping faith in me from the first day of my study. I am very honoured and blessed for being supervised by them. Special thanks to Dr Mingfu Guan who supervised me and support me during the second year of my PhD. I appreciate all his helpful valuable advice. I would like to thank Dr Yonghui Zhu who provided me with the data of the experimental measurements that he had taken in his work.

I am very grateful and thankful to Ministry of Higher Education and Scientific Research (MOHESR) in Iraq for giving me the opportunity to study the PhD and for the fully funded scholarship. I also thankful to the University of Anbar in Iraq which nominate me for the PhD scholarship. Special thanks to Dr Yaser Al-Anii for his encouragement and support to finish my PhD.

In addition, I would like to acknowledge School of Civil Engineering at the University of Leeds for giving me the opportunity to finish my PhD in this great institution and for providing all the needed support.

Last but not least, I would like to thank my father and my mother for their support and encouragements for me to keep working hard. Their encouragement provided me with the strength to go on. All the words cannot express my feeling or my appreciation for them. Many thanks to my brother and my sisters for their encouragement. I would like to thank my lovely daughters Maryam, Sarah, and Afnan for being beautiful gifts to make my life happier. Special thanks to the great woman, my wife, for her sacrifices, patience, and support through my study journey to achieve my goals. To my family, may Allah bless you all.

Abstract

In this work, a robust two-dimensional model is constructed to simulate river erosion and deposition of cohesive and non-cohesive sediment. The numerical model is constructed based on the shallow water equations with sediment-flow interactions that incorporates a sediment transport model including, significantly, the evolution of the bed profile. The governing equations are solved explicitly using finite volume method using a Godunov type approximate Riemann solver. A spatially first order accurate and numerically robust Harten-Lax-van Leer (HLL) solver is utilised to calculate the fluxes at cell faces. A Courant-Friedrichs-Lewy (CFL) type criterion governs temporal stability of the solver.

The sediment transport component of the model consists of two different elements: the first, HMD-NC, is constructed to simulate flow over a movable bed with non-cohesive materials; and the second, HMD-C, is constructed to simulate the flow over a movable bed of cohesive materials. The models are tested and validated against experimental and theoretical works from published literature. The results show good agreement with the measurements, demonstrating that the models are both capable of predicting the spatial and temporal changes of the flow and bed change effectively. In a case study is used to demonstrate the cohesive model, HMD-C, which shows the impact of employing different formulations for erosion rates of the channel bed in which significant differences are seen in resulting solutions. An intensive investigation of the model parameters on the numerical result is presented. It is found that the model is particularly sensitive to certain parameters such as erodibility, Manning's roughness, and the critical shear stress for erosion. While others such as critical shear stress for deposition, bed porosity, and the settling velocity show very low influence on the erosion.

Table of Contents

List of Tables

List of Figures

Chapter 1 Introduction

1.1 Background

In river engineering and related areas, water and sediment transport is one of the most important topics that represents a big challenge for researchers and water engineers. Large efforts have been utilised to investigate this specially in rivers and open channels. Problems are characterised by: changing flow patterns; high concentration of sediment; the interaction between the water flow and the sediment transport; and the associated morphological changes. Furthermore, the rivers and channels are characterised by: there irregular topography that can vary with distance and time, and the variety of the bed materials.

Figure 1-1: Sediment transported down the Rhone River into Lake Geneva (Fundamentals of Environmental Measurements. 2014.)

In addition to above, rivers have embankments and dams that are very important for water management which may break and breach naturally. Embankment breaching is a complex process that threatens the downstream infrastructures and flood plain because of the high destructive energy of the formed waves. These waves are formed during the breaching process which

occurs because of overtopping or piping. This complex process is characterised by unsteady flow, high concentration sediment transport, and severe morphological changes (Gilvear (1999)).

Natural disasters such as active volcanic eruption, landslides, earthquakes, and tsunamis can increase flood hazards (Alho *et al.* (2005); Carrivick *et al.* (2010); Carrivick and Rushmer (2006); Dai *et al.* (2005); Guan *et al.* (2015b)). Moreover, different factors can increase the flooding likelihood such as extreme heavy rain, and dam breaks. Despite that the flooding can be beneficial by increasing the soil fertility in the flood plain, it can severely influence rivers and the surrounding area. All these factors threaten human life and their cities. In 1998, China suffered from the largest flood disaster since 1954 (Yin and Li (2001)) when the Yangtze drainage area was exposed to massive flooding. The floods occurred as a result of heavy rains falling at the end of July. The economic loss was about 20 billion US dollars. Many people died and many more became homeless. The total reported inundated area was around 1400 km^2, including almost 50 km^2 of residential land and 68000 ha of cultivated land (Zhang *et al.* (2002)). This is one example that demonstrates the importance and need to predict water flow and sediment transport. With good prediction and results from appropriate simulations even these very large and complex flow can be managed and controlled so that risk are minimised and the benefits of the water is taken and the impact of heavy rains and disasters is reduced.

The development of technology and numerical methods has become the main way to enable models computations that predict flood events, fluvial flow, sediment transport, and geomorphological changes. These models reproduce results with lower cost, more flexibility, and more accuracy and efficiency compared to physical models. A wide range of numerical models has been presented, many employing shallow water theory. This theory is based on mass and momentum conservation principles with the main simplifying assumption being that the vertical velocity is very small and can safely ignored in the models and computations. These models are capable of dealing with sediment transport by including additional source terms that are represent the

momentum transfer that results from the sediment exchange between water column and the erodible bed boundary, and represent the streamwise sediments concentrations. In addition to above, it is incorporated with sediment transport model and morphological model to reproduce that erosion deposition and bed change processes. Models presented and used in practice vary in their complexity from simple 1D to the slightly more complex 2D shallow water equations to full 3D solutions of the Navier Stokes equations. While the 1D models are applied for narrow, constrained, channels they do not represent the whole conditions of the flow in rivers when they are in flood. in contrast, 3D numerical models are very accurate with most of the flow conditions are included. However, because of the scale of the computation for river simulation they are is computationally too expensive and too time consuming. Two-dimensional models are, however, very attractive to modellers because they are lower cost than the three-dimensional model and more representative of flood simulation then one dimensional models.

Different numerical methods have been implemented in these models such as the finite difference method, the finite element method, and the finite volume method. Recently, many researchers have utilised the Godunov-type approximate Riemann solvers based on finite volume technique to produce new numerical solutions (Zoppou and Roberts (2000); Zhou *et al.* (2002); Liang *et al.* (2004); Liang and Borthwick (2009); Guan *et al.* (2015a)). These solvers vary from first order accuracy to high order accuracy. These techniques are robust and accurate and capable of reproducing rapidly changing flows (incorporating sub and super critical changes) numerically.

It is well known that the bottom of rivers and channels consist of different materials with different particle sizes. These particles include, coarse particles and fine particles. Fine particles material is one that may form the bed of a river. They have cohesive properties and have different mechanisms causing erosion, transportation, and deposition. Cohesive sediment particles are affected by electrochemical forces that acting between them. These forces cause flocculation and consolidation processes which is not the case in non-

cohesive sediments (Teisson (1991)). Cohesive sediments are transported in suspension as flocculated materials (Franz *et al.* (2014)).

Many researchers and engineers have produced and implemented different numerical hydro-morphodynamic models to simulate different cases of water flow, sediment transport and morphological change. The majority of these models have been utilised intensively to study the water flow over a movable bed with non-cohesive materials. However, it is very rare to find hydro-morphodynamic models that are capable for dealing with cohesive materials. Therefore, new models with capability of dealing with cohesive bed materials are more realistic and can truly represent the physical conditions with accurate numerical results.

1.2 Research Gap and Research Questions

Based on a review of the previous modelling efforts, it has been identified that, despite the availability of studies and investigations which have been undertaken to understand erosion, deposition and sediment transport processes in rivers or open channels, it is found that most of these have focused on flow over non-cohesive beds neglecting the cohesive effect. In nature, the majority of river beds consist of a mixture of cohesive and non-cohesive material (Morris (2011)). However, it is rare to find numerical models and reported research studies which include a representation of the cohesive soil property. Furthermore, cohesive soil is used widely in embankment construction and has a significantly different failure mechanism during the breaching process than non-cohesive soil due to overtopping. Therefore, we can ask ourselves the following questions which are important to get a better understanding about the whole processes to make advances in this field of study:

1- How does the bed in rivers that consist of cohesive or non-cohesive influence the numerical results?
2- What is the effect of cohesive soil in the breaching process in earth embankments due to overtopping and how can we improve the available numerical models to take into account this issue?

3- Does the use of different erosion formulae have a significant impact on the numerical results?
4- What are the parameters that influence the erosion process and the numerical result in for the numerical models when the bottom consists from cohesive materials?

1.3 Aim and Objectives:

This work aims to produce a two-dimensional model that is capable of reproducing the water flow over complex movable beds that consist of different materials by including representations of the more complex physics of cohesive soil based on the particle diameters. To achieve this aim, the research objectives include:

1- Construction of a two-dimensional model that is capable of dealing with water flow over non-cohesive materials.
2- Introduction of a novel one-dimensional model that is capable of simulating the water flow over a movable bed that consist of either fine materials or cohesive materials.
3- Extension of the one-dimensional numerical model to a novel two-dimensional one that is capable of simulating the water flow over movable bed of fine materials or cohesive materials.
4- Application of the new model to study different entrainment formulae to find the optimum formula that is convenient to the presented model.
5- Employment of the new model in a significant parametric study to investigate how the many different parameters affect the simulations to understand better their influence on the numerical results.

1.4 Research Significance

This research contributes to knowledge by introducing a novel two-dimensional numerical model. This model is capable of simulating water flow over movable bed that consist of cohesive and non-cohesive materials with complex topography. This model reproduce the results based on the particle diameters and soil properties. This model can be considered as a basis for the next

generations of models that deal with rivers that have non-homogeneous bed materials.

1.5 Thesis Organisation

The thesis is organized in six chapters. A brief description of the content of each chapter is given below.

Chapter 1: This chapter, provides the general background, motivation for this work, research gap, research questions, the objectives of the research, and the organisation of the thesis.

Chapter 2: In this chapter, a literature review shows the related research scopes that include the hydro-morphodynamic modelling in regular flow and dam beaching. It demonstrates the progress in research in numerical methods based on the shallow water theory.

Chapter 3: In this chapter, the construction of the base numerical models are presented. These models are the one-dimensional and two-dimensional hydrodynamic models, and the one-dimensional and two-dimensional hydro morphodynamic models. Results of intensive tests for the constructed models are also demonstrated. Moreover, sensitivity tests of some parameters that influence the model are shown and discussed in this chapter.

Chapter 4: In this chapter, the construction of a new novel one-dimensional hydro-morphodynamic model, that deals with water flow over movable cohesive bed, is presented. The validation of this model is demonstrated and discussed. A comparison of different entrainment flux formulae is given. Sensitivity tests for the parameters that influence the entrainment flux is presented.

Chapter 5: In this chapter, the novel one-dimensional hydro-morphodynamic model that was presented in Chapter 4 is extended to a two-dimensional hydro-morphodynamic model. A comparison of the numerical result of this model with the two-dimensional model that was presented in Chapter 3 is given and discussed. Results of an important parametric study is presented that exam the influence of different parameters on numerical result. At the end of this chapter, a unified model, is introduced and its significance demonstrated.

Chapter 6: In this chapter, a discussion based on the conclusions drawn from each model is presented and some specific features of the studies are listed.

Chapter 2 Literature Review

2.1 Introduction

In this chapter, a general review is presented that covers the previous studies and investigations which have been done to predict the water flow over movable beds. While most models are well defined for their flow and it is accepted in literature that the shallow water equations provide a sufficiently robust way of simulating the flow (Guan *et al.* (2013); Liang and Marche (2009);Yoon and Kang (2004); Vázquez-Cendón (1999); Sleigh *et al.* (1998)), the choice of model for the sediment movement and its effect are less well accepted. Movable beds may consist of different materials that vary in sediment particles size, bio-chemical properties and mechanism of transport, and they may include either or both non-cohesive soil and cohesive soil. The majority of the numerical models have been focused on non-cohesive sediment transport where the sediment is transported by suspension or as a bed load. A large number of models have been presented to deal with this case. However, in reality, rivers usually consist of cohesive materials that are fine materials and are transported by suspension. It is therefore important for scientists and engineers to undertake more investigations to get a better understanding water flow when combined with all aspects of sediment transport. It is thus identified that there is a real need for the development of a hydro-morphodynamic model that is capable of predicting rapid sediment laden flow with different kinds of sediment materials.

2.2 Numerical Solution of Shallow Water Equations

For the last fifty years, many numerical approaches have been developed and used for solving the hyperbolic partial differential equations that are the shallow water equation (SWE) which are specifically and routinely used in flood water and river flow simulations (Guan (2014)). Three numerical solution techniques where reported that are solved using a variety of discretisation techniques, i.e. the finite difference method, the finite element method and the finite volume method. Most models employ the finite difference method (FDM).

Despite the wide use of the finite difference technique in dam-break simulations, it possess a major obstacle in that it does not observe strict conservation of mass and momentum (Liang *et al.* (2004)). A growing number of hydrodynamic models employ finite elements (FEM) or finite volume (FVM) approaches. Such models show good geometric flexibility that allow better incorporation of the often irregular geometry. These weighted residual methods have been utilised for simulating dam-break hydrodynamics with different shaped flow domains. However, FEM can face difficulty when both subcritical and supercritical flows are included in the simulation (Liang *et al.* (2004)), a feature of all dam-break flows. Thus, FVM is commonly used for simulating dam-break flows. The use of FVM has been shown to be superior to the FDM in terms of accuracy for steep bottom slope and complex coastal geometry (Chen *et al.* (2003); Chen *et al.* (2007)). The methods employ the integral form of the conservation laws, and thus conserves mass and momentum correctly.

The SWEs are composed of a mass conservation equation and momentum conservation equations for each dimension. They can be derived by integrating the Navier–stokes equation through the depth. In these equations, the velocity in the vertical direction is taken as being zero. They are widely used to be implemented in 2D numerical models that reproduce the hydrodynamics of water flow in natural rivers, natural and artificial channels, lakes, flood plain and embankment erosion processes (Zoppou and Roberts (2000); Zhou *et al.* (2001); Liang *et al.* (2004); Lee and Wright (2010)).

Many numerical methods have been used to solve SWEs. Each method has its specific benefit, but for rapidly changing flows on feature of great importance is the method's ability to capture shocks and discontinuities which occur at relatively low speeds and regularly in the situation of rivers and flooding. The capturing of these discontinuities by conservative discretisation is formally addressed and its importance emphasised by (Lax and Wendroff (1960)). Godunov-type schemes are considered as the most attractive for the researchers for the last two decades (Liang and Marche (2009)). Alcrudo and Garcia-Navarro (1993) utilised the finite volume method based on a high-order accuracy Godunov-type scheme (MUSCL) with slope limiters to increase

discretisation accuracy when solving the two-dimensional SWEs. In their work an approximate Jacobian (Roe solver) of the normal flux function was presented. The scheme presented allows a conservation solution of the whole domain on a unstructured mesh. Zhao *et al.* (1994) introduced a two-dimensional unsteady flow model that is discretised using a FVM. In this model the mass and momentum fluxes where calculated at the cell interfaces using the Osher scheme. This scheme enables the model to deal with wetting and drying problem in different cases of water flow modelling. Anastasiou and Chan (1997) employed the Godunov-type second-order upwind finite volume scheme to solve their two dimensional model. The Roe's flux function was utilised to calculate the fluxes in the presented system on the unstructured triangular meshes. The scheme shows high accurate results with a Superbee limiter. Later, Mingham and Causon (1998) introduced a high resolution time marching method to solve the two-dimensional equations. This technique employs a cell centred formulation with collocated data. An approximate Riemann solver with MUSCL reconstruction in a two-step Runge-Kutta time step scheme were used to avoid oscillations. This model was applied to different cases of dam breaks and bore wave propagation. More recently, Sleigh *et al.* (1998) employed the finite volume method to discretise the two-dimensional shallow water equations on an irregular grid. An approximate Riemann solver was utilised to determine the direction of the flow in coupling with an effective means of dealing at boundaries that have wetting and drying problems. A novel error estimating time stepping algorithm controlled accuracy in their solution. Later, Rogers *et al.* (2001) discretised the two-dimensional shallow water equations using a finite volume method and solve it by utilizing a second order accurate Godunov scheme. Roe's flux function was employed for the convection terms at the cell interfaces, while for the spurious numerical oscillations that can occur in high-order schemes, these were prevented by applying a non-linear limiter. In this work, no need for numerical treatment of the balancing between the source terms source and flux gradient terms. Liang *et al.* (2004) solved the shallow water equations by using the second order Godunov-type finite volume based on dynamically adaptive quad-tree grids. The (HLLC) approximate Riemann solver was employed with the MUSCL-Hancock method to calculate the fluxes

at the cell interfaces for wet-dry cases. The model was validated against experimental work and qualitatively showed a good agreement with measurements.

From the above, it can be seen that a large number of numerical methods and different solvers have been utilised to solve the shallow water equations. In this research, the finite volume method is utilised to solve the governing equations. A Godunov type approximate Riemann solver, Harten-Lax-van Leer (HLL) solver, is adopted to calculate the fluxes at the cells.

2.3 Challenges of Solving the SWEs

2.3.1 Bed Slope Source Term Treatment.

One of the main concerns in shallow water equations is the treatment of the source term which is related to the bed geometry. This term has an important influence on the numerical result and may cause numerical errors in the solution when an imbalance between the source terms and the gradient of the flux exists. Different techniques have been presented to deal with this issue.

Bermudez and Vazquez (1994) presented an upwind method to deal with general hyperbolic systems of conservation laws with source terms. In their method they used the upwind discretisation of the source terms while the flux is treated by utilising the flux-difference or flux-splitting techniques. The linear stability meant that simulation showed better stability compared to the previous centred schemes.

LeVeque (1998) developed the wave propagation algorithm by incorporating the source term to introduce a new discontinuous Riemann problem at the cell's centre for the whole grid. As a result, the flux difference exactly cancels the source term at the cell centre. However, the approach is complicated when it is utilised and not appropriate for trans-critical flow with shocks.

Later, the upwind scheme that had been presented by Bermudez and Vazquez (1994) was employed in the two-dimensional case that was presented by Bermúdez *et al.* (1998). Later still, Vázquez-Cendón (1999) presented an extensions of the Q-schemes of van Leer and Roe to produce upwind

discretisation for the source terms, which is improved. A comparison was presented between the described scheme and high order methods such as the TVD scheme that was presented in Garcia-Navarro *et al.* (1992).

New development for the upwind scheme was introduced by Hubbard and Garcia-Navarro (2000). They employed the higher order total variation diminishing (TVD) and utilised flux and slope-limiting techniques. The aim was to get an approximate discretisation for the source terms. Thus, it can be ensured that the source term will be discretised in the same manner as the flux derivatives. The effectiveness of the technique was tested in both the one and two-dimensional shallow water equations. This comparison was found satisfactory, however, despite the accurate solution of the upwind source term treatment scheme, the main weakness is the complexity of this scheme utilization in the numerical model.

Later, Garcia-Navarro and Vazquez-Cendon (2000) adopted the upwind scheme to treat the source terms. Roe's discretization was used to discretize the source term which is not straightforward. The scheme deals with rectangular sections only which represents a weakness point for general application in practice.

A novel scheme to incorporate the bed source term was presented by Zhou *et al.* (2001), where they introduced the Surface Gradient Method (SGM). In this method, the water surface level is considered as the data reconstruction basis. The piecewise linear reconstruction was used to produce second order scheme. A slope limiter is utilised to prevent spurious oscillations for the reconstructed data at the cell interfaces. The main advantage of this scheme is the simplicity, where centred discretization is used to treat the source terms. This method was applied to steady and unsteady flow and showed a good result and efficiency.

A new mathematical technique was presented by Rogers *et al.* (2003). This technique was used for balancing the flux gradient and source terms in case of applying the approximate Riemann solver in finite volume schemes. This method was first applied to the shallow water equations applications and showed a good agreement with the analytical solutions. Later, it was applied to

a coupled system of shallow water equations and the hyperbolic period- and depth-averaged ray-type wave conservation and showed reasonable agreement with the laboratory measurements. However, this technique is complex in implementation.

A further different technique was introduced by Benkhaldoun *et al.* (2007) that uses an upwind scheme. They incorporated the upwinded numerical fluxes and the slope limiters in the approximate Riemann solver based on an unstructured mesh. This method enhanced the accuracy according to the ability to provide mesh refinement at a specific zone for the unstructured meshes. The numerical result shows that this technique simulates the pollutant transport effectively.

Another technique was introduced by Caleffi *et al.* (2007). They presented a fourth order accuracy central weighted essentially non-oscillatory (CWENO) scheme to solve the one-dimensional shallow water equations over movable bed. In this scheme, the Runge–Kutta method was used to obtain time accuracy. While conservative variables were constructed using WENO for specific accuracy. The new scheme was tested and showed good agreement with analytical solutions and with numerical results available in previous work.

Recently, Guan *et al.* (2013) proposed a numerical model based on shallow water equation to solve the flow over complex topography. They used a Godunov-type numerical solver scheme to solve the 2D SWEs. To deal with the SWEs, the bed slope term, a homogenous flux method is employed. The researchers extended the work which had been done by Lee and Wright 2010 to 2D to deal with the homogenous source term. The second order total variation diminishing of weighted average flux scheme. (TVD-WAF) and the Harten-Lax van-Leer Contarad (HLLC) was adopted to solve the shock-capturing problems with wet/dry fronts. This method produced second order accuracy in space and time.

The methods described in the paper above are often complicated – and often improvements are of not seen when applied to practical problems. The incorporation of an upwind and pointwise approach is one of the most attractive techniques that utilise the direction of the wave propagation in the solution and capable for dealing with the flux terms and source terms (Bermudez and

Vazquez (1994); Toro (2001)). It is convenient and adequate to be adopted in this research.

2.3.2 Wetting and Drying Problems.

One of the most difficult problems in shallow water flow modelling is the wetting and drying problem. This problem appears during the modelling of the moving wet–dry interface at a shallow water wave front (Liang and Borthwick (2009)).In such problem, erroneously high velocities are predicted at wet–dry fronts. The reason of that is that the depth-averaged velocities are computed by dividing the discharge per unit width by the local water depth, where the water depth is equal to zero or extremely small at the dry bed.

Simple techniques assumes a minimum water depth for the dry cell. In this case, the negative affect of the zero water depth will be eliminated. It is important to examine all options for implementation of addressing this problem as it occurs regularly, and can lead to sever numerical solution problems.

Zhou *et al.* (2002) enhanced the surface gradient method SGM to make it capable of dealing with a vertical bed step, and dealt with wetting and drying problem by modifying the left and right wave speed calculation. Then they utilized the same technique in the work of numerical prediction of dam break test cases in Zhou *et al.* (2004).

Audusse *et al.* (2004) presented a flexible approach that involves a hydrostatic reconstruction to introduce a first order well-balanced finite volume method that overcomes the wetting and drying problem. Later, this approach was utilised in the presented well-balanced method by Audusse and Bristeau (2005). In this work, a second order upwind kinematic solver was utilised. The disadvantage of this technique is its complexity.

A new method was introduced by Begnudelli and Sanders (2006) based on unstructured triangular grid. The researchers classified the cells into wet cells, if the three nodes are wet, and dry cells. In this method, algebraic equations relate fluid volume to the free surface elevation in partially wetted cells. This relationship reconstructs the free surface in partially wetted cells to compute

fluxes at the interfaces. Different test cases were accurately predicted using this scheme. This powerful technique is compatible with a triangular mesh.

Another technique was introduced by Gallardo *et al.* (2007). In this technique, the numerical fluxes are modified based on the wet/dry transition kind. Moreover, the variable reconstruction is involved to preserve the water height positivity. The scheme is third-order accurate at wet cells while it is first-order accurate near shocks and wet/dry transitions.

Liang and Borthwick (2009) presented a second-order Godunov-type shallow flow solver on adaptive quad-tree grids to simulate the flood flows over natural topography. In this scheme, a new artificial mathematical formulation is presented to balance the flux gradient and the source terms in the cases that involve wetting drying issues. Where the local modification of bed slope is implemented at the interface where the wetting and drying issue is formed. The solver is tested against three bench mark tests and showed that the result of the presented scheme works well for the range of laboratory experiments.

Recently, Hou *et al.* (2013) proposed a 2D Godunov-type cell-centred finite volume model with a new approach that is capable of distinguishing the problematic cells with edges that have wetting and drying problems. The researcher imposed a first-order scheme to avoid the numerical instability. They employ the MUSCL linear reconstruction to compute the values of variables at cell edges. A modification with a non-negative water depth reconstruction is applied on these values. The numerical fluxes are computed by the HLLC approximate Riemann solver utilising the modified values. These modified values are then employed to evaluate the slope source terms. The new approach is capable of handling the wetting and drying problem over complex topographies in an accurate way with good stability. However, the approach was applied and suggested for the numerical models on unstructured grids.

More recent, Guan (2014) adopted a simple artificial method to deal with wetting and drying problem. He assumed a water depth tolerance to define the wet cells and dry cells. The cell is treated as a dry cell when it has a water depth smaller than the tolerance. Moreover, the source term flux should be

considered to handle the wet/drying front where the source term is incorporated into flux term. He demonstrated that this method is working very well for challenging problems. This technique is attractive and it is accurate enough to be adopted in the new model while the other techniques are very complicated or not necessary to be included in the model.

2.4 Applications of SWEs

As mentioned earlier, the shallow water equations have been utilised widely in numerical modelling for different applications such as flow in rivers, embankments breaching and breaks, sediment transport and flood simulations. The numerical modelling takes into account the sediment type whether it is non-cohesive or cohesive materials. These models are validated with experimental. These experimental works are very important for understanding the physical effect of different parameters on the measurements. In the next sections, a list of experimental works and numerical modelling is presented based on the type of sediment materials. This leads to better understanding about the development of the study field.

2.4.1 Non-cohesive Sediment Materials

2.4.1.1 Experimental Work

Dam break flow is one of the most interesting subjects that attracts hydraulic engineers and scientists. This is because of complexity of the process that combines the dam breaking which is characterised by unsteady flow, high concentration sediment transport, and severe morphological changes (Gilvear (1999)). Different approaches have been implemented to produce good models that are capable of simulating flow in such cases. Three generations of dam break models have been developed and produced which include: dam break over fixed bed, dam break over movable bed and dam breaching models. The models of dam break over movable bed are worthwhile for studying the water flow hydrodynamics (Cao *et al.* (2004)). However, this type of models does not represent the real case in nature where sediment transport is involved in the flow. Recently, the efforts of the researchers have been focused on the dam

break over movable bed during their experimental and numerical works. These experiments provide the researchers with more realistic measurements to gain better understanding about water flow hydraulics and sediment transport and how they interact and influence at each other. Moreover, these measurements are considered as a data bank for researchers to validate their numerical models. Later, the new generation of experimental studies have been undertaken to understand the embankment breaching process due to overtopping. These studies gave a good understanding about the breaching mechanism and gave a real data for the whole process and the effect of different parameters that include embankment height, sediment particles, inflow and outflow discharge and etc.

In his work, Rozov (2003) investigated the dam breach erosion process with laboratory experimental work. The researcher produced a mathematical model to simulate both the dam breach process and the important properties of the process to evaluate the wave parameter of the dam breaching. The main equations of this model are the reservoir water-mass depletion and breach-width enlargement. The researcher found that the model is suitable for predicting the embankment breaching process. This work dealt with the non-cohesive materials, therefore it still has weaknesses.

In the same year, experimental work was done by Chinnarasri *et al.* (2003) to investigate the flow patterns and breaching process during water overtopping a dike. The researchers observed that the dike surface showed two types of phenomena: erosion, and erosion and sliding. The researchers observed four stages of the overtopping flow and these stages that could be affect by the slope of the downstream of the dike. They concluded that the decay in these stages is higher when the downstream slope is steeper. This work did not consider cohesive materials.

An important overview has been presented by Morris *et al.* (2007). They investigated the embankment breaching process due to overtopping in field and laboratory tests. They introduced five field tests that were included as a part of IMPACT project and Norwegian National research program as well. Four different types of materials were used in the field tests as shown in Figure (2-1).

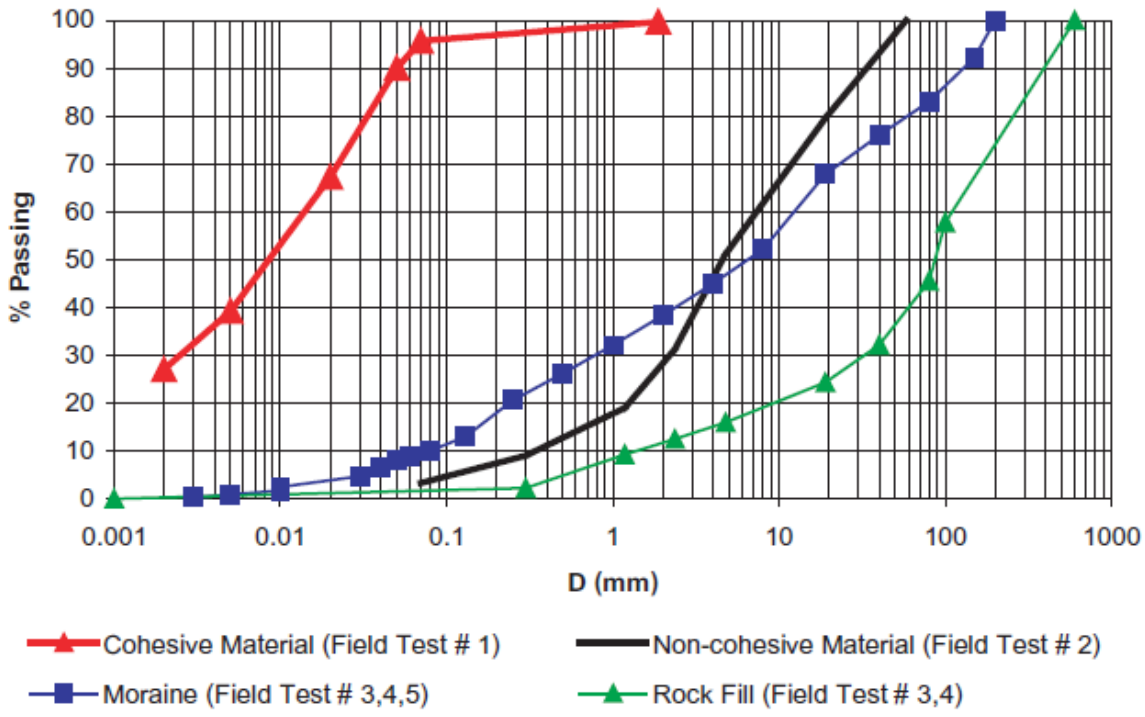

Figure 2-1: Grading Curves for Material Used in the Five Field Tests Morris *et al.* (2007).

To monitor the rate of breach growth, movement sensors were placed under the ground within the dam body. The authors concluded that, through the breaching process, the curved weir that occurred during the erosion process represents the control section, and it allows the flow to move on a length which is much longer than the breach width. In addition, they assumed that the lateral growth occurs at the base and the sides of the breach with failures at the side slope of the breach with minimal sediment transport at the centre. On the other hand, three series of laboratory tests were done with geometric scale 1:10 between the field and laboratory test. The first and second test series investigated the breaching growth due to overtopping in non-cohesive and cohesive material respectively. The researchers noted that in cohesive materials, the erosion process formed single or multi steps called head cutting which had been seen clearly in the field and in the laboratory tests. The moister content has an effect on the erodibility rate of the cohesive materials. In addition, the compaction efforts have a significant effect on the breach formation (Morris *et al.* (2007)).

In 2009, a valuable experimental work has been done by Schmocker and Hager (2009). They investigated embankment failure processes by water overtopping. The researchers conducted 39 laboratory experiments considering scaling issues. All the dikes had a trapezoidal shape with uniform non-cohesive materials. Neither a surface layer nor a core was included in dike. The details of sediment and water surface change are considered. They concluded that there is a minimum dimensions for dike height and width, limitation in sediment particles diameter and breaching discharge. Despite the importance of this work, the cohesive materials were not taken into account.

More investigations were executed by Pickert *et al.* (2011). They studied the non-cohesive embankment breaching process due to overtopping. This work provide a good measured data for water level, erosion rate, the breach discharge, the side slope of the breach and the pore-water pressure within embankments. The researchers divided the breach development process in two phases. The first phase starts when the overtopping begins and the erosion moves from the downstream to the upstream face with low discharge, while the second phase can be recognized by rapid erosion process with high breach outflow. The researchers noted that the slowest failure was happened in fine sand in vertical eroded cross section and the fastest failure was noted in the coarse sand in transverse and vertical cross section direction, while it was in between for the medium sand as shown in Figure (2-2).

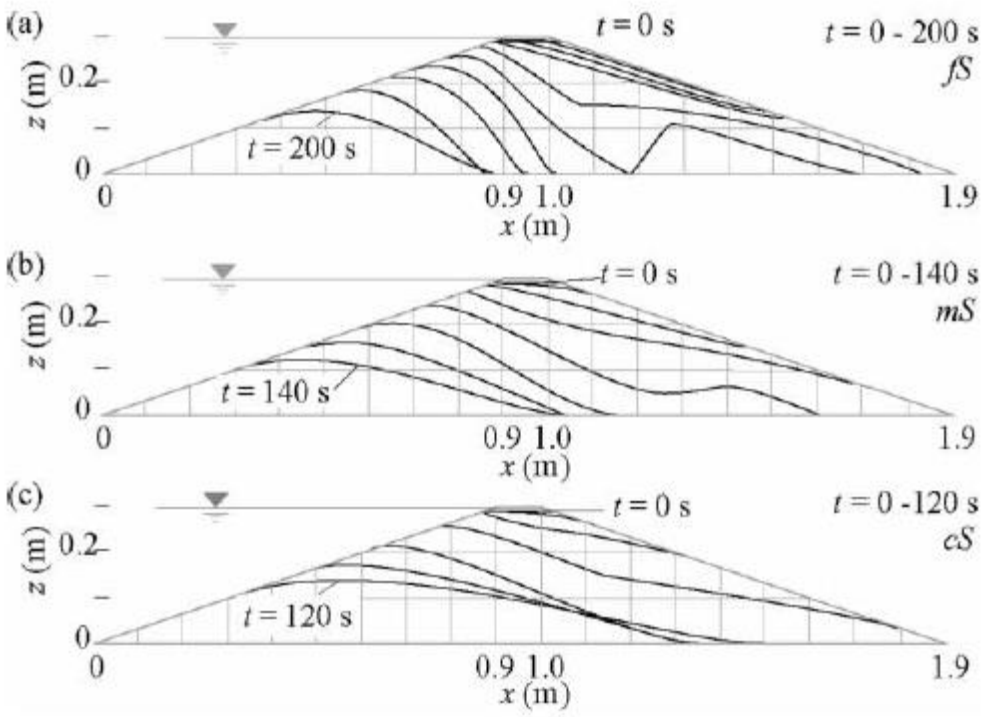

Figure 2-2: Development of longitudinal breach bottom profile at y=0 m each 20s for (a) fS, (b) mS and (c) cS (Pickert *et al.* (2011))

The researchers concluded that the apparent cohesion has a significant influence on the breach side slope stability and the complete breach process as a result.

Goutiere *et al.* (2011) produced an experimental work to study the dam break flow on a mobile bed in widening channels. The wider channel has twice the width of the narrow channel. The sediment used was uniform coarse sand. The geometry of the channel was fixed in all tests. A well-compacted fully saturated sediment layer of the bed was used. The wave propagation spread directly in the wide channel causing progressive morphological change in the bed. Scouring processes occurred in the corners and sediment deposition in the wider channel was observed. The flow evolution measurements and bed morphological processes were monitored using ultrasonic sensors and digital imaging techniques. This experiment produced good data of temporal water level, final bed elevation at various locations, and velocity field at free surface at various times. The experiment results are of practical value for validating numerical models.

Based on his previous work Schmocker and Hager (2009), Schmocker and Hager (2012) investigated a dike breach process due to overtopping. The researchers presented a simple hydraulic model to achieve this goal. The parameters of the study were the sediment diameter, the height of the dike, and the inflow discharge. The hydraulic test conditions which were included are the same as that of Schmocker and Hager (2009), i.e. the dikes are trapezoidal, the soil is homogenous and non-cohesive, neither core nor surface layer has been used, bottom drainage was used to control the seepage, and the inflow is steady. It is found that for the small discharge, the eroded particles deposited suddenly after the dike. While for higher discharge, the particles are transported far away resulting in a steeper downstream dike face. In addition, for the small dike heights, the erosion process is considerably faster. Furthermore, it is concluded that the breach process has two phases and the dike erodes faster with increasing diameter of the sediment, while it will slow down during the second phase. The researcher introduced the relationship between the breaching process and the governing parameters which is

$$Breach\ process \sim \frac{hc}{w,d} \tag{2.1}$$

It is found that besides the inflow Qc and the critical flow depth hc, the sediment diameter d is a very important parameter that controls the equilibrium stage of the breach profiles by sediment transport.

Recently, Schmocker *et al.* (2014) presented experimental work investigating the influence of the grain size distribution on the breaching process of the dike due to overtopping. Two test groups consisting of uniform non-cohesive sediment were used as reference and three additional different sediment mixtures were tested. Each different mixture group was tested for three different inflow discharges. Sediment particles were limited in size where (1mm ≤d≤ 8mm), to exclude the cohesion and bottom drainage effects. Neither surface layer or core layer were added, nor was dike material compacted. The researchers found that the grain size distribution has a small influence on the whole process, and the effect of the Qc or hc is more distinct than the grain size distribution. The dikes with coarse materials show that the slope in the downstream is unstable in the beginning of the overtopping and the erosion

process progressed faster, then the dike face in the downstream region start to settle again. In this stage the erosion process will be controlled by the sediment transport and will proceed slower. It is very clear that the researcher excluded the cohesion property and this represent a short-coming in understanding of different real soil erosion mechanisms.

2.4.1.2 Numerical Work

In addition to the experimental work listed above and regarding the availability of high-performance computing hardware, interest in computational fluid dynamic (CFD) has increased and it has been widely used to simulate a real life cases of breaching and flooding events.

In his early study, Wang and Bowles (2006) presented three dimensional model of dam breaching to simulate the overtopping breach of non-cohesive dam materials. The topography of the site is accounted for by the model and the slope stability is checked through the breach channel. The researcher solved the two-dimensional shallow water equations to propose a hybrid type of total variation diminishing finite-different method to simulate the outflow of the dam breach. The two-dimensional model can represent the three-dimensional phenomenon of the dam break because the flow stream become two-dimensional not far from the dam location. In addition to that, the flow stream become two-dimensional after very small time period after the dam break. The numerical test showed that this scheme can accurately predict the dam-break out flow and the final breach width. They found that the breach location and reservoir shape have an important effect on the peak breach discharge and the shape of the out flow hydrograph. By comparing the numerical model with the field and laboratory dam breach tests, the researcher found that the shape of breach channel during breaching process is successfully modelled. This work neglected the cohesion property.

Later, an interesting study was presented by Aliparast (2009) to simulate dam break flow. In this, the author solved the shallow water equations by developing a numerical model based on the finite volume method employing a second order upwind cell-centred scheme. The researcher used the HLL approximate Riemann solver to handle both of wet/dry treatment and the

discontinuous solution. A multidimensional slope limiting scheme is applied to get second order spatial accuracy and to avoid unphysical oscillations. The friction source term was treated using fully implicit scheme in order to minimize the problems that are associated with numerical instabilities due to small water depth near a wet/dry boundary. The Runge Kutta method was used for time integration of the semi-discrete equations. This model simulated the dam break of Torogh in Iran. The model is capable of handling with different geometries by using unstructured grids and solving the discontinuous solution by an approximate Riemann solver. This model is able to obtain second order spatial accuracy by using multidimensional reconstruction technique and continuously differential multidimensional limiter.

Later, Pontillo *et al.* (2010) presented a one-dimensional numerical model. In this model, the two-phase model which was suggested by Leopardi (2001), was used. In this model the shallow water equations was coupled with a sediment erosion model. The mass and momentum conservation equation was solved separately to represent each phase. This model was validated against an experimental work. Figure (2-3) shows the experimental setup and the dam dimensions. In these tests, the sediments are homogenous and non-cohesive. Neither compaction were applied to the dike material, nor core or surface protection layer were used. steady approach flow discharge without tail water submergence was ensured. The three tests were undertaken using the arrangement as shown in Table (2-1).

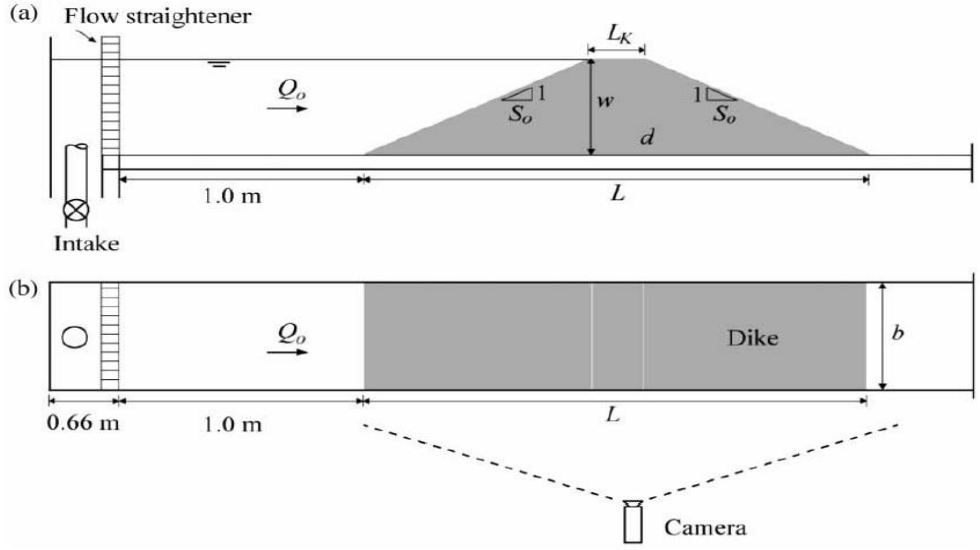

Figure 2-3: Dam dimensions Pontillo *et al.* (2010)

Table 2-1: Hydraulic model tests and basic test parameters

Test	w(m)	L_k(m)	b(m)	d(mm)	Q
1	0.20	0.1	0.2	2	11.31
2	0.20	0.1	0.2	2	5.66
3	0.20	0.1	0.2	4	11.31

The numerical model parameters are as shown in Table (2-2).

Table 2-2: Selected parameters of numerical model

H	α	C_D	φ	φ'	C	P	θ_c
1.0	0.025	0.01	37˚	25˚	0.19	0.43	0.035

The model requires a calibration for all the parameters. The researcher found that, according to their sensitivity analysis, the model results are more sensitive to dynamic sediment friction angle, while least sensitive to drag coefficient C_D, Shield's mobility parameter, and fluid velocity reduction close to

bed, and the results depend on sediment concentration and Bagnold's collisional shear coefficient. The comparison between the hydraulic and numerical models showed a deviation. This deviation resulted from the initiation of overflow with small flow depth, the curvature effects of the bed and the underestimate of flow velocities near to the surface of the sediment, and the saturation changing in the dike body which is ignored in the model. The authors found that, regarding the comparison between water surface and bed surface profile, the overall agreement is reasonable.

A new simple technique was presented by Lee and Wright (2010). This technique was used for solving the shallow water equations that include the source terms. In this method, the researchers converted the equation to a homogenous equation by changing the source term to a new form to represent a new flux that is added later to the original numerical flux. The result will be a homogenous equation that could be solved by well-known numerical schemes, such as TVD and HLL Roe solvers. This technique, was developed later by Guan *et al.* (2013) for two-dimensions.

An interesting investigation was executed later by Van Emelen *et al.* (2011). They presented an experimental and numerical work to investigate the breaching process in sand dikes. Different measurement techniques were employed to evaluate the water and the bed evolutions. The researchers used two numerical models and tested them according to the experimental work. The first one is a two-dimensional SWEs model and the second one is the same model but coupled with the bank failure operator. The finite volume scheme was used with unstructured triangular mesh. The researchers found that the first numerical model could not simulate the lateral erosion process and the breach width remained constant according to the initial pilot channel width, while the vertical erosion was overestimated due to high velocity. On the other hand, the second model is efficient to simulate the lateral and vertical erosion. At the end of the research, the authors compared results between the second model and the experimental work and good comparison was found, especially when the mesh is fine.

In the same year, Singh *et al.* (2011) presented a two-dimensional numerical model to solve the shallow water equation during dam-break flow. The researchers adopted a well-balanced-central upwind scheme proposed by Karganove and Petrove (2007) for less numerical diffusion. The proposed scheme guarantees the positivity of the flow depth at the cell centre. The model was verified against four one-dimensional analytical solutions for water surface elevation and discharge for test cases and this showed a good agreement between the two schemes. In addition, the well-balanced property test was done. The new model was validated against experimental work of dam-break cases qualitatively and it showed a good agreement. The model was used for simulating a 2D experimental work for dam-break flow on horizontal bottom and the result showed a good agreement between the numerical model and the experiment work. The researchers concluded that the model is suitable for simulating real life cases by using this model to simulate the Malpasset dam-break event in 1959. The model showed that the arrival time of the propagated wave in the model matches the real case. The researcher concluded that this model is capable of simulating dam break flows in real life cases with high accuracy.

Recently, a new experimental and numerical work has been done by Emelen *et al.* (2014) to estimate the process of breaching in non-cohesive earthen dams. To achieve this purpose, the shallow water equations- Exiner model was used. Two types of experimental works were included. The first one, which done by Van Emelen *et al.* (2013), has been used to understand the vertical erosion process by overtopping and the second one employed the full 3D breach model that had produced by Van Emelen *et al.* (2011) to study the breaching problems according to lateral erosion of the dike due to overtopping. Different formulations of sediment transport are tested, including the classical bed load formulation and sheet flow formulation. The steep slope correction factor was evaluated to understand its impact on the breaching process and it is found that there is no significant effect on the whole process. Other formulations have been used for bed load sediment transport to understand the full breaching process employing a bank failure operator, because these formulations do not account for the presence of the steep slope directly. The

researcher found that Smart and Jäggi (SJ) and Meyer-Peter and Müller (MPM) formulae give the most accurate results to predict the hydrograph.

More recently, Guan *et al.* (2014) presented a morphodynamic model based on shallow water equations to simulate flood events which are resulted from dam breach. The researcher employed the second order Godunov-type FVM to solve the model. The model was validated by using experimental tests which has been done by previous work for other researchers. The authors found that the model is efficient and capable of predicting flood events that could result from the dam breach due to overtopping. These flood events include the outflow hydrograph, dyke erosion process and the sediment deposition in the downstream area.

The sections above shows the interest of the researchers and engineers on water flow, sediment transport, and dam break cases. Intensive investigations have been executed, whether they are experimental or numerical, to get better understanding about the whole processes. It is very clear that most of these efforts were focused on cases with non-cohesive sediment materials.

2.4.2 Cohesive Sediment Transport

As mentioned previously, the cohesive property is very important to be simulated in the numerical model to make such models capable of dealing with real life flood events and breaching processes. Some studies focused on the cohesive property and how it affects the embankments erosion process due to overtopping. Some studies tried to classify the mechanisms of erosion process in cohesive materials and they tried to explain each mechanism. To get better understanding of the whole process, it is very important to work through all experimental and numerical studies in this field.

2.4.2.1 Experimental Work

An important experimental work was done by Feliciano Cestero *et al.* (2014) to understand the influence of the soil properties on the dike breach. Eight small-scale dikes were used in the experiments. The researchers focused on the breach width evaluation and headcut migration and how they were affected by soil properties. The authors found that the increasing of non-

cohesive fine materials (45% of silt) reduced the peak discharge by 50%, subsequently, the time of the peak of the discharge increased compared to a dike that is constructed with pure sand. In contrast, they found that the increasing of kaolin clay raised the unconfined compressive strength, thus, the failure resistance of the dike is increased. The researchers developed non-dimensional equations using a multivariate analysis depending on the experimental data in order to link the headcut migration and the breach width to the soil properties.

A classification of the erosion phenomena of cohesive embankment was presented by Zhao *et al.* (2014). He divided the erosion phenomena of such embankments to surface erosion, headcut erosion and helicoidal erosion. He suggested that the surface erosion starts in the initial breach stage and excites the primary damage of the embankments, while the headcut erosion controls the breaching process by cutting the slope of the embankment and lowering the crest level. In addition, helicoidal erosion represents the process of the collapse due to the undermining of the breach side slope toe.

Another study was presented by Luo *et al.* (2014). They observed three different erosion types in cohesive soil due to overtopping flow in dams, which are shear erosion, head-cut erosion and collapse. The authors explained the difference between the three types as below:

1- The shear erosion represents the erosion process that occurs in the surfaces of the embankments which erodes the dam materials and deposits them away from the dam body by the shear stress due to overtopping water flow. This kind of erosion occurs when the critical shear stress (τ_E) is smaller than the flow shear stress (τ).
2- The head cut erosion is the process of scouring that occurred in the downstream surface in a vertical slope, then the flow moves through the scoured area to form a turbulent overflow with strong scouring ability. Two conditions are needed to form the head-cut erosion: first, τ at the edge of the dam crest is smaller than τ_E, this makes a stable overflow point at the edge of the dam crest; second, sufficient dam height to ensure the greater flow kinetic and potential energy

conversion to further make erosion rate at the dam crest edge smaller than that at the lower part of dam slope, namely forming erosion zones. The embankment body will face high shear erosion when it fails to satisfy the first condition, and wetting shear erosion when it fails to satisfy the second condition but satisfies the first.

3- The collapse includes slump and capsizing. Slump occurs when the destructive shear stress is greater than the shear strength, while capsizing is caused when the materials tensile strength is smaller than any destructive tensile stress. Small scale slump occurs repeatedly on the downstream slope of the dam when the strength of the materials is weakened by wetting process. In the breaching process, water flow hollows and scours the lower part of lateral sides of the breach, and as a result, the side wall loses its stability and capsizes.

The headcut erosion phenomenon is the most important in the cohesive embankment. The headcut formation process happens in cohesive materials that have a low erodibility Morris (2011). This phenomenon is very clear in cohesive embankment in breaching process due to overtopping and has a special mechanism to form. Morris (2011) mentioned that the headcut is formed when the erosion materials form steps in the downstream slope of the embankment. During the process, these steps become deeper and migrate upstream to form larger steps. Later the steps cut the downstream face reaching the upstream edge of the crest. This process leads to the creation of a series of cascading water jets. These water jets impact the embankment surface and erode back into the step as well as the step surface.

2.4.2.2 Numerical Work

As mentioned earlier, most of the numerical works focused on non-cohesive embankments. Only a few numerical works have attempted to model erosion process of cohesive bed such as the two-dimensional numerical model that was presented by Cole and Miles (1983) to model cohesive sediment transport in coastal water and estuaries. This model is based on finite difference method. The erosion mechanism was neglected to avoid the

complexity in the equation solving. Therefore, this represents the weakness of this method. This model applied to two siltation studies with availability of field data regarding the bed core samples for verification and calibration purposes. This model could be used for engineering predictions works such as dredging needs in rivers, estuaries and flood plains.

Wu *et al.* (1999) introduced a three dimensional layer-integrated numerical model to predicted cohesive sediment transport fluxes in the Humber Estuary, UK. The authors split the three-dimensional model into a vertical one-dimensional equation, and horizontal two-dimensional equations to overcome the differences in length scales between the vertical and the horizontal planes. The author developed a two-dimensional QUICKEST scheme, based on one-dimensional QUICKEST scheme that have been presented by Leonard (1979) to solve the horizontal two-dimensional layer-integrated transport equation. To avoid any unphysical oscillations according to numerical dispersion, the authors used the one-dimensional ULTIMATE algorithm. The governing equations were solved using a combined explicit and implicit finite difference scheme. The authors compared the measured and predicted velocity and they found a good agreement between the depth-mean velocities. In addition, a comparison of the suspended cohesive sediment concentration conducted and showed a good agreement for the deposition phase. However, the variation over the water column was much smaller for the predicted result than for measured data. This could be because during the erosion phase, the difference in the vertical concentration distribution is due to the mixture of non-cohesive and cohesive sediment fluxes occurring in-situ, where the non-cohesive sediment transport is neglected.

A two-dimensional model was presented by Liu *et al.* (2002) based on finite difference method. This model is used for simulating cohesive sediment transport and hydrodynamics in the Tanshui River estuary. The model simulates the currents, salinity distributions, and the water surface elevation. The model results showed a good agreement with measurements. This model employs the FDM, with the previously discussed limitations.

An important numerical study was presented by Lumborg and Windelin (2003). They employed a numerical model that deals with water flow over

cohesive beds in estuaries. The researchers aimed to set up and calibrate a numerical model so that the sediment transport is described in a physically correct way, and to model the cohesive sediment transport in the Rømø Dyb tidal area in the Danish estuary over a long period. The hydrodynamic model utilised the MIKE 21 Hydrodynamic (HD module). while the model MIKE 21 Mud Transport (MT module) is employed to model the sediment transport. The description of the bed is presented in a way to describe the differences in erodibility of the sediment. Further, the description of critical shear stress, erosion and deposition processes of the cohesive sediment bed, is presented describing the morphological changes. The numerical results were compared to measured data and shows a good agreement for the suspended sediment transport concentration and the bed level.

Later, Pandoe and Edge (2004) presented a numerical model built by extending the three-dimensional FEM ADCIRC model. This model was used to study the hydrodynamic circulation and sediment transport. The model showed good result with flat bottoms, while slopes cause errors in the results. However, it is applicable for estuarine areas that have fairly gentle slopes.

The model that presented by Lumborg and Windelin (2003) was utilised later by Lumborg (2004) to study the Lister Dyb tidal area in Danish Wadden Sea. The simulation was performed for long time period to investigate the suspended sediment concentration and the bed level change. It was found that the comparisons with the observations shows unrealistic numerical result for sediment concentration over a long period of time. However, the model was capable of predicting the sediment transport dynamics in the Lister Dyb tidal area and shown that it can be used for elaborating on the dynamics in this area. Despite the limitations of the hydrodynamic model in MIKE 21, this model is utilised for simulation of water levels and flows in estuaries, bays and coastal areas.

Later,Lumborg and Pejrup (2005) re-employed the MIKE 21 numerical modelling system in their study. The system consists of a combination of models. The depth-averaged hydrodynamic conditions in the area were calculated by the hydrodynamic module (MIKE 21 HD), the near-shore Spectral

Waves module (MIKE 21 NSW) was employed to calculate the waves that are generated by winds. The complicated processes of the cohesive sediment transport were modelled by incorporating the Mud Transport module (MIKE 21 MT). The aim of the study was to model and quantify the annual net transport of cohesive sediment for the Lister Dyb tidal area in the northern part of the European Wadden Sea. The hydrodynamics were satisfactorily reproduced by the model as well as the suspended cohesive sediment concentration. A combination of field data and calibration parameters were employed to calibrate the model. Again, this model was applied to study suspended sediment concentrations in estuaries.

Recently, Lopes *et al.* (2006) introduced a two-dimensional numerical model that include a sediment transport model that is coupled to a hydrodynamic model. This model is applied to study the dynamics of the suspended cohesive sediments in the Ria de Aveiro lagoon and to assess the impact of the extreme situations of tides, river input and wind stress.

More recent, Yang *et al.* (2015) developed a numerical model by integrating an atmospheric-wave-3D hydrodynamic and cohesive sediment transport model. This model consists of the Weather Research and Forecasting (WRF) model Simulating Waves Nearshore (SWAN) model, and the Finite-Volume Coastal Ocean Model (FVCOM). The flocculation and hindered settling velocity were included in the sediment transport model. The model was applied to simulate the sediment transport process in the Lianyungang Harbor, China, during Typhoon Wipha in 2007. The comparison between the numerical result and the observations showed a good agreement. This model was developed to predict cohesive sediment transport in storm events around harbours and coasts.

Despite very few numerical models dealing with the cohesive soil, most of them utilised the finite difference method and finite element methods. None of the published work has presented significant detail of the hydraulic models that were employed nor about the erosion and deposition formulae that employed. They have not demonstrated a good understanding of the parameters that

influence the whole hydro-morphodynamic processes when cohesive sediments are present.

2.5 Summary

In this chapter, the researcher introduced a brief literature review about the flow over a movable bed. The literature review includes different sections which are: the development of the numerical approaches that are utilised in numerical modelling; the shallow water equations and their challenges in numerical solution, and the applications of the shallow water equations. The researcher summarised each section with his findings, these have formed the basis of the model to be presented in later chapters. Specifically the model will use the finite volume method to discretise the governing equations incorporating a Godunov type approximate Riemann solver, Harten-Lax-van Leer (HLL) to calculate the fluxes at the cells. An upwind and pointwise approach will be adopted to deal with the flux terms and bed source terms. The source term flux is considered to handle the wet/drying front where the source term and flux term are treated in artificial way to handle the wetting and drying issue.

In the applications of the shallow water equations section, the researcher shows the development of the numerical modelling and how these models dealt with sediment transport based on the sediment materials type. It is very clear that the majority of the efforts of the aforementioned researches and works, whether they were experimental or numerical, were applied to study the non-cohesive sediment materials. Moreover, it is very rare to find a numerical study that considers cohesive soil or even a cohesive property in soil. The reason of this lack of interest appears to be because that the cohesive property adds more complexity to the model. Thus, it is important to understand the effect of the cohesive property on sediment transport mechanism and simulate it accurately by using suitable numerical models.

Chapter 3 Construction of the Hydrodynamic Model and the Hydro-Morphodynamic Model

3.1 Introduction

Hydraulic engineers and scientists have been working on sediment transport in rivers for the last hundred years Einstein (1950). Sediment movement influences the roughness and the frictional resistance of the channels and rivers and in certain circumstance can cause a significant effect on the water movement. To understand this the question of the water flow and sediment transport relationship must be addressed. Scientists who have studied the sediment transport have the goal of a better understanding about its influence on flow patterns. In this chapter the construction of the hydraulic model combined with a hydro-morphodynamic model is presented with the objective of understanding this coupled flow–sediment motion.

3.2 Construction of the Hydrodynamic Model

3.2.1 The Governing Equations of Two-Dimensional Model

The Hydrodynamic model used in this work is developed based on the traditional two-dimensional shallow water equations (SWEs), that consist of the mass and momentum conservation equations of the water flow as shown in Equations (3.1), (3.2) and (3.3) Guan *et al.* (2013). In the hydrodynamic model, the effect of mass and momentum exchange between the water flow phase and the sediment phase will not be included.

$$\frac{\partial h}{\partial t} + \frac{\partial hu}{\partial x} + \frac{\partial hv}{\partial y} = 0 \tag{3.1}$$

$$\frac{\partial hu}{\partial t} + \frac{\partial}{\partial x}\left(hu^2 + \frac{1}{2}gh^2\right) + \frac{\partial huv}{\partial y} = gh(S_{ox} - S_{fx}) \tag{3.2}$$

$$\frac{\partial hv}{\partial t} + \frac{\partial huv}{\partial x} + \frac{\partial}{\partial y}\left(hv^2 + \frac{1}{2}gh^2\right) = gh(S_{oy} - S_{fy}) \tag{3.3}$$

Where h is water depth at the cell centre, u and v are the velocities in x and y directions, t is time step, g is acceleration due to gravity, S_{ox} and S_{oy} are the bed slopes in x and y directions respectively, S_{fx} and S_{fy} are the friction slopes in x and y directions respectively.

The friction slopes and the bed slopes can be represented as

$$S_{fx} = \frac{n^2 u\sqrt{u^2+v^2}}{h^{\frac{4}{3}}} \quad , \quad S_{fy} = \frac{n^2 v\sqrt{u^2+v^2}}{h^{\frac{4}{3}}} \tag{3.4}$$

$$S_{ox} = -\frac{\partial z_b}{\partial x} , \qquad S_{oy} = -\frac{\partial z_b}{\partial y} \tag{3.5}$$

The friction slopes S_{fx}, and S_{fy} are defined based on Manning's roughness coefficient n. The z_b is the bed elevation at a specific location of the grid of (x, y) dimensions.

From the SWEs (3.1), (3.2) and (3.3), it is clearly seen that there is no specific term representing the turbulence. The turbulence effect is propagated by the gravitational force and it is included by the influence of the friction slope terms S_{fx} and S_{fy} within the friction coefficient n (Chow (1959)). These terms are calculated by Equation (3.4).

The hyperbolic system, which is represented by the Equations (3.1), (3.2), (3.3), (3,4) and (3.5), can be solved numerically using a number of different schemes as described by Toro (2001). To do so, it is convenient to convert the above Equations (3.1), (3.2), and (3.3) into a compact form as below:

$$\frac{\partial \boldsymbol{U}}{\partial t} + \frac{\partial \boldsymbol{F}}{\partial x} + \frac{\partial \boldsymbol{G}}{\partial y} = S \tag{3.6}$$

Where $\boldsymbol{U}$ is the vector that containing the conserved flow variables

$$\boldsymbol{U} = \begin{bmatrix} h \\ hu \\ hv \end{bmatrix} \tag{3.7}$$

$\boldsymbol{F}$ and $\boldsymbol{G}$ are the flux vectors in x and y directions, respectively.

$$\boldsymbol{F} = \begin{bmatrix} hu \\ hu^2 + 0.5gh^2 \\ huv \end{bmatrix} \tag{3.8}$$

$$\boldsymbol{G} = \begin{bmatrix} hv \\ hvu \\ hv^2 + 0.5gh^2 \end{bmatrix} \tag{3.9}$$

Where $\boldsymbol{S}$ is the source term vector

$$\boldsymbol{S} = \begin{bmatrix} 0 \\ gh(-S_{ox} - S_{fx}) \\ gh(-S_{oy} - S_{fy}) \end{bmatrix} \tag{3.10}$$

To solve Equation (3.6) numerically, it can be discretised using finite volume method at rectangular mesh as shown in Figure (3.1), to be written as in equation (3.11):

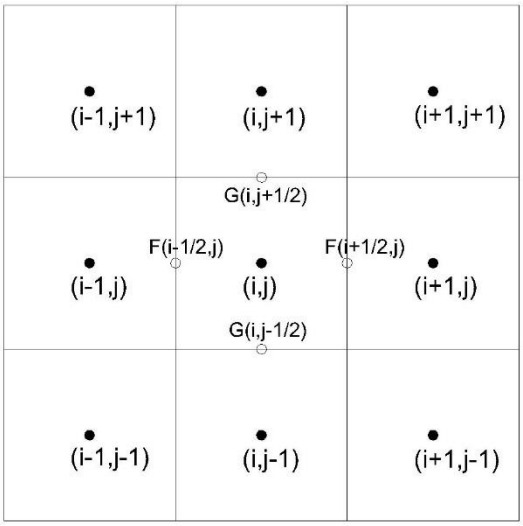

Figure 3-1: Two dimensional finite volume mesh

$$\boldsymbol{U}_{i,j}^{t+1} = \boldsymbol{U}_{i,j}^{t} - \frac{\Delta t}{\Delta x}\left(\boldsymbol{F}_{i+\frac{1}{2},j} - \boldsymbol{F}_{i-\frac{1}{2},j}\right) - \frac{\Delta t}{\Delta y}\left(\boldsymbol{G}_{i,j+\frac{1}{2}} - \boldsymbol{G}_{i,j-\frac{1}{2}}\right) + \Delta t\boldsymbol{S}^{t} \tag{3.11}$$

Where $\boldsymbol{F}_{i\mp\frac{1}{2},j}$ and $\boldsymbol{G}_{i,j\mp\frac{1}{2}}$ are the numerical flux values at the cell interfaces in x and y direction respectively.

3.3 Numerical Solution

A wide range of numerical schemes had been introduced by Toro (2001). In the current work the HLL (Harten-Lax-van Leer), see Figure (3-2), is employed to solve the system in Equation (3.11). The HLL numerical flux, in Equation

(3.12), is derived by applying the integral form of the conservation laws in appropriate control volume.

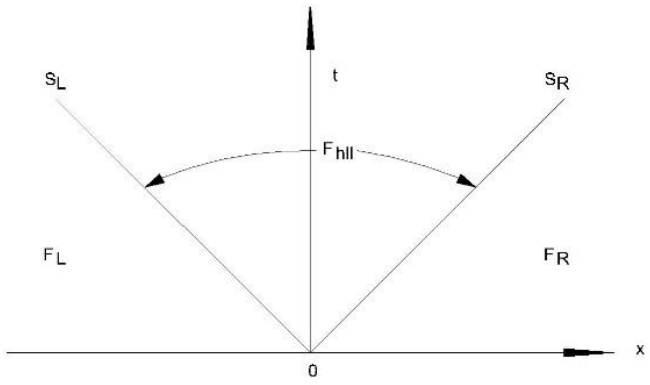

Figure 3-2: The two wave structure of Riemann problem solution using HLL solver

$$F_{i+\frac{1}{2}} = \begin{cases} F_l & if\ S_l \geq 0 \\ F_R & if\ S_R \leq 0 \\ F^{hll} & S_L \leq 0 \leq S_R \end{cases} \quad (3.12)$$

$$F^{hll} = \frac{S_R F_L - S_L F_R + S_R S_L (U_R - U_L)}{S_R - S_L} \quad (3.13)$$

Where F_l and F_{R} are the conservative variable vectors at the left and right sides of each cell interface. F^{hll} The numerical flux at the star region. S_L, and S_R are the wave speeds at the right and left sides of the cell interfaces.

$$S_l = \begin{cases} \min\left(u_i - \sqrt{gh_i}, u^* - \sqrt{gh^*}\right) & if\ \ h_i > 0 \\ u_{i+1} - 2\sqrt{gh_{i+1}} & if\ h_i = 0 \end{cases} \quad (3.14)$$

$$S_R = \begin{cases} \min\left(u_{i+1} + \sqrt{gh_i}, u^* - \sqrt{gh^*}\right) & if\ \ h_i > 0 \\ u_{i+1} + 2\sqrt{gh_{i+1}} & if\ h_i = 0 \end{cases} \quad (3.15)$$

Where

$$u^* = \frac{1}{2}(u_i + u_{i+1}) + \sqrt{gh_i} - \sqrt{gh_{i+1}}; \quad (3.16)$$

$$\sqrt{gh^*} = \frac{1}{2}\left(\sqrt{gh^*} + \sqrt{gh^*}\right) + \frac{1}{4}(u_i - u_{i+1}) \quad (3.17)$$

3.4 Model Stability

The governing equations of the numerical model are solved explicitly. Explicit method needs a special attention to ensure the model stability. To ensure the model stability, an additional condition is required. This condition can strictly ensure a small time steps for the simulation. In the present work, the Courant-Friedrichs-Lewy (CFL) stability condition is utilized (Krámer and Józsa (2007; Sanders (2008)). Therefore, the time step Δt is computed by multiplying the Courant number by the smaller value of the time steps for *x* and *y* directions as below:

$$\Delta t = CFL * \min(min\frac{dx}{|u| + \sqrt{gh}}, min\frac{dy}{|v| + \sqrt{gh}})$$

Where, *CFL* is the Courant number and 0<*CFL*<1.

3.5 Bed Discretisation

In shallow water equations for the purely hydrodynamic case, the source terms consist of two terms that are the bed slope S_o and friction slope S_f. The bed slope S_o, plays a significant role to maintain the balance of the flux (Guan, M. 2013). Therefore, it is very important to evaluate the source term in order to update the flow variables to a new time step and ensure that the non-physical non-negative water depth does not form part of the solution. Different techniques have been used to reconstruct the bed slope to a new form (as discussed earlier) to incorporate it in the flux term to maintain such a property. In this work, a simple central-differencing forward technique, based of values at the cell centre, is implemented to discretise the bed slope term. Where

$$-ghS_{ox} = -gh\frac{\partial z_b}{\partial x} = -gh\frac{(z_{b(i+1,j)} - z_{b(i,j)})}{\Delta x}$$

$$-ghS_{oy} = -gh\frac{\partial z_b}{\partial y} = -gh\frac{(z_{b(i,j+1)} - z_{b(i,j)})}{\Delta y}$$

Where $z_{b(i,j)}$ and $z_{b(i+1,j)}$ are the bed level in x direction at the cells i and $i+1$ respectively, and $z_{b(i,j)}$ and $z_{b(i,j+1)}$ are the bed level in *x* direction at the cells j and $j+1$ respectively.

3.6 Mesh independence

In numerical modelling, mesh size is one of the important parameters that influences the accuracy of the result. To find the compatible mesh size for the simulations, mesh independence test is required. To perform this test for the new model, the dam break case that had been presented in Cao *et al.* (2004) is utilised. To represent the 50000m length of the channel, different cell sizes were selected. This includes 1m, 5m, 10m, 25m, and 100m. The measured water level at x = 25075m is tasted against the mesh size values. Figure (3-3) shows the influence of the mesh size on the water level. It is found that the mesh cell size of dx = 1m gives the most accurate value with water level error equal to 0.178%, but it is time consuming. While the mesh cell size of 100m produce high water level error that equals to 26.7% but with good time saving. The mesh cell size of dx = 10m shows low error percentage that equals to 0.3% and good time saving of 0.8% less than time required for that of dx = 1m. Therefore, the mesh cell size with dx =10m is chosen considering the accuracy of the result with reasonable execution time. To generalise the mesh cell size dx to employ in different simulations, it is converted to a dimensionless value as a percentage of the channel length. It is found that the cell dimensionless value is equal to 0.02% of the channel length.

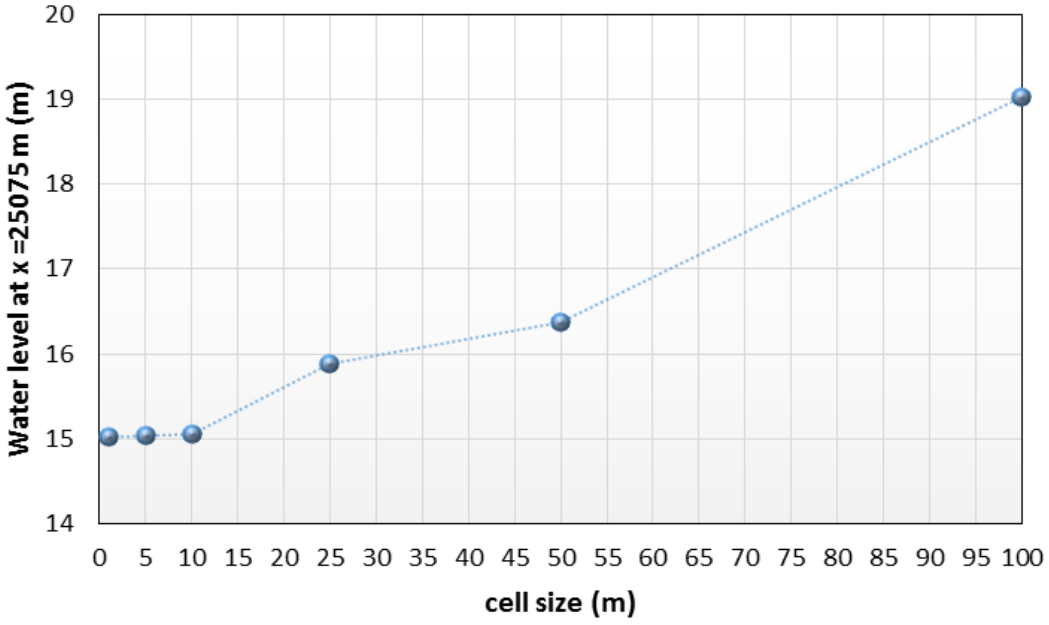

Figure 3-3: Mesh independency test.

3.7 Wetting and Drying

The most common problem that faces the researchers in water flow modelling is the wetting and drying problem. The problem is that small water depth produces high velocities which in turn cause numerical instability. Many researchers (Perthame and Simeoni (2001); Kurganov and Levy (2002); Zhou *et al.* (2002); Zhou *et al.* (2004); Audusse *et al.* (2004); Liang and Borthwick (2009)) have presented different techniques that deal with such problems.

In this research, the simple technique that uses minimum water depth as tolerance is employed. This minimum water depth is specific to each computational cell itself. If the cell has a water depth less than the water depth tolerance, it will be treated as a dry cell otherwise it will be considered as a wet cell. Based on the definition above, and assuming that the flow direction is from left hand side to the right hind side, there are four different cases of wet/dry cell to deal with as below:

1- If the left cell (i) is wet and the right cell ($i+1$) is wet, the numerical flux will be calculated at the interface ($i+1/2$) based on the numerical scheme and no more special treatment is required and the flow direction will be from the high water level cell to the lower water level side.

2- If the left cell (i) is dry and the right cell ($i+1$) is dry, the numerical flux will equal zero where no numerical flow occurs at the cell interface.

3- If the left cell (i) is wet and the right cell ($i+1$) is dry, and the water level $wl_{(i)}$ >bed level $z_{b(i+1)}$, the numerical flux will be calculated based on the numerical scheme and no special treatment is required and the flow direction will be from the wet cell to the dry cell.

4- If the left cell (i) is wet and the right cell ($i+1$) is dry, and the water level $wl_{(i)}$ < bed level $z_{b(i+1)}$, the numerical flux will be equal to zero where no flux moves through the cell interface ($i+1/2$).

Figure (3-4) shows the four cases of the wet-dry relationship for two neighbour cells.

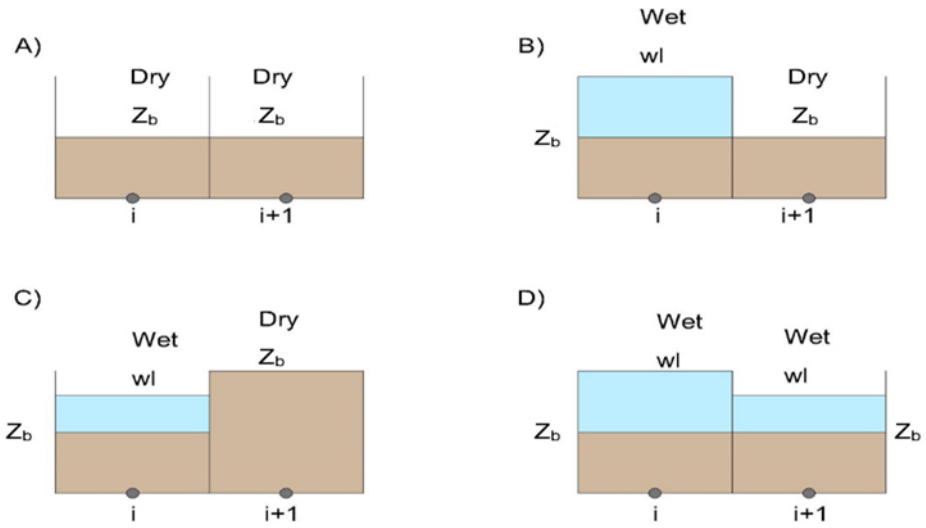

Figure 3-4: The four cases of wet-dry relationship of two neighbour cells.

3.8 One-Dimensional Numerical Testing

3.8.1 Dam break Flow Over a Flat Bed

3.8.1.1 Testing of the One-Dimensional Hydrodynamic Model

In this section, a validation test was undertaken to examine the ability of the hydrodynamic model to predict the front wave evolution and time of arrival of this wave in comparison with a dam break case presented in Cao *et al.* (2004). The channel length is 50 km, and has a dam that is located at the centre of the channel, at x=25 km, far from the upstream. The initial water depths are 40m and 2m at the upstream and the downstream respectively. The bed is assumed to be fixed with a horizontal level.

For numerical simulation the channel is divided into 5000 cells with dx=10m. the boundary condition at the upstream is assumed to be a closed boundary, while the downstream boundary condition is assumed to be an open boundary. The simulation is executed for 20s. Figure (3-5) shows the comparison between the numerical model and Cao's simulation. It is seen that the numerical result has a good agreement with the Cao model which is taken to

mean that the model is able to simulate such cases of dam break over horizontal fixed bed.

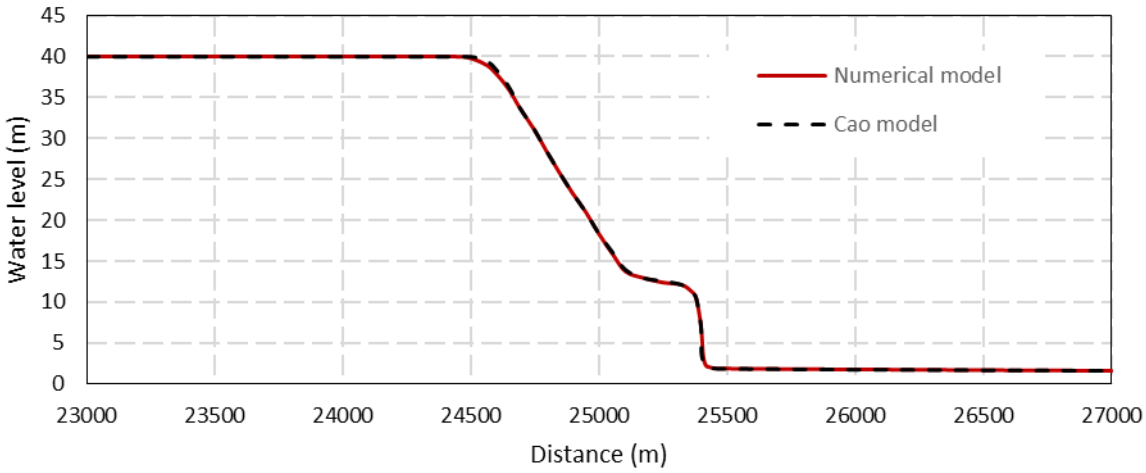

Figure 3-5: Hydrodynamic model compared to Cao et al. (2004) at 20s

In a similar dam-break case that had been presented by Zhang and Duan (2011), the dry and wet bed were taken the account. This channel is 1200m long with a dam located at 100m upstream from the centre of the channel. The initial water level was assumed to be 10m depth, while the downstream water level was assumed to be 1m and 0.001m was used as the criteria for the wet and dry bed. Manning roughness is assumed as n=0 where the bed is frictionless.

For the simulation, the domain was divided into structured mesh with cell size of 10m. And the simulation was executed for 20s. Figure (3-6) shows the comparison between the new numerical model and the result that presented by Zhang and Duan (2011). It shows that the model can predicted the shock wave, that propagate because of the dam break, which advances over a fixed dry bed with a slight diffusion.

Figure (3-7) shows the same dam break simulation, but over a wet bed, which shows predicts the wave front nicely with slight diffusion.

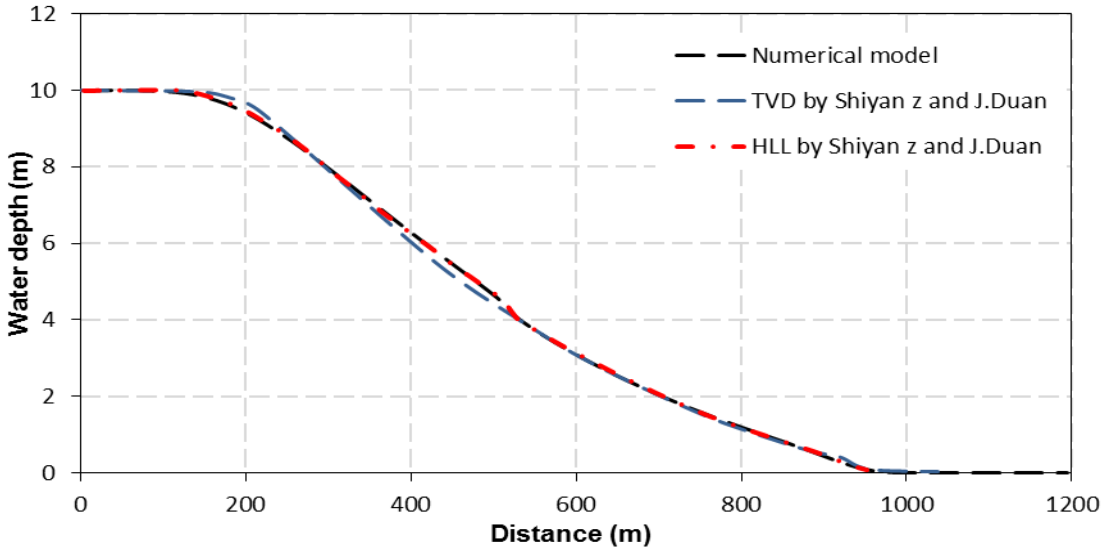

Figure 3-6: Hydraulic model compared to Zhang and Duan (2011) model at t= 20s

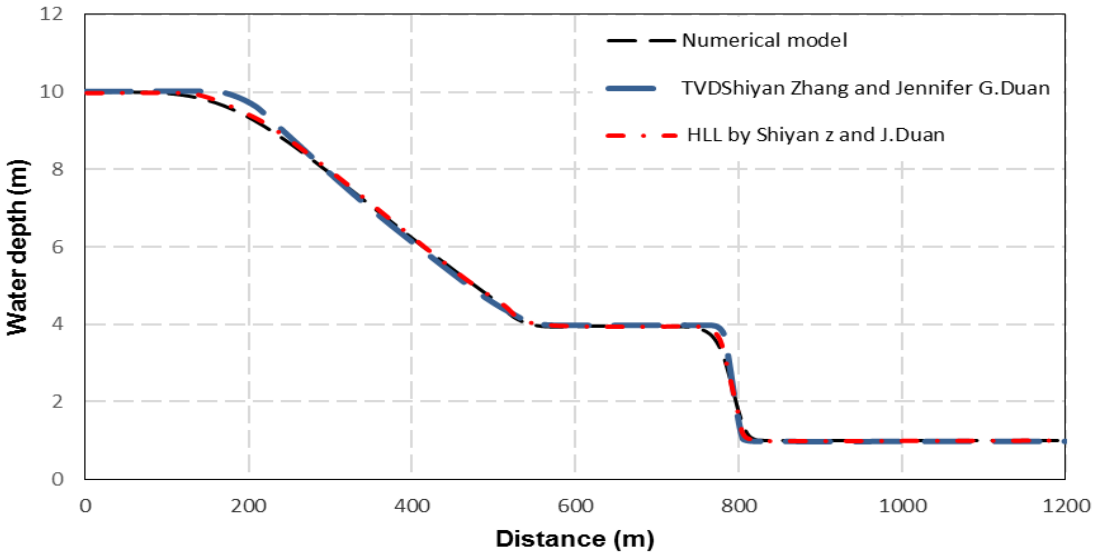

Figure 3-7: Hydraulic model compared to Zhang and Duan (2011) model at t= 20s

3.8.1.2 One-Dimensional Dam-Break Flow Over a Triangle Hump

It is very important to check the model capability to deal with irregular bed topography when the wet/dry case is involved. To test the model, a lab experimental work that recommended by the EU CADAM project is applied (Liang and Marche (2009)). Figure (3-8) shows the experimental setup, where the experiment had been undertaken in a channel with a 38m length with a

dam location of 15.5m away from the upstream channel edge. The water level at upstream where the reservoir is located is 0.75m height. A symmetric triangular obstacle is located 10m from the dam at the downstream. The upstream end is assumed as a closed boundary while the downstream end is assumed to be free flow boundary. In this experiment, seven gauges were installed to monitor the water level at the locations 2m, 4m, 8m, 10m, 11m, 13m and 20m respectively. The bed boundary is assumed as dry bed at the downstream with Manning roughness equal to n=0.0125.

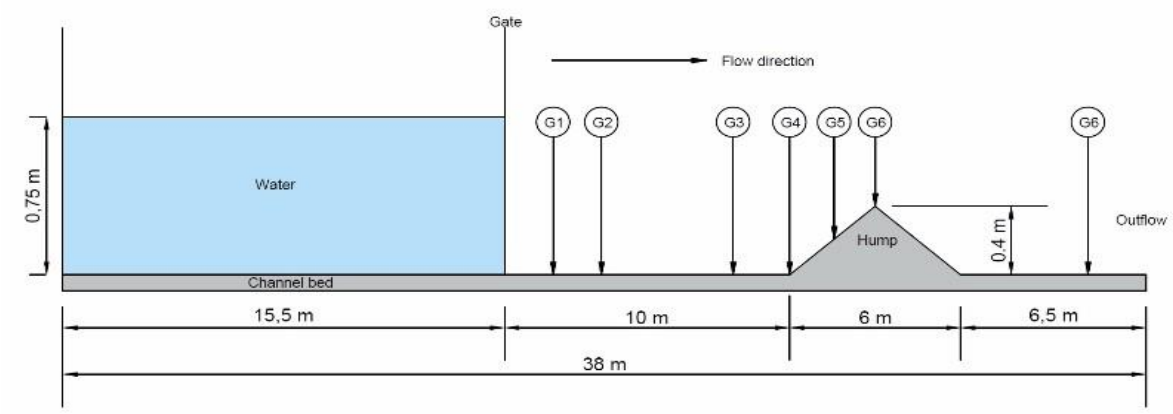

Figure 3-8: Dam break flow over a triangle hump

For the simulation purposes, the channel domain is discretised using dx=0.05m and it was run for 90 seconds.

At time t =0s, the dam is opened suddenly and water at the reservoir falls to propagate a wave that moves toward the hump in the downstream. The wet/dry front wave reaches the obstacle at t =3s and continue to overcome it. After around 2 seconds, at t =5s, the wave reaches the end of the hump at the other side. At the same time, the interaction of the incoming wave and the triangle hump propagates a shock wave that moves towards the upstream of the channel, while a rarefaction wave is propagated to move towards the downstream. This process will decrease the water level at the hump crest. After that, at t=24s, the shock wave reaches the wall boundary at the upstream and reflected from it to toward the hump, in the same time the hump at the downstream side will be totally dry while the upstream side is drying out continually until the new shock wave hits the triangular hump. The energy of the wave covers the hump completely with water and a new shock wave will

propagate and move to the upstream direction. These processes will continue until the momentum of the reflected wave is weak enough to be damped by the bed friction. Figure (3-9) shows the water level comparison between the numerical and the experimental lab work. It is shown that the water depth and the arrival time agree with the measurements fairly well at the Gages 1 to 6. Gage 7 shows a reasonably good prediction for the arrival time but with a water depth discrepancy. It is believed that a combination of numerical errors and measurement errors cause such discrepancy.

The description and the result of the numerical model are matched very well to other researchers' work such as that presented in Liang and Marche (2009). The proposed numerical model shows a good agreement with the measurements and shows its capability to simulate water flow over irregular topography in a wetting/drying case with a good stability.

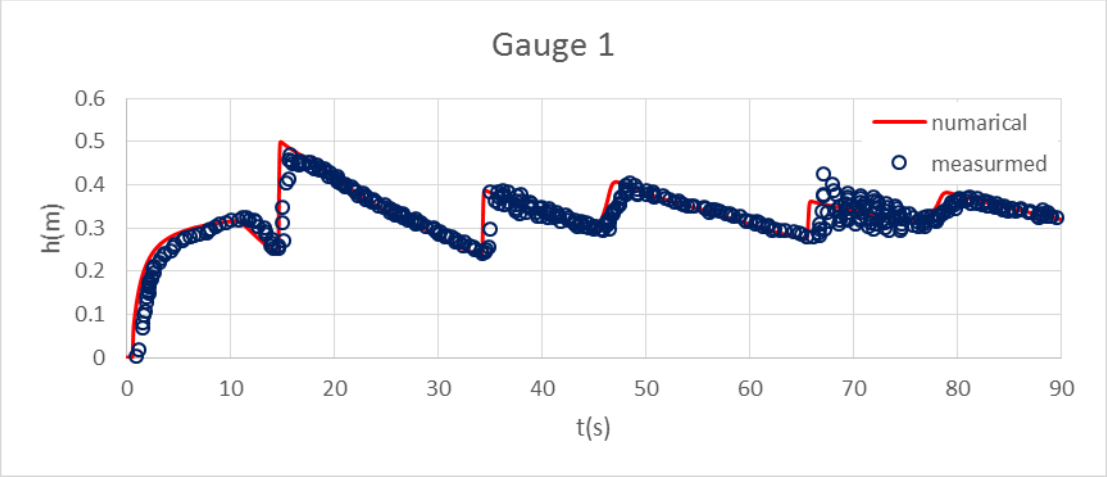

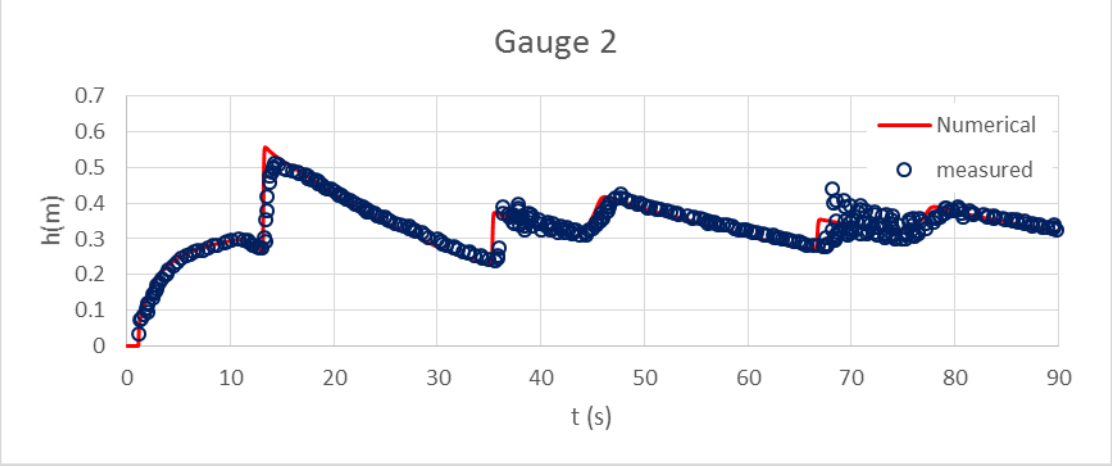

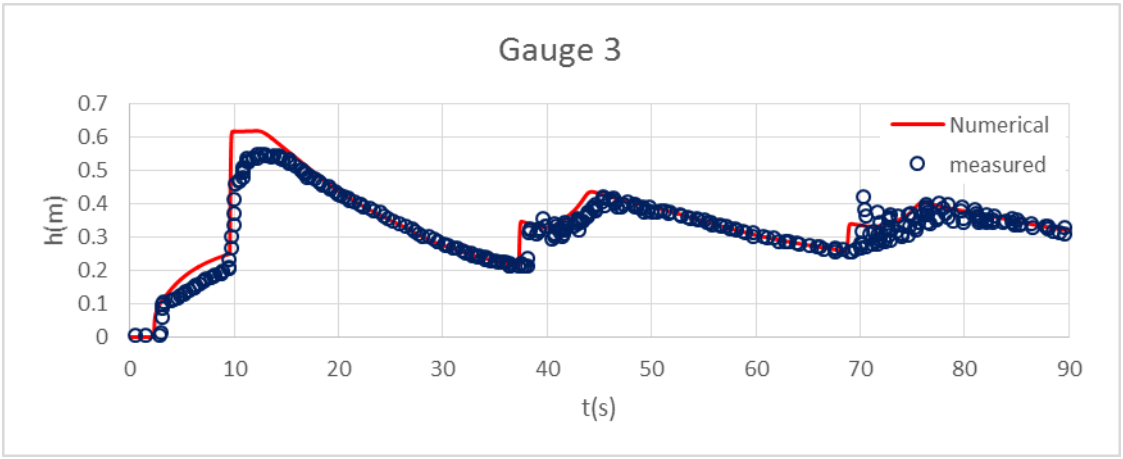
Gauge 3
h(m)
t(s)
Numerical
measured
0.7
0.6
0.5
0.4
0.3
0.2
0.1
0
0
10
20
30
40
50
60
70
80
90

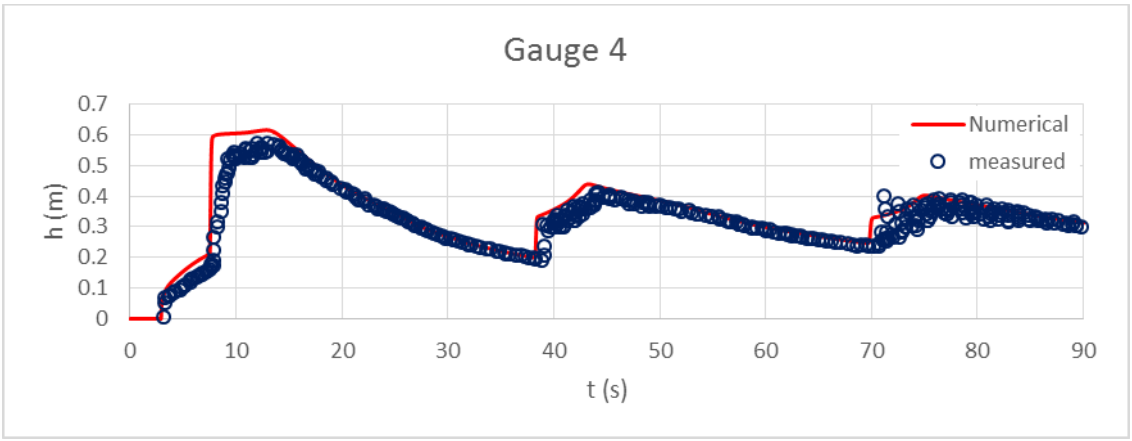
Gauge 4
h (m)
t (s)
Numerical
measured
0.7
0.6
0.5
0.4
0.3
0.2
0.1
0
0
10
20
30
40
50
60
70
80
90

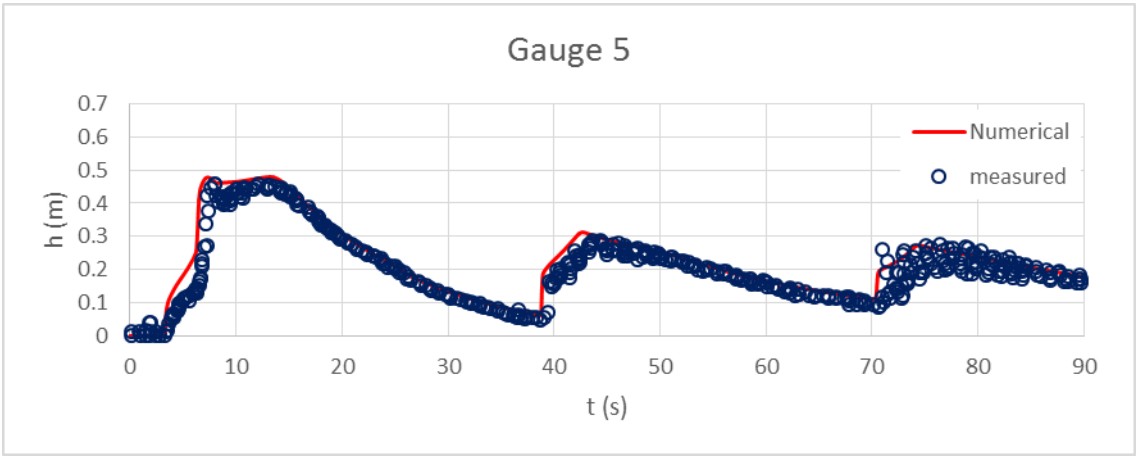
Gauge 5
h (m)
t (s)
Numerical
measured
0.7
0.6
0.5
0.4
0.3
0.2
0.1
0
0
10
20
30
40
50
60
70
80
90

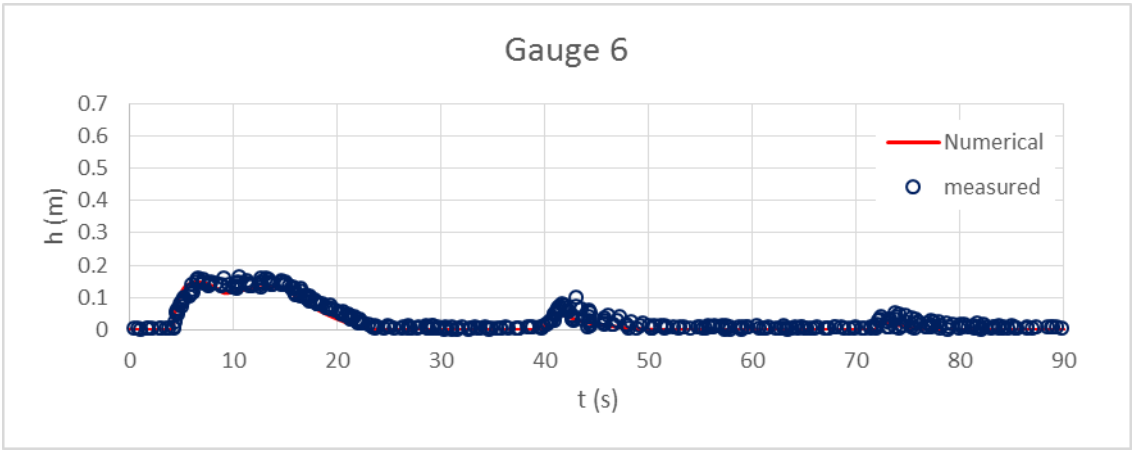

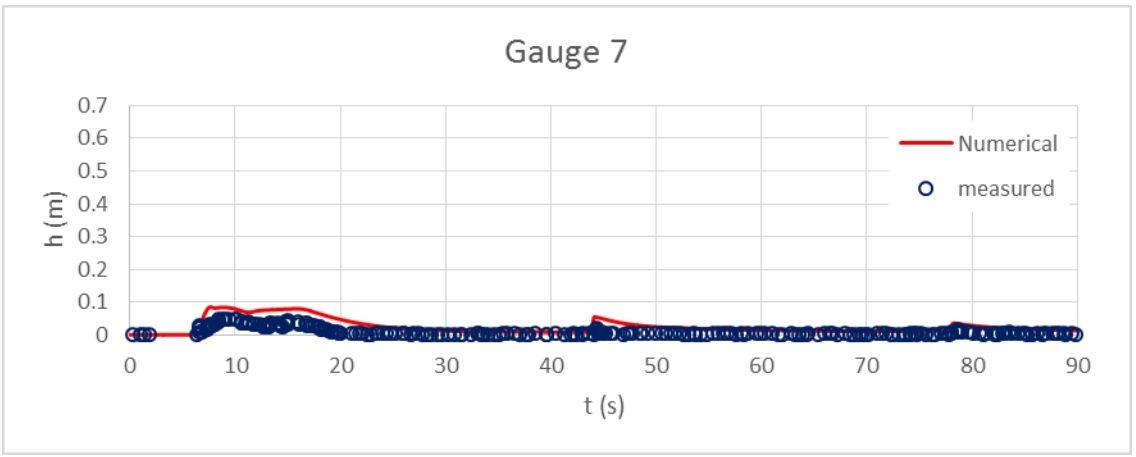

Figure 3-9: Comparison between the numerical and measured water level evolution during time at gages G1, G2, G3, G4, G5, G6, and G7

3.8.2 Two-Dimensional Dam Break Case Over Three Bumps

Once the one dimensional model had been tested, it is important to be extended and be tested for two dimensional channels with irregular bed topography as these allow a full range of practical simulations. For this purpose, the model was implemented to simulate a dam break case over a channel with three humps. This case was originally proposed by Kawahara and Umetsu (1986) and employed later by many researchers (Liang and Marche (2009); Guan (2014)). The dam break occurs on a channel with a 75m length with 30m width with three humps. Two small hump with base diameter of 8m are located at x=30m, y=6m, and x=30m, y=24m respectively, while the bigger hump with 10 m base diameter is located at x=47.5m and y=15m. The bed of

the channel, with Manning coefficient of n=0.018, have an irregular topography based on the following:

$$z_b(x,y) = \max\begin{bmatrix} 0, \\ 1-\frac{1}{8}\sqrt{(x-30)^2+(y-6)^2}, \\ 1-\frac{1}{8}\sqrt{(x-30)^2+(y-24)^2}\,, \\ 3-\frac{3}{10}\sqrt{(x-47.5)^2+(y-15)^2} \end{bmatrix}$$

The upstream water elevation is still at 1.875m while the downstream is totally dry which separated by a dam that located at 11m from the upstream edge. The upstream boundary condition is considered as a closed boundary, while the end boundary at the downstream considered as an open boundary.

Figure (3-10) shows the initial condition of the case at t=0s.

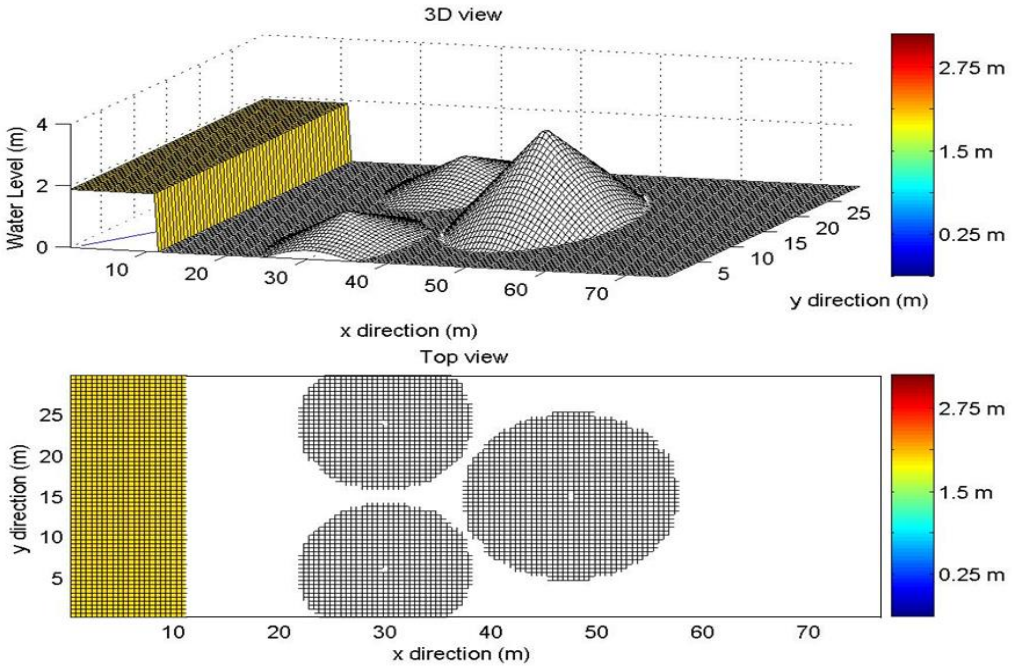

Figure 3-10: The initial conditions of the numerical model at t=0s.

For the simulation purposes, the channel domain is discretised using dx=0.5m with 150 cells in x direction and $\mathrm{d}y$ =0.5m with 60 cells in y direction respectively, and it was run for 300s. When t=0s, the dam breaks and water falls to the floodplain and propagate a wave that moves toward the humps at the downstream. The wet/dry front wave reaches the first two small humps at

around *t*=3s, Figure 3-11(a), and continues to rise over them and keeps climbing until they are totally submerged by water, Figure 3-11(b). At the same time, reflective waves are started that move from these two humps towards the upstream of the channel, while part of the wet/dry wave keeps moving in between the two humps in the downstream direction. At *t*=6s, Figure 3-11(c), the two small humps are entirely covered by water, and the wet/dry wave front has reached the big hump. Part of this wave tries to climb the big hump and part of that wave swerves around the two sides of the hump while a reflective wave propagate upstream. These different waves interact with each other and the energy dissipates gradually because of the bed friction. This complicated processes takes the water flow to steady state which is reached around t=300s, Figure 3-11(e).

The result of this simulation, shown in Figure (3-11), could be compared with other numerical models that had been presented by other others (Liang and Marche (2009); Guan (2014)) which in turn show a good agreement and similar descriptions.

The results from this simulation give confidence that the model is capable of simulating two-dimensional dam break cases on irregular topography even when the wetting and drying problem is involved, with good efficiency.

A)

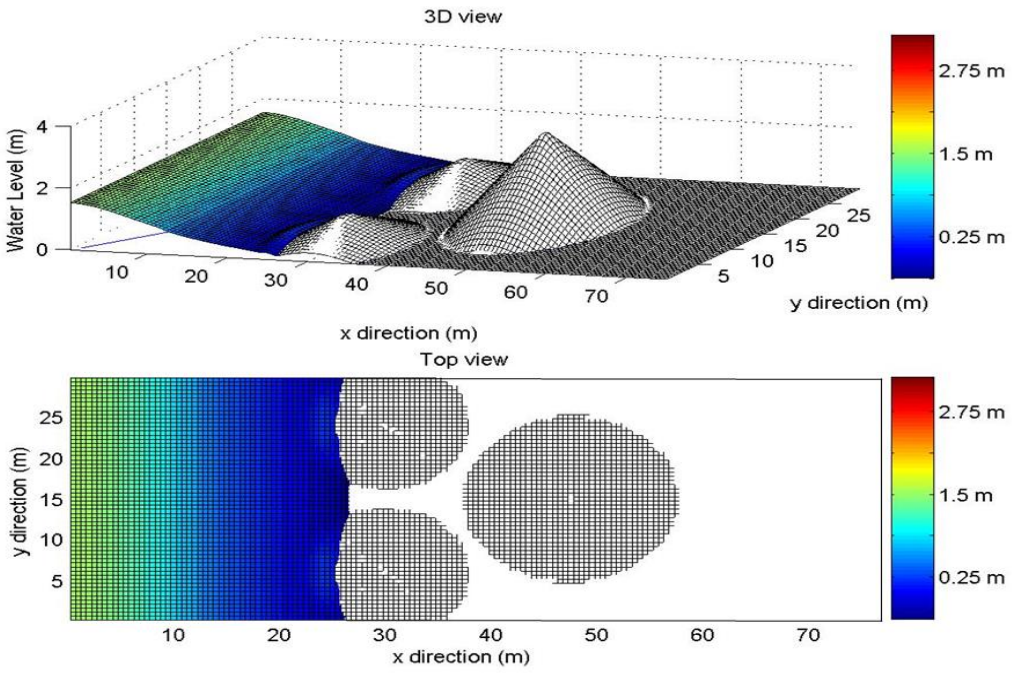

B)

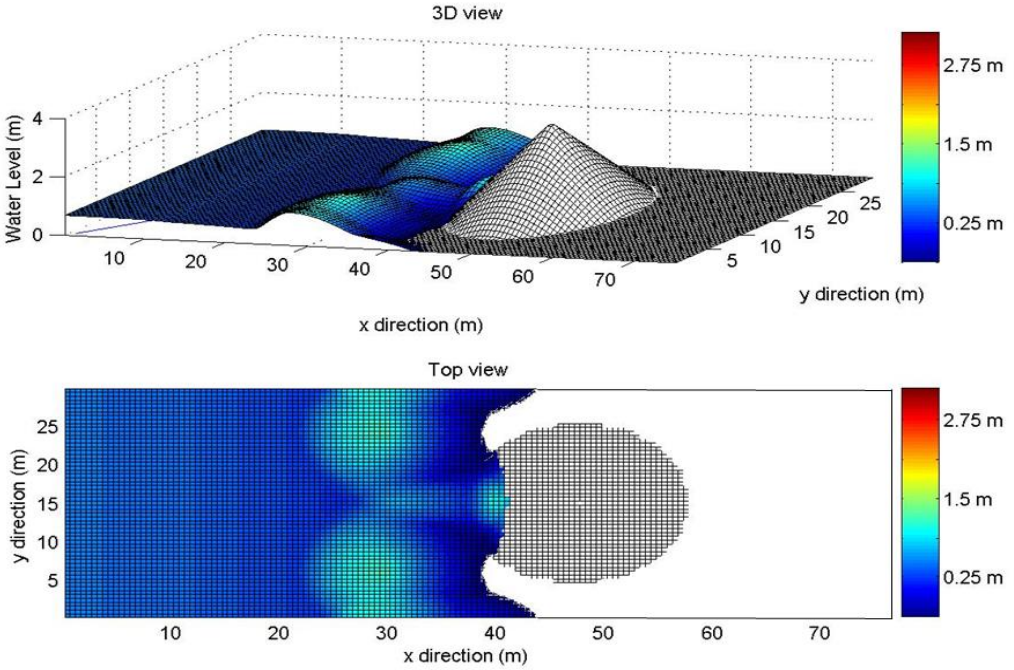
3D view
Water Level (m)
x direction (m)
y direction (m)
2.75 m
1.5 m
0.25 m
Top view
y direction (m)
x direction (m)
2.75 m
1.5 m
0.25 m

C)

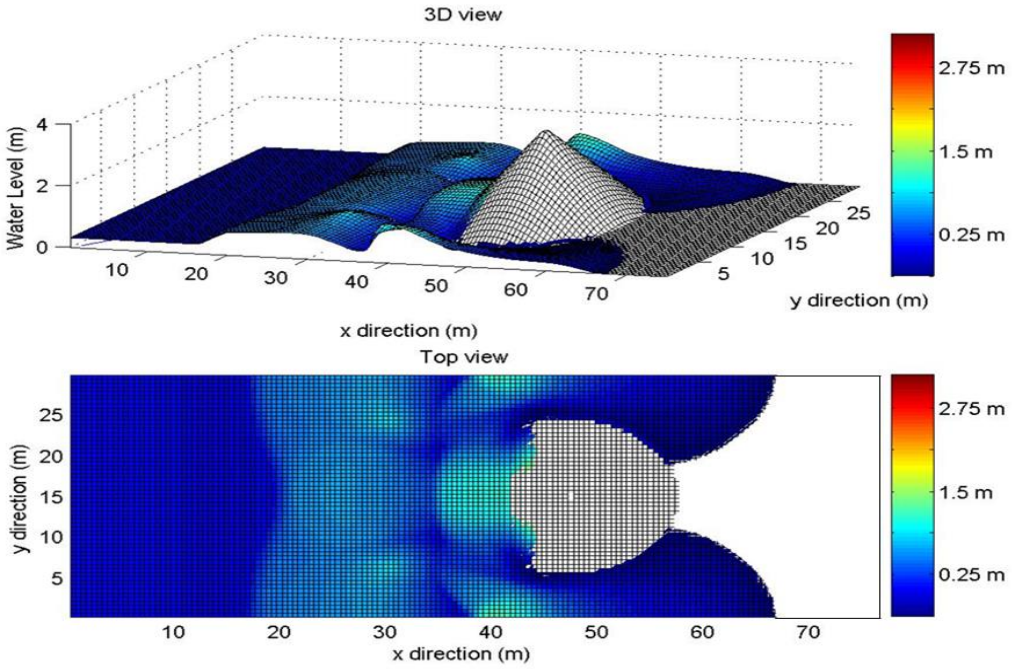
3D view
Water Level (m)
x direction (m)
y direction (m)
2.75 m
1.5 m
0.25 m
Top view
y direction (m)
x direction (m)
2.75 m
1.5 m
0.25 m

D)

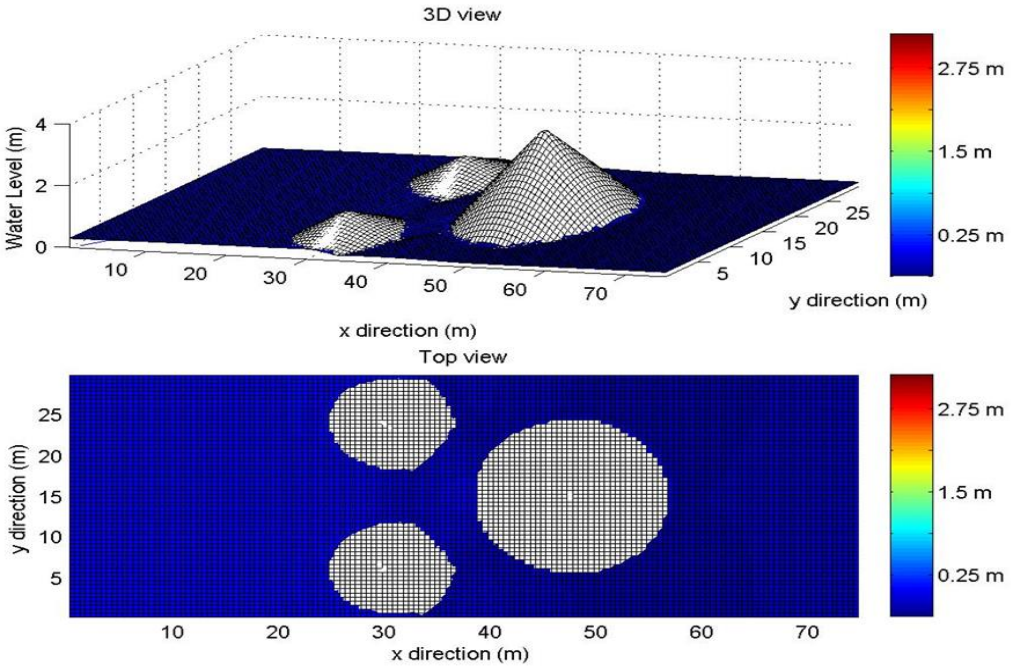

E)

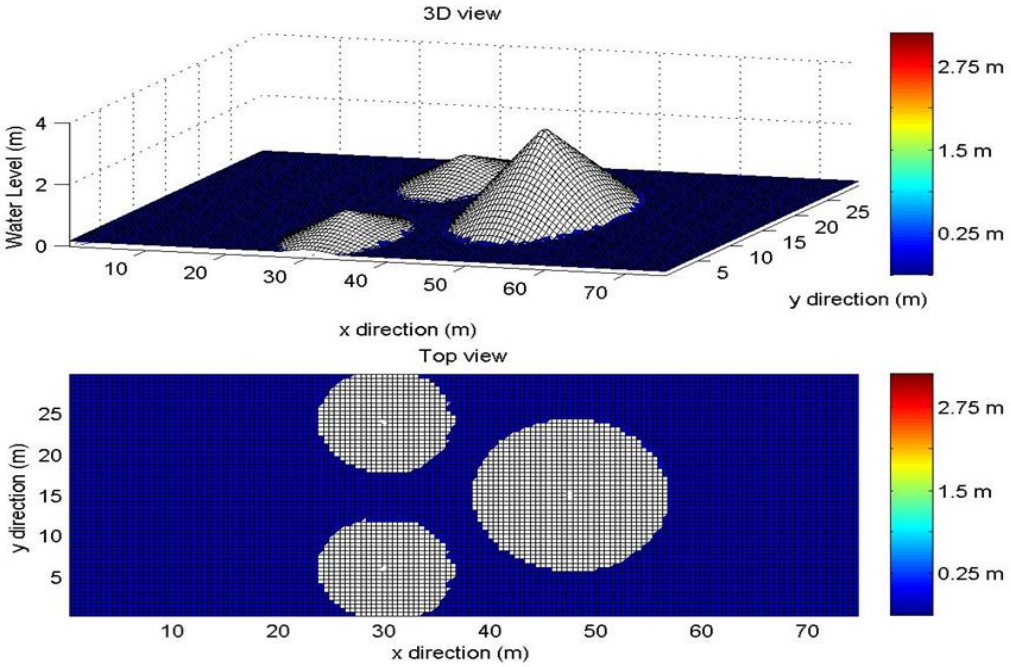

Figure 3-11: The numerical simulation of water flow over non-erodible bed with three humps.

3.9 The Construction of the Non-Cohesive Hydro-Morphodynamic Model (HMD-NC)

In this section the construction of a hydro-morphodynamic model that is designed to deal with water flow over a non-cohesive soil bed is presented.

3.9.1 One-Dimensional Model

Sediment transport is one of the most important issues that faces hydraulic engineers. This is because of its effect on water quality, hydraulic structure collapse, topography change, bank erosion, and dam the breaching process. For that reason, this research presented a simple hydro-morphodynamic model that is capable of simulating the water flow over movable beds that consists of non-cohesive materials. This model is built by incorporating a sediment transport model and bed evolution model with the hydrodynamic model described previously in this chapter. The details of this hydro-morphodynamic model extension is described below.

3.9.2 Governing Equations

Water flow hydrodynamics, as mentioned above, can be represented by the use of shallow flow theory. In this section the one-dimensional model is presented to simulate the water flow over movable bed that consist of uniform non-cohesive sediment particles. The mass and momentum conservation equations for water-sediment mixture can be written (for simplicity, in 1D) as in Cao *et al.* (2004):

$$\frac{\partial h}{\partial t} + \frac{\partial hu}{\partial x} = \frac{-\partial z}{\partial t} \tag{3.18}$$

$$\frac{\partial hu}{\partial t} + \frac{\partial}{\partial x}\left(hu^2 + \frac{1}{2}gh^2\right) = gh\left(S_{ox} - S_{fx}\right) - \frac{(\rho_s - \rho_w)gh^2}{2\rho}\frac{\partial C}{\partial x} - \frac{(\rho_0 - \rho)(SE - SD)u}{\rho(1-P)} \tag{3.19}$$

Where, $\rho = \rho_w(1-c) + \rho_s$ is the density of water-sediment mixture, $\rho_o = \rho_w P + \rho_s(1-P)$ is the density of the saturated bed, ρ_w, ρ_s are the densities of water and sediment, respectively, C is the sediment concentration, P is the porosity, and SE,SD are the sediment entrainment and deposition flux at the bed boundary, representing the exchange process of the sediment between the movable bed and water column.

It is very clear that the mass conservation continuity Equation (3.18) differs from the classical continuity equation for clear water flow in shallow water hydrodynamics by the mass exchange between the water flow and erodible bed. The right hand side of the equation, $\frac{-\partial z}{\partial t}$ is the important term that represents the morphological evolution process following the sediment transport process.

The momentum Equation (3.19) has a different form compared to the single phase clear water momentum equation. An additional two source terms are incorporated in the equation to represent the physical case of the sediment-water mixture. The first extra term, (the second on the right hand side), brings to light the influence of the streamwise variable concentration. This term is particularly significant in the cases of high sediment concentration such as dam break cases and debris flow cases. The second new term, (the third one on the right hand side), represents the momentum transfer that results from the sediment exchange between water column and the erodible bed boundary.

To represent the sediment transport mechanism, a suitable sediment transport model is required to be incorporated and coupled with the hydrodynamic model. This model is suitable for the bed with fine particles that exposed to flow with high shear stress. A simplified advection-diffusion equation, that had been presented by Cao *et al.* (2004), is adopted and adapted to represent the suspended load transport and bed load transport by the following:

$$\frac{\partial hC}{\partial t} + \frac{\partial huC}{\partial x} = SE - SD \tag{3.20}$$

The sediment entrainment and deposition flux over the bed boundary, SE and SD, can be computed based on using one of the formulae presented by other researchers over the years. This will be discussed in the following sections.

The final governing equation that is important to close the model is the bed morphological change model which is represented as below:

$$\frac{\partial z}{\partial t} = \frac{SD - SE}{1 - P} \tag{3.21}$$

The new compact form of the morphodynamic model of the previous equations is:

$$\frac{\partial \boldsymbol{U}}{\partial t} + \frac{\partial \boldsymbol{F}}{\partial x} = S \tag{3.22}$$

Where $\boldsymbol{U}$ is the vector that containing the conserved flow variables

$$\boldsymbol{U} = \begin{bmatrix} h \\ hu \\ hc \end{bmatrix} \tag{3.23}$$

$\boldsymbol{F}$ and $\boldsymbol{G}$ are the flux vectors in x and y directions, respectively.

$$\boldsymbol{F} = \begin{bmatrix} hu \\ hu^2 + 0.5gh^2 \\ huc \end{bmatrix} \tag{3.24}$$

Where $\boldsymbol{S}$ is the source term vector

$$\boldsymbol{S} = \begin{bmatrix} \frac{SE-SD}{1-P} \\ gh(S_{ox} - S_{fx}) - \frac{(\rho_s-\rho_w)gh^2}{2\rho}\frac{\partial C}{\partial x} - \frac{(\rho_0-\rho)(SE-SD)u}{\rho(1-P)} \\ SE - SD \end{bmatrix} \tag{3.25}$$

3.9.2.1 Erosion Flux

There are many different formulae that could be used to simulate the erosion process for non-cohesive sediment. A study by Guan *et al.* (2012) that compared different entrainment formulae concluded that the van Rijn's formula is more powerful and applicable to different circumstances that include low shear stress and high shear stress cases. Therefore, van Rijn's formula is adopted for the current study. Thus the following were used:

$$SE = w_0 C_{ac} \tag{3.26}$$

$$C_{ac} = 0.015\frac{d}{a}\frac{T^{1.5}}{d^*} \tag{3.27}$$

$$T = \frac{(u_*)^2-(u_{*,cr})^2}{(u_{*,cr})^2} \tag{3.28}$$

It is very important to know that the erosion process occurs when $T > 0$.

$$d_* = d\left[\frac{g(s-1)}{V^2}\right]^{\frac{1}{3}} \tag{3.29}$$

Where, SE is the erosion rate, w_0 is the settling velocity, $C_{ac}$is the near bed concentration, a is a reference level, u_* shear velocity, $u_{*,cr}$is the critical bed shear velocity, d_* is the dimensionless particle diameter, V is the kinematic viscosity coefficient of water, and T is the transport stage parameter.

3.9.2.2 Deposition Flux

A transported particle will deposits when its weight exceeds the value of uplift force that is applied on the particle by the water flow. This means that the flow shear stress is weak and incapable of eroding this particle again.

It is important to understand that the majority of deposition flux formulae are empirical, and they were derived from measured data with relatively low shear stresses that $\theta \leq 2.0$ (Cao *et al.* (2004)). In this research, the equation that had been used in Guan (2014) is adopted. This represents the value of particle settling velocity times the concentration at the reference level:

$$SD = w_0 C_a \tag{3.30}$$

$$C_a = \delta C \tag{3.31}$$

Where, SD is the deposition flux, C_a is the near bed concentration at reference level a, δ is an empirical coefficient that is defined in previous works (Cao *et al.* (2004)) where the relationship is presented as:

$$\delta = min\left\{2.0\,, \frac{1-P}{C}\right\} \tag{3.32}$$

3.9.2.3 Settling Velocity

When the weight of the transported non-cohesive particle is larger than the uplift force, the particle tends to settle and deposit on the bed. The non-cohesive particles settle as individual particles. This settling process has a velocity of settling w_0. The settling velocity depends on the particle size and sediment concentration.

There are many different formulae that are used to compute the settling velocity. van Rijn (1984a) presented several different formulae to calculate the settling velocity based on particle size as following:

$$w_0 = \begin{cases} \frac{0.056(s-1)gd^2}{V} & for\ d < 100\ \mu m \\ 10\ \frac{v}{d}\left[\left(1+\frac{0.01(s-1)gd^3}{V^2}\right)^{0.5} - 1\right] & for\ 100\ \mu m < d < 1000\ \mu m \\ 1.1[(s-1)gd]^{0.5} & for\ d > 1000\ \mu m \end{cases} \quad (3.33)$$

Where, g=9.81 m/s^2 is the gravitational acceleration, s is the sediment relative density, d is the particle diameter (m), and V is the water kinematic viscosity coefficient m^2/s.

For normal flow condition with particle sizes that range from 50μm to 500μm, van Rijn (1984b) suggested another equation to calculate the settling velocity as following:

$$w_{0,s} = (1-c)^4 w_0 \quad (3.34)$$

Also, another formula, which is adopted in this research, was presented by Soulsby (1997) to calculate the settling velocity for individual particle as following:

$$w_0 = \frac{V}{d}[\sqrt{(10.36)^2 + 1.049d_*^3} - 10.36 \quad (3.35)$$

Where, d_* represents the dimensionless particle size.

$$d_* = d\left[\frac{g(s-1)}{V^2}\right]^{1/3}$$

3.9.3 Testing of One-Dimensional Hydro-morphodynamic Model

3.9.3.1 Suspension Dominant Dam break Case

Model testing was carried out to check performance when simulating erodible bed situations. A dam break experiment flow over movable bed that was executed in Taipei University (University of Taiwan) is employed. The physical set-up and instrumentation was reported in Capart and Young (1998). The experiment is performed on horizontal channel with dimensions of 1.2m long, 0.2m wide, and 0.7m deep. In this experiment, artificial spherical particles were used with diameter of 6.1mm with a density of 1,048kg/m^3, and settling velocity of about 0.076m/s. A sediment layer with a thickness of 5-6mm was placed along the channel. To represent the dam, a sluice gate was installed at the middle of the channel, to release the dam break wave by sudden lifting for the

sluice gate. The initial water depth were 0.1m and 0.0005m at the upstream and the downstream respectively. The flow and sediment transport evolution was filmed using charge-coupled device (CCD) camera that fixed at the channel sides.

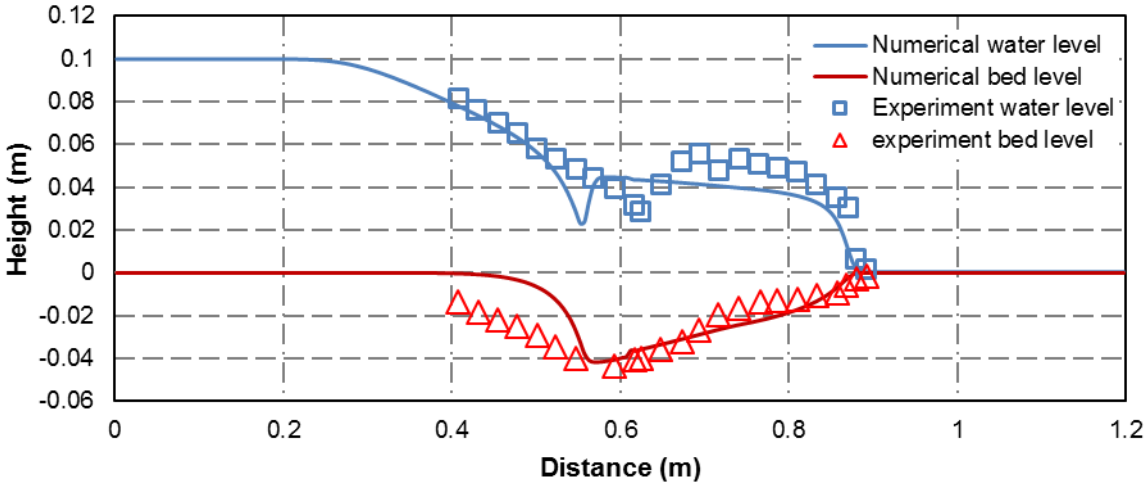

Figure 3-12: Dam-Break validation with Taipei University experimental work (Capart and Young (1998)) at t = 0.303s

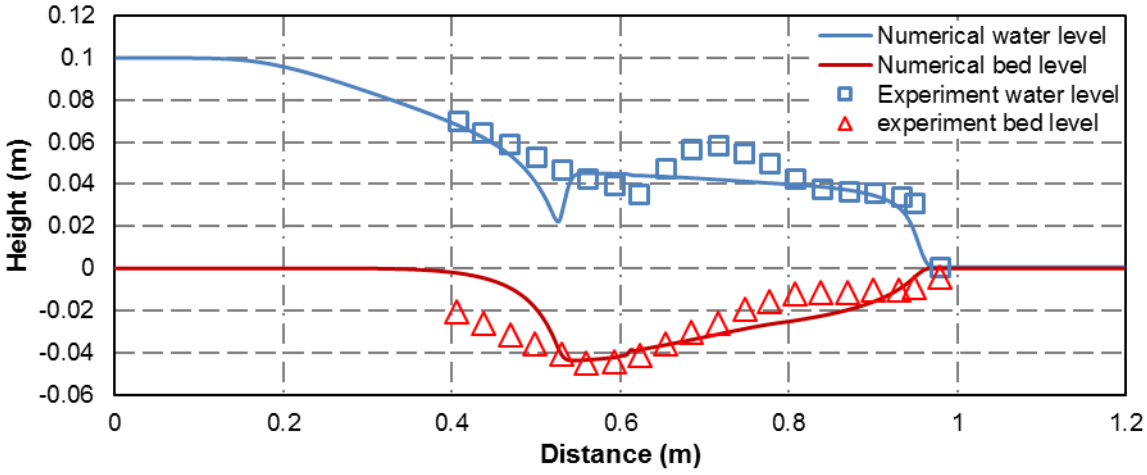

Figure 3-13: Dam-Break validation with Taipei University experimental work (Capart and Young (1998)) at t = 0.404s

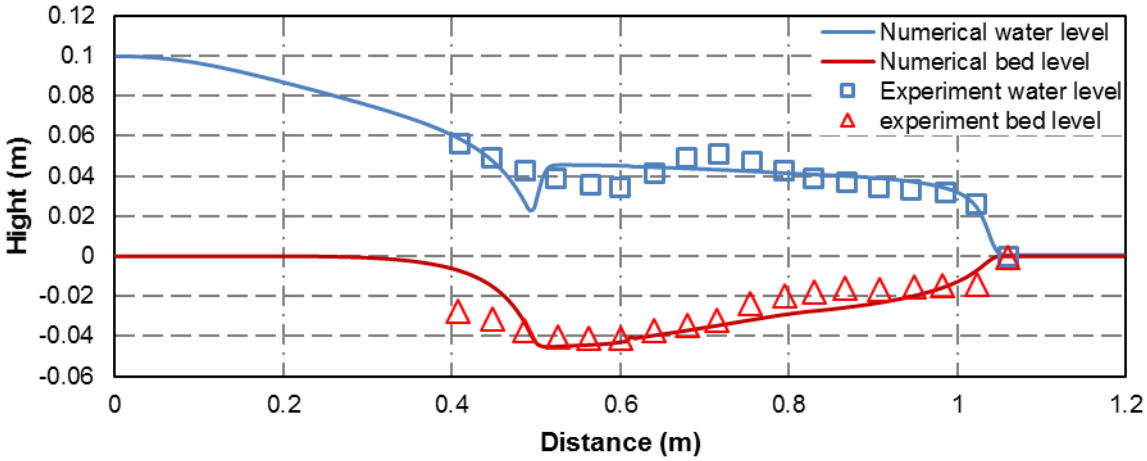

Figure 3-14: Dam-Break validation with Taipei University experimental work (Capart and Young (1998)) at 0.505s

In the numerical simulation, a uniform mesh is employed with a grid spacing of 0.005m to form 500 cells that represent the whole channel length. An initial water depth of 0.0005m is employed for the wet-dry bed tolerance. The value of 0.025 is used as the Manning roughness of the bed. The sediment porosity is given as 0.28. The van Rijn (1984b) sediment transport formula to simulate the entrainment and the deposition process of the sediment particles. A constant value of reference level a = 0.005m, is used. The simulation is run for 0.505s.

Figures (3-12), (3-13), and (3-14) show that the qualitative agreement between the simulation and the measurements is quite good. The bed change and the wave front location are well described by the model. To determine whether the flow is laminar flow or turbulent flow, the Reynolds number criteria is employed. It is computed based on the following equation:

$$R = \frac{uL}{V} \tag{3.36}$$

Where R is Reynolds number, u is the flow velocity, L is a characteristic length, and V is the water kinematic viscosity. It is found that the Reynolds number equals to 32100. This demonstrates that the flow is turbulence (Lowe (2003); Chow (1959)).

The simulation shows that the propagated hydraulic jump is located at the upstream area. It is clearly observed that the hydraulic jump shifts upstream during the simulation.

3.9.3.2 Bed Load Dominant Dam Break Case

The model was tested against an experiment work to check its capability to predict the bed evolution process in case of bed load sediment transport. To perform this experiment, the dam break experiment of flow over a movable bed that was carried out in Louvain-la-Neuve University is utilised. The experiment was reported in Fraccarollo and Capart (2002). The experiment was performed on channel with dimensions of 2.5m long, 0.1m wide, and 0.25m deep. In this experiment, artificial cylindrical PVC pellets were used with diameter of 3.2mm with height of 2.8mm (hence the equivalent spherical particles diameter is 3.5mm. These particles have density of 1,540/m^3, and settling velocity of about 0.18m/s. A sediment layer with a thickness of 5-6mm was set up along the channel. A sluice gate was installed at the middle of the channel to represent the dam. The dam break is represented by sudden lifting for the sluice gate. The initial water depth were 0.1m and 0.0005m at the upstream and the downstream respectively. The flow and sediment transport evolution was monitored by set up CCD camera that fixed at the channel sides.

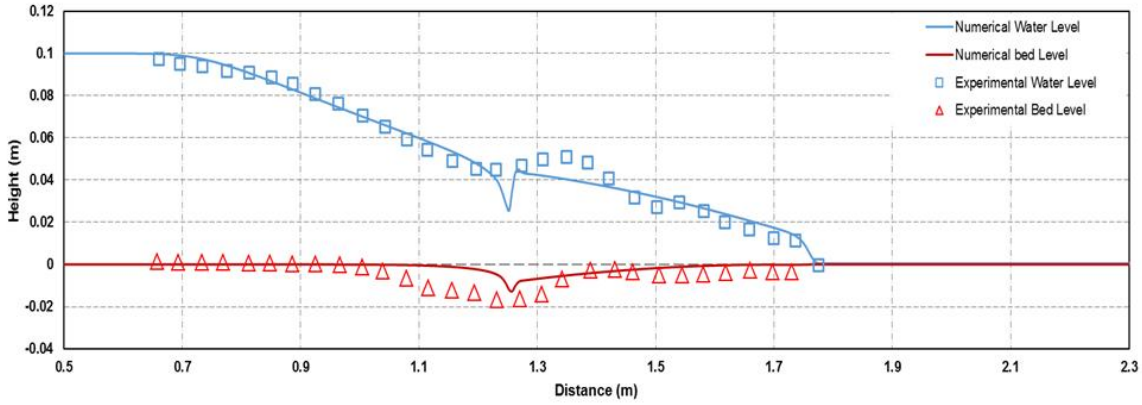

Figure 3-15: Dam-Break validation with Louvain University experimental work at 0.505s

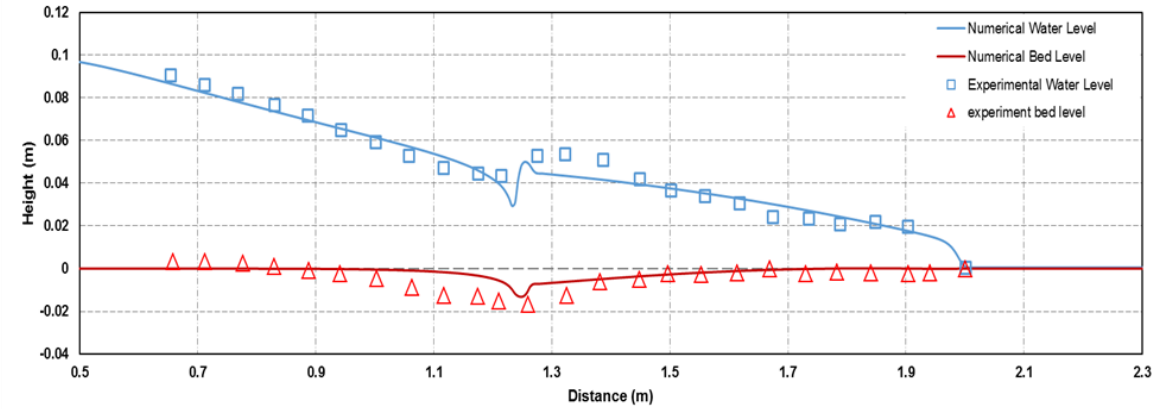

Figure 3-16: Dam-Break validation with Louvain University experimental work at 0.758s

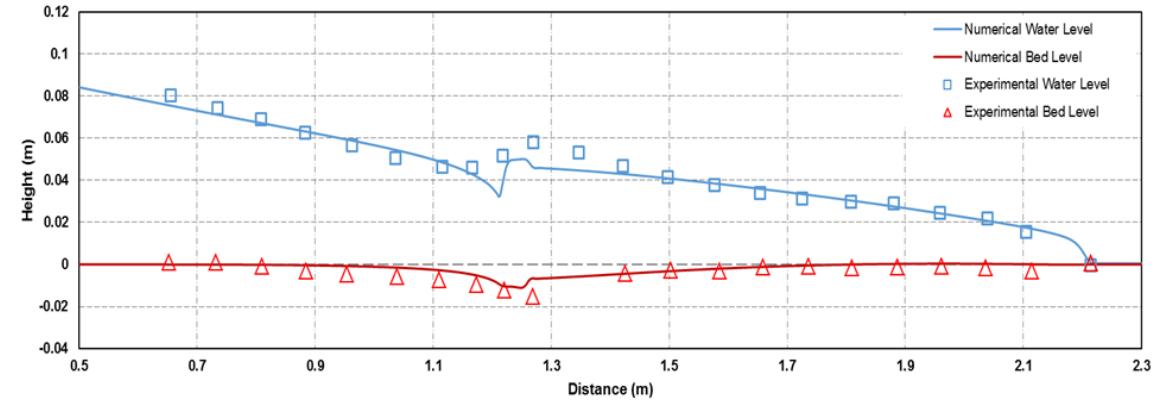

Figure 3-17: Dam-Break validation with Louvain University experimental work at 1.01s

In the numerical simulation, a uniform rectangular mesh is utilised to generate a grid that have 500 cells with spacing of 0.005m to represent the whole domain. An initial water depth of 0.0005m is employed for the wet-dry bed tolerance. The value of 0.025 is used as the Manning roughness of the bed. The sediment porosity is given as 0.3. The van Rijn (1984b) sediment transport formula to simulate the entrainment and the deposition process of the sediment particles. A constant value of reference level a = 0.005m, is used. The simulation is run for 1.01s.

Figures (3-15), (3-16), and (3-17), demonstrate the comparison between the numerical results and the measurements at 0.505s, 0.758s, and 1.01s. The

comparison shows a good agreement between the two results. The numerical model reproduces the bed change and the wave front location accurately. It can be seen that the hydraulic jump shifts upstream during the simulation evolution.

For this simulation, it is found that the Reynolds number R equals to 24900. This demonstrates that the flow is turbulence (Lowe (2003); Chow (1959)).

The model is capable of predicting the water flow over a movable bed with non-cohesive soil when the transport is bed-load dominant.

3.9.4 Sensitivity Tests

To study the numerical model sensitivity to different parameters, a group of tests have been undertaken. The parameters that were tested include Manning roughness n, the reference level a, and settling velocity w. To perform the tests, the dam break experiment flow over movable bed that was executed in Taipei University (University of Taiwan) is employed. In the numerical simulation, a uniform mesh is employed with a grid spacing of 0.005m to form 500 cells that represent the whole channel length. An initial water depth of 0.0005m was used for the wet-dry bed. The tests were run for 20 seconds.

Figure (3-18) shows the effect of Manning roughness coefficient value on the simulation result. The values of 0.025, 0.023, and 0.022 were used. This small variation of n values can demonstrate the model sensitivity to n value. It is found that the Manning roughness has a significant influence on the simulation. Notably increasing of the scoured hole can be seen when small values of Manning roughness, 0.022 and 0.023 were used, which increased significantly when bigger value of 0.025 were employed. This increase of erosion rate is caused by the increasing of the shear stress that influenced by the Manning roughness.

Figure (3-19) shows how the value of the reference level influences the simulation results. The reference level (a) ,which is a layer with a small depth that is close to the bed at which the sediment exchange occurs between the water column and the bed, has the values of 0.01m, 0.02m, and 0.005m in the

tests. It can be seen that the thickness of the reference level plays a significant role in influencing the results because of its effect on the entrainment magnitude. The increasing of *a* value will decrease the erosion and vice versa. The decrease of *a* value shows of increasing of the scour hole at the dam location. The value of 0.005m shows over an predicted erosion process compared to measurements. The reason of the increase when using a small value of the reference level is, the small value of the reference level will increase the magnitude of the near bed concentration C_{ac}, based on the relationship of $C_{ac} \propto \frac{1}{a}$, and the consequence is an increase in the erosion rate which is calculated by:

$$SE = w_0 C_{ac}$$

Figure (3-20) illustrates the influence of the range of the different values of the settling velocity on the results of the simulation. The values of 0.06m/s, 0.075m/s, and 0.08m/s were employed in the test. It can be clearly seen that the settling velocity has a tenuous influence on the numerical result in comparison to the a level test. However, the settling velocity plays a significant role in both erosion and deposition process. The increasing of the settling velocity will increase the erosion rate based on the previous formula.

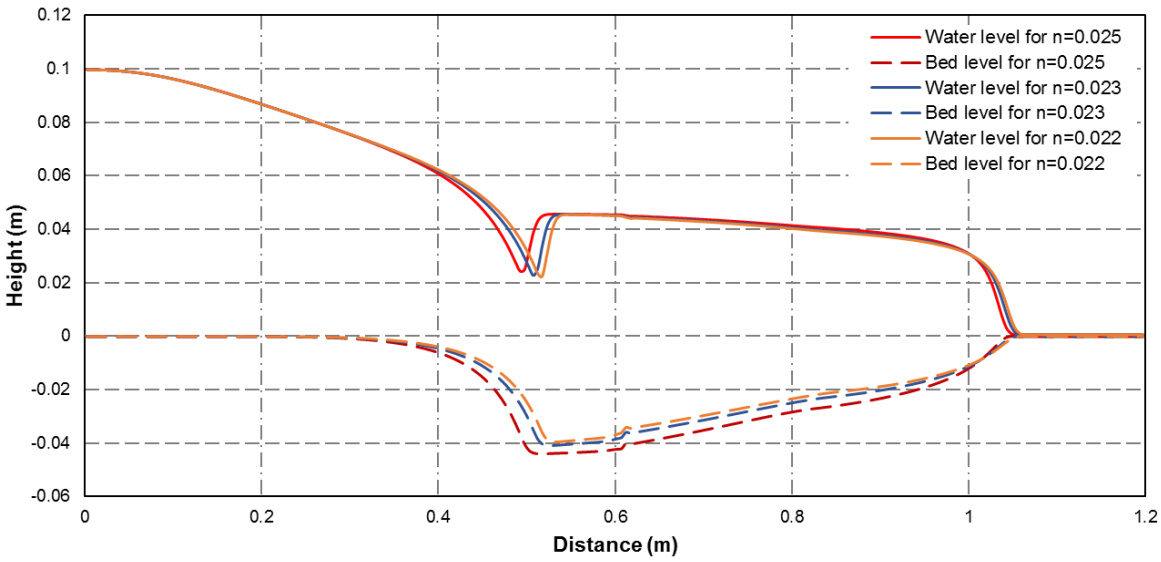

Figure 3-18: Sensitivity test of n

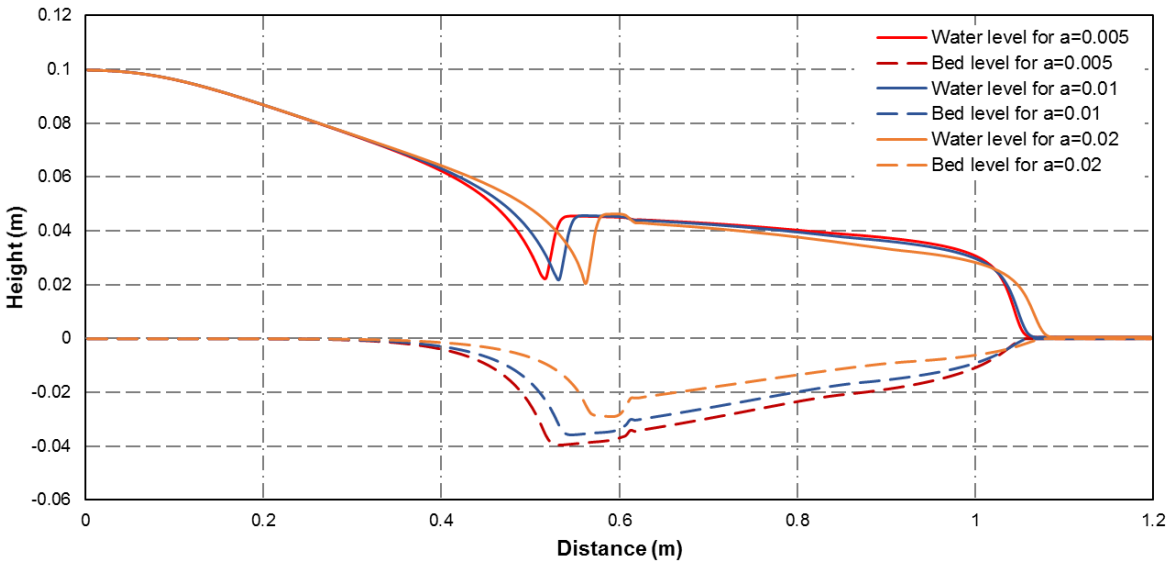

Figure 3-19: Sensitivity test of a

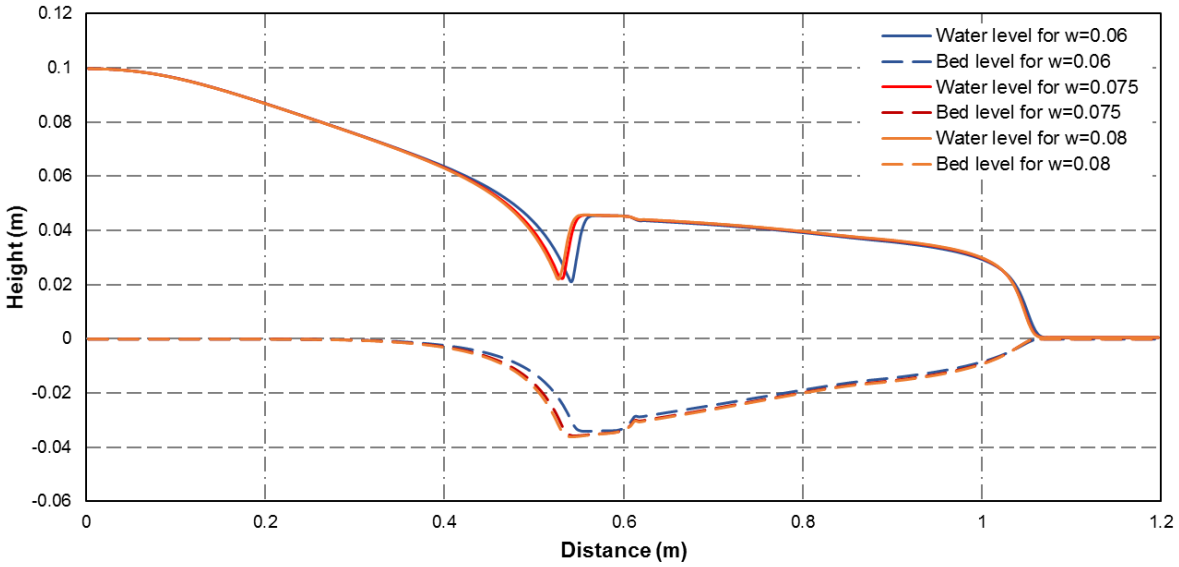

Figure 3-20: Settling velocity sensitivity

3.9.5 Two-Dimensional Model

In this section, the previous one dimensional model is extended to a two dimensional version. This is to make the simulation is more realistic according to the involvement of y direction influence on the solution.

3.9.6 Governing Equations

$$\frac{\partial h}{\partial t} + \frac{\partial hu}{\partial x} + \frac{\partial hv}{\partial y} = \frac{-\partial z}{\partial t} \tag{3.37}$$

$$\frac{\partial hu}{\partial t} + \frac{\partial}{\partial x}\left(hu^2 + \frac{1}{2}gh^2\right) + \frac{\partial huv}{\partial y} = gh\left(S_{ox} - S_{fx}\right) - \frac{(\rho_s - \rho_w)gh^2}{2\rho}\frac{\partial C}{\partial x} - \frac{(\rho_0 - \rho)(SE - SD)u}{\rho(1-P)}$$

(3.38)

$$\frac{\partial hv}{\partial t} + \frac{\partial huv}{\partial x} + \frac{\partial}{\partial y}\left(hv^2 + \frac{1}{2}gh^2\right) = gh\left(S_{oy} - S_{fy}\right) - \frac{(\rho_s - \rho_w)gh^2}{2\rho}\frac{\partial C}{\partial y} - \frac{(\rho_0 - \rho)(SE - SD)v}{\rho(1-P)}$$

(3.39)

The simplified advection-diffusion equation that was presented in Equation (3.21), which represent the suspended load transport and bed load transport, is extended to represent the two dimensions by the following:

$$\frac{\partial hC}{\partial t} + \frac{\partial huC}{\partial x} + \frac{\partial hvC}{\partial y} = SE - SD \tag{3.40}$$

The bed morphological change model is represented as below:

$$\frac{\partial z}{\partial t} = \frac{SD - SE}{1-P} \tag{3.41}$$

The new two-dimensional compact form of the hydro-morphodynamic model of the previous equations is:

$$\frac{\partial \boldsymbol{U}}{\partial t} + \frac{\partial \boldsymbol{F}}{\partial x} + \frac{\partial \boldsymbol{G}}{\partial y} = S \tag{3.42}$$

Where $\boldsymbol{U}$ is the vector that containing the conserved flow variables

$$\boldsymbol{U} = \begin{bmatrix} h \\ hu \\ hv \\ hc \end{bmatrix} \tag{3.43}$$

$\boldsymbol{F}$ and $\boldsymbol{G}$ are the flux vectors in x and y directions, respectively.

$$\boldsymbol{F} = \begin{bmatrix} hu \\ hu^2 + 0.5gh^2 \\ huv \\ huc \end{bmatrix} \tag{3.44}$$

$$\boldsymbol{G} = \begin{bmatrix} hv \\ hvu \\ hv^2 + 0.5gh^2 \\ hvc \end{bmatrix} \tag{3.45}$$

Where $\boldsymbol{S}$ is the source term vector

$$\boldsymbol{S} = \begin{bmatrix} \frac{SE-SD}{1-P} \\ gh(S_{ox} - S_{fx}) - \frac{(\rho_s-\rho_w)gh^2}{2\rho}\frac{\partial C}{\partial x} - \frac{(\rho_0-\rho)(SE-SD)u}{\rho(1-P)} \\ gh(S_{oy} - S_{fy}) - \frac{(\rho_s-\rho_w)gh^2}{2\rho}\frac{\partial C}{\partial y} - \frac{(\rho_0-\rho)(SE-SD)v}{\rho(1-P)} \\ SE - SD \end{bmatrix} \quad (3.46)$$

3.9.7 Testing of the Two-Dimensional Hydro-Morphodynamic Model

To test the model capability to deal with dam break over a mobile bed changes in two dimensions, the experimental work of Goutiere *et al.* (2011) is used to compared with the numerical work. The laboratory experiment was performed at the Universitě Catholique de Louvain, Belgium. The test flume was 6m long with glasses side walls. The channel has 0.25m width then suddenly widens after 4m to be 0.5m wide. The dam is located at the centre of the flume. The initial water depth at the upstream and the downstream of the channel are 0.25m and 0m respectively. The channel was filled with 0.1m height uniform sand layer. The median diameter of the sand is 1.72mm, with specific density of ρ_s/ρ_w=2.63, and 39% of porosity. The boundary conditions were a closed boundary at the upstream of the flume, while at the downstream was open boundary with free outflow. The experimental setup is presented in Figure (3-21).

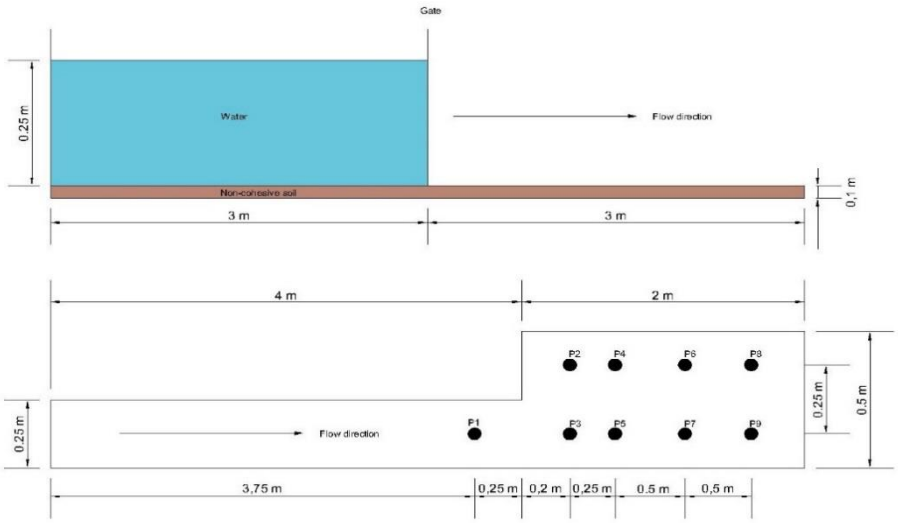

Figure 3-21: Dam break experiment setup

For simulation, the channel domain was discretised by 120 x 60 structured cells with dx = 0.05 and dy = 0.025 respectively. The Manning coefficient is taken to be 0.023 as in the experiment. The simulation was run for 10 seconds and the numerical result was compared with the measurements at seven gauges, P1, P2, P3, P4, P5, P6, and P7, that are shown in Figure (3-23).

When t=0, the dam breaks and the water level falls into the flume and propagates a wave that moves toward the widening channel. When the wet/dry front reaches the opening, the wave front spreads to the left side of the channel as shown in Figure 3-22(a) at *t*= 1s. Later, at 1.5s, the wave reflects from the wall forming a wave bore that moves from the left wall as shown in Figure 3-22(b).

A

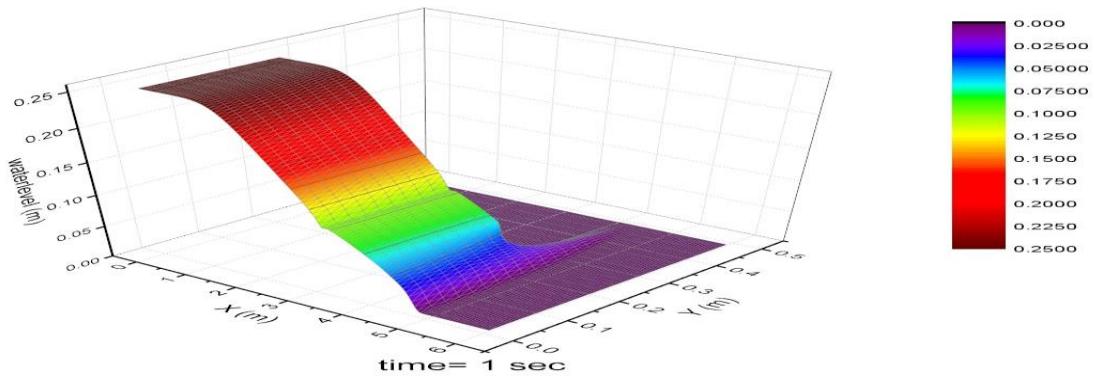

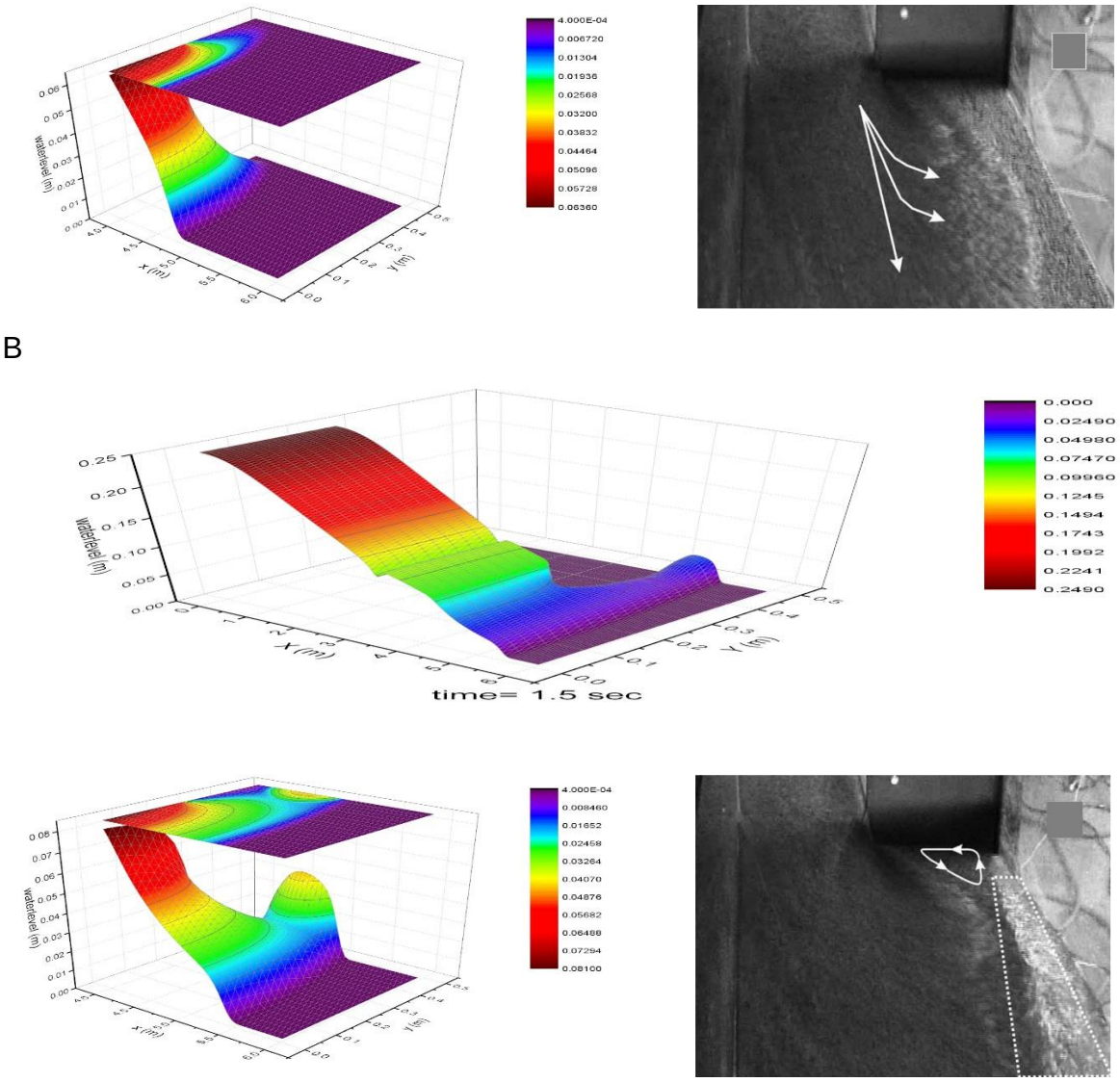

Figure 3-22: The 3D simulation and comparison between simulated water contours and experimental observations at t=1s and 1.5s for A and B respectively

Figure (3-23) shows the water level comparison for the whole numerical simulation time, that is 10s, between the water level of the numerical result and the measurements at the gauges, P1, P2, P5, and P6. The qualitative comparison between the numerical result and the measured data shows a good agreement. However, some slight differences appear between the two results in some gauges such as gauge at P2, the temporal simulation of water flow process through the channel domain is well predicted. Some discrepancies can be seen at the location of P2 that is the closest point to the widening corner than other points. This significant discrepancy in this surface level is due to

lower performance of predication of the bed elevation at this point as shown later.

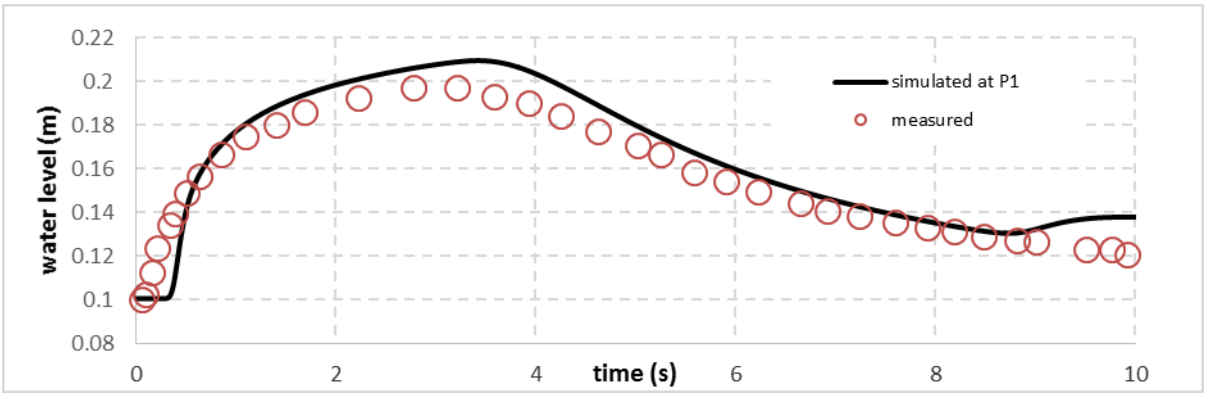

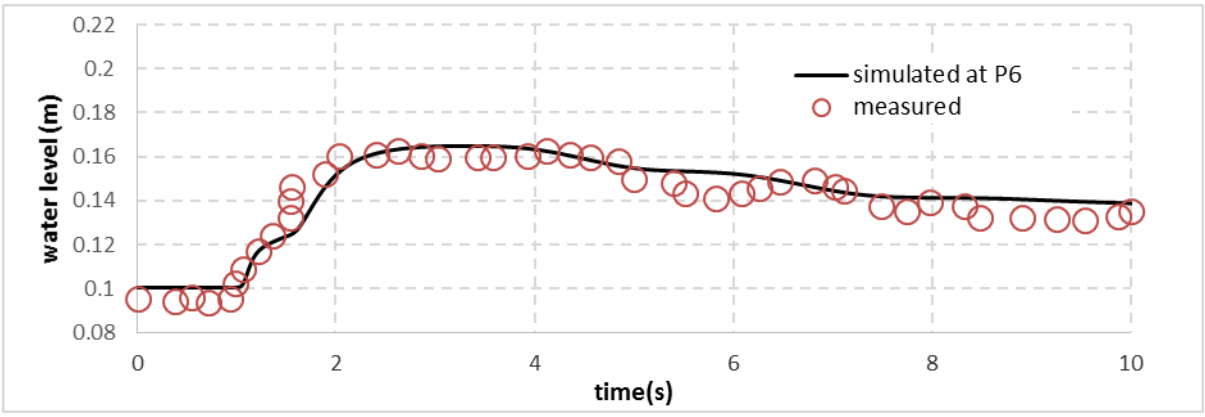

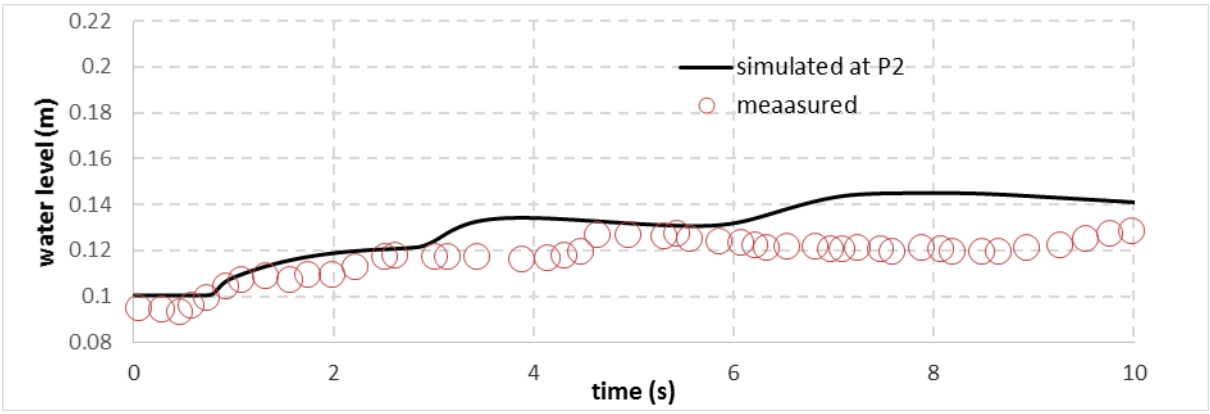

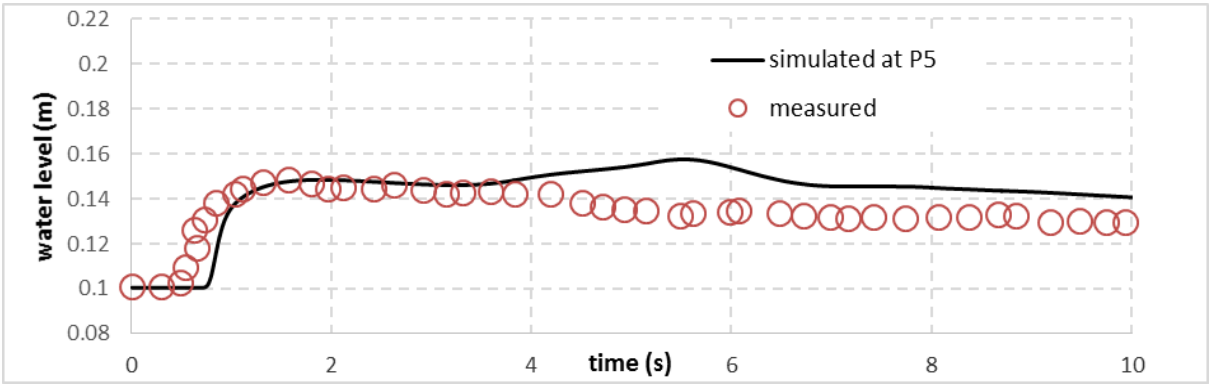

Figure 3-23: Comparison between simulated and measured water level at P1, P2, P5 and P6

The spatial simulation of the bed evolution is examined in Figure (3-24) by showing the comparison of cross sections of the channel at the opening of the model simulation, experimental measurements and the SWE-Exner model simulation that done by Soares-Frazão and Zech (2011) for the final bed topography. The main features that are very noticeable are the erosion where the scoured hole occurs at the beginning of the widening, and the deposition area where the mound is formed. At x=4.2m and x=4.3m, it is clearly seen that the numerical simulation has a discrepancy compared to the measurements, where the scouring and the deposition process are over estimated. However, the simulation shows trends of erosion and deposition similar to that observed in the experiment with smoothed patterns – probably because the secondary current effects are neglected in the present model. While at x=4.5m, the simulation shows a good agreement compared to the measurements and the final bed topography is well predicted. The discrepancy is reasonable if the following reasons are taken into the account: firstly, the secondary current influence is neglected in the model; secondly, the inability of the model to represent some physical processes such as the particle-particle collision which is ignored in the model ; thirdly, the neglect of the turbulence viscosity term which means that the rapid formation of horizontal circulating flow may not be predicted by the model (Guan (2014)).

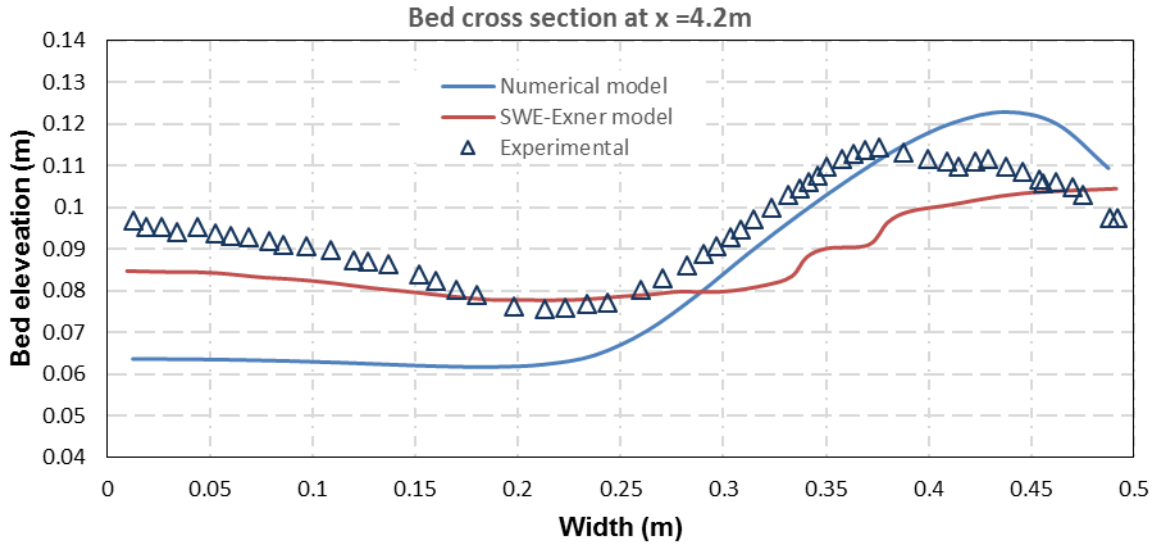
Bed cross section at x =4.2m
Numerical model
SWE-Exner model
Experimental
Bed eleveation (m)
Width (m)
0.14
0.13
0.12
0.11
0.1
0.09
0.08
0.07
0.06
0.05
0.04
0
0.05
0.1
0.15
0.2
0.25
0.3
0.35
0.4
0.45
0.5

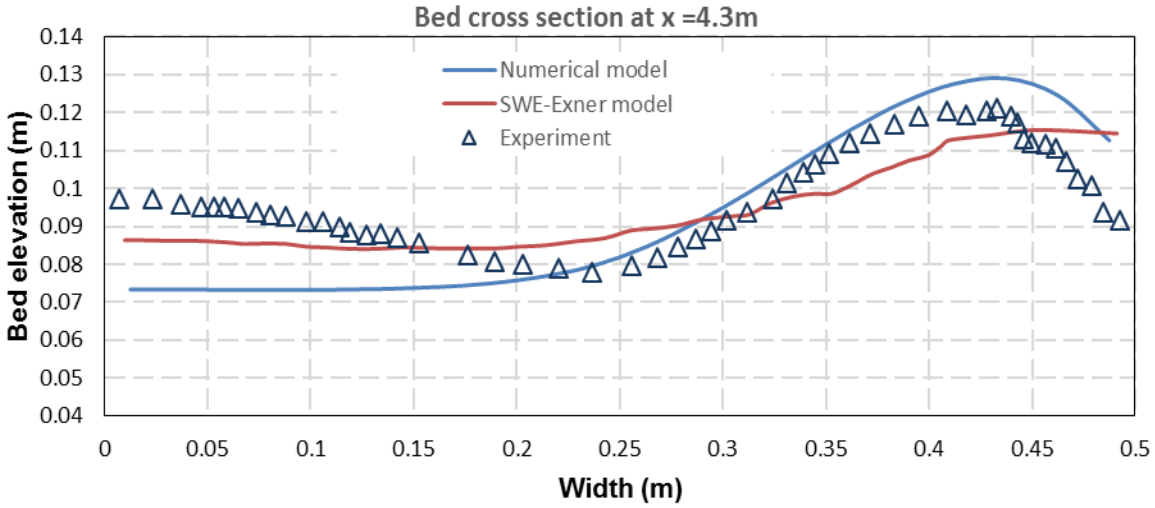
Bed cross section at x =4.3m
Numerical model
SWE-Exner model
Experiment
Bed elevation (m)
Width (m)
0.14
0.13
0.12
0.11
0.1
0.09
0.08
0.07
0.06
0.05
0.04
0
0.05
0.1
0.15
0.2
0.25
0.3
0.35
0.4
0.45
0.5

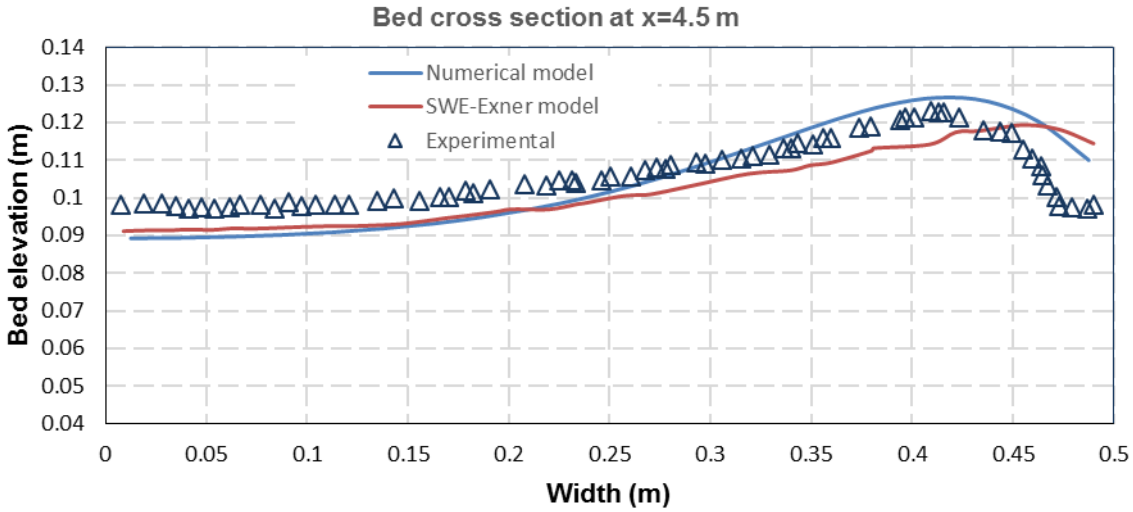

Figure 3-24: Bed topography of channel cross section at x=4.2m. x=4.3m, and x=4.5m.

3.10 Summary

This chapter introduces the development of the models required for this study, these include: a one-dimensional hydrodynamic model, a two-dimensional hydrodynamic model, a one-dimensional hydro-morphodynamic model, and a two-dimensional hydro-morphodynamic model. These models are based on the shallow water equations with a simple technique for source term treatment that had been previously presented and which is capable of dealing with water flow over a complex topography. The bed slope in the source term is discretised by implement a simple central-differencing forward technique at the cell centre. To solve the governing equations, the 1st order accurate HLL flux based, explicit time stepping, finite volume method is implemented.

The hydro-morphodynamic models were built by combination of the shallow water equations and additional two equations that are a sediment transport model and a bed evolution model. The sediment transport model that is presented in this study is capable of dealing with suspended sediment transport load and the bed-load sediment transport.

The models presented were tested and validated using previous experimental work. The numerical results of these tests showed a good agreement, in both

hydrodynamic and morphodynamic aspect, when compared to measurements. This demonstrates the models' capabilities to deal with such complex water flow over movable bed cases.

To sum up, the presented schemes can be applied in a straight-forward manner and are applicable for predicting flow over irregular topography for the fixed bed case as well as a movable bed when the suspended transport mode or the bed load transport mode dominates the sediment transport.

Chapter 4 One-Dimensional Hydro-Morphodynamic Model With Cohesive Bed Materials.

This chapter contains the core of the research work of this thesis. A new hydro-morphodynamic model is introduced that is robust and capable of dealing with cases that include water flow over movable beds that consist of cohesive sediments.

4.1 Introduction

In rivers, the bed materials may consist of cohesive or mixed material in which, the effects of the cohesion influences the erosion or deposition of the sediment particles. This can influence the hydraulic flow, sediment transport and bed evolution. Subsequently, it will affect different aspects such as the stream or riverbank stability, navigation, scouring around bridge piers, and the water quality as fine particles can carry chemical materials that affect natural life in the river. In addition to the above, the breaching mechanism in cohesive embankments is differ from that of non-cohesive embankments. It may include sudden mass failure that produces large outflow discharge with high destructive energy causing serious flash floods. Having to work with cohesive sediment transport is common and a frequent issue in disciplines that are related to water-hydraulic engineering as it plays a key role in many engineering projects.

As discussed in Chapter 2, the majority of the models that are employed to simulate water flow and sediment transport, either based on the flow over fixed bed or, water flow over movable bed that consist of non-cohesive materials. This is despite the fact that the science of cohesive sediment transport has been studied for some time; as Ongley writes:“ a few researchers have been investigating cohesive sediment transport processes for more than twenty years, conventional wisdom in the sediment transport field holds that suspended fine-grained sediment is transported in rivers in a continuous mode without significant deposition” (Ongley *et al.* (1992)).

Based on the discussion above, following substantial questions need clear answers:

1- How do cohesive sediments influence the erosion and deposition processes?
2- How do cohesive sediments influence the hydrodynamic process of water flow in rivers and channels?
3- How do cohesive sediments affect the bed morphological change during the flow in rivers?
4- How do different erosion formulae vary the erosion results in the numerical models?
5- What are the parameters that influence the erosion process for cohesive bed materials?

According to the works discussed previously, it is very important to understand what is the constituency and properties of the cohesive sediment in order to start working on a new generation of models that are capable of simulating water flow over mobile beds with cohesive sediment materials.

4.2 Cohesive Sediment

Cohesive sediments are fine sediment particles ($< 63\mu m$). Cohesive sediment transport is governed by hydrodynamic forces (e.g., drag force ,and lift force), biological forces (e.g. bacterial bonding and bacterial glue), and electrochemical force (e.g., van der Waals bonding, Coulombic repulsion, etc.) (Hayter and Mehta (1986)). The sediment make up bed material with the appearance of “mud”. Properties of the mud vary based on a variety of factors: first, sediment nature, which includes mineralogical composition of the mud, organic contents etc., second, on the water environment this including temperature, PH, ionic composition…etc. (Teisson (1991)). According to Teisson (1991), to characterize the overflowing fluid, seven parameters are required. While eighteen parameters are required to find the physio-chemical properties of mud. This large number of parameters demonstrates the complexity of studying cohesive sediments and as a result, poor understanding of such properties has made it difficult to handle within numerical models.

4.3 Cohesive Sediment Transport

Large efforts have been made and many studies undertaken which have had results presented to enable better understanding of the complex mechanism of cohesive sediment transport, erosion and deposition as reported by Mehta (1984). The cohesive sediment transported in suspension mode where the bed load transport is assumed to be zero. The long journey of the particles from the bed to the water column then to the bed again is complicated and takes place due to different phenomenon and mechanisms. These include erosion, suspension, flocculation, deposition, and self-consolidation.

Erosion is the process where the sediment particles are detached from the bed when the flow shear stress exceeds a critical shear stress of the bed. While suspension is the process that represents the sediment particles' transport status during their migration in the fluid column. During the suspension, the fine particles tend to flocculate. Flocculation is the process of formation and break up of flocs of cohesive sediments and is a key process in differentiating non-cohesive and cohesive sediments. Flocs could settle to the bed by the deposition process which is the process that occurs when the flocs' weight is higher than the outer forces and the flow shear stress is smaller than the critical shear stress for deposition. After the flocs rest on the bed consolidation occurs by the upper particles' weight. More details about flocculation processes and how it influences the settling velocity are introduced in Section (4.5.3.2).

Figure (4-1) presents the whole processes of cohesive sediment transport. This figure shows that in Zone 1, the particle exposed to the water flow with high shear stress τ that exceeds the critical shear stress for erosion τ_E is detached from the bed to suspend in the water column by the lifting forces. In this zone, the flocculation process forms different floc sizes. It is very important to notice that the erosion process is dominant in Zone 1 where ($\tau > \tau_E$) and no deposition occurs. In Zone 2, the flow shear stress τ is smaller than the critical shear stress for erosion τ_E. This means that the flow shear stress is unable to erode the cohesive particles which are still stuck to the bed. In other words, no erosion process occurs in this zone. At the same time, the flow shear stress τ is

larger than the shear stress for deposition τ_D and this prevents the sediment particles from being deposited on the bed. This means that there is no deposition process in Zone 2. According to above, the only processes that occur in Zone 2 are the flocculation process where different floc size are formed, and the suspension process that transport the flocs and the sediment particles. In Zone 3, the flow shear stress τ is lower than the critical shear stress of deposition τ_D where the flocs and sediment particles tend to settle towards the bed due to gravity. This process forms a new layer of the bed that is then consolidated with time. Consolidation is considered as self-weight consolidation that occurs by the deposited cohesive sediments under the effect of their own weight. The flocs settle on the bed forming an accumulated flocs layer then a new layer of flocs settle on top of the old one. The new layer squeezes the underneath layers to make the pore water driven out of the spaces between the lower flocs. The consolidation processes influence the vertical bed deformation (Amoudry and Souza (2011)). Consolidation does not occur for the zones where the erosion process is the dominant.

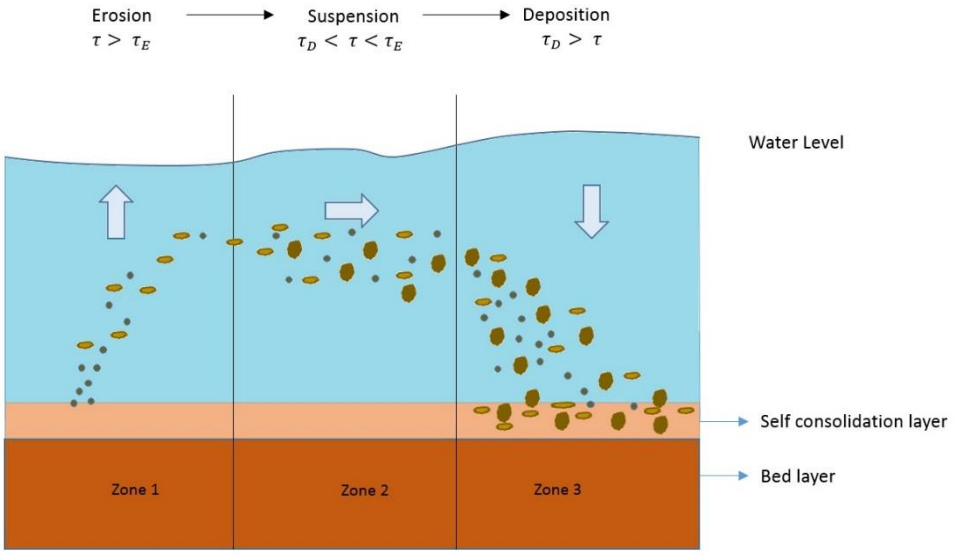

Figure 4-1: The Erosion-Suspention-Deposition processes

The numerical modelling of such processes in a cohesive bed is complicated and still in need of more simplification for application in numerical models. From

above, four different physical states of the cohesive sediments are shown to exist. They can be found as a mobile suspension, a stationary suspension, a partially consolidated bed and fully consolidated bed Hayter and Mehta (1986).

Generally, a specific cohesive formulation for erosion, settling, suspension and deposition are considered, while the flocculation process and consolidation are neglected (Amoudry and Souza (2011)). These processes have been implemented in the numerical models of the 1970's by Odd and Owen (1972).

4.4 Mechanism of Cohesive Sediment Erosion

The water flow in a channel or a river exerts a force on the bed sediment particles. This force can be calculated as the product of the flow shear stress τ and exposed surface area to this stress. This force is resisted by the submerged weight of the particle, grain particles frictional interlocking, and cohesion in cohesive soil. Black *et al.* (2002) explained the erosion process as "Erosion can thus be thought of as a see-saw type interplay between a hydrodynamic driving force, which usually is turbulent, and a resisting force, which dominantly is attributable to cohesion". In general, erosion occurs when the flow shear stress τ exceeds the critical shear stress for erosion τ_E. Subsequently, the erosion carries on at a rate, E, proportional to the shear stress with a constant rate with time or decreasing through time depending on the structure of the bed. Once sediment transport occurs, a series of erosion and deposition processes will deform the sediment bed. If the lift force, exceeds the grain particle weight, sediment particles may be entrained into suspension (Amoudry and Souza (2011)).

4.5 Construction of the One-Dimensional Hydro-Morphodynamic Model (HMD-C)

4.5.1 Governing Equations of the One-Dimensional Model

To represent the water flow over moveable beds with cohesive sediment, a range of techniques and governing equations have been employed by researchers. The most common technique is to employ the shallow water

theory for the such fluid flow purposes and build other models around this (Fagherazzi and Sun (2003); Cao *et al.* (2004); Simpson and Castelltort (2006)). The SWEs, that consist of the mass and momentum conservation equations for a water-sediment mixture, are presented as below:

$$\frac{\partial h}{\partial t} + \frac{\partial hu}{\partial x} = \frac{-\partial z}{\partial t} \tag{4.1}$$

$$\frac{\partial hu}{\partial t} + \frac{\partial}{\partial x}\left(hu^2 + \frac{1}{2}gh^2\right) = gh\left(S_{ox} - S_{fx}\right) + v_t\left(\frac{\partial^2 hu}{\partial x^2}\right) - \frac{(\rho_s - \rho_w)gh^2}{2\rho}\frac{\partial C}{\partial x} - \frac{(\rho_0 - \rho)(E-D)u}{\rho(1-P)} \tag{4.2}$$

The presented SWEs in this chapter are similar to those in Chapter 3, Equations (3.18) and (3.19), but the key difference is the additional source terms that are added to the conservative momentum Equation (4.2). The second order turbulent viscosity term that had used in Fiedler and Ramirez (2000), which represents the diffusive turbulent momentum transfer associated with Reynold stresses, $v_t\left(\frac{\partial^2 hu}{\partial x^2}\right)$, is added to the equation. The coefficient v_t is called the coefficient of turbulent viscosity or eddy coefficient. The dependence of coefficient v_t on the flow velocity or water depth are neglected in this research and utilised as a calibrated constant value (Fiedler and Ramirez (2000); Simpson and Castelltort (2006)). This term , turbulence viscosity term, is added to predicted the rapid formation of horizontal circulating flow (Guan (2014)) by the model.

The sediment transport model aims to predict the suspended sediment concentration, the erosion, and the deposition processes. The sediment model is represented using the non-capacity approach that has become attractive to researcher in recent years (Cao *et al.* (2004); Simpson and Castelltort (2006)). This approach treats the erosion and deposition of the sediment as independent empirical functions, which influence the sediment flux based on the mechanism of mass exchange between the fluid and the bed across the flow bottom boundary. The sediment transport model is represented using the advection diffusion model

$$\frac{\partial hC}{\partial t} + \frac{\partial huC}{\partial x} = \frac{1}{h}\frac{\partial}{\partial x}\left(hD_x\frac{\partial C}{\partial x}\right) + SE - SD \tag{4.3}$$

To represent the morphological change of the bed, the following equation is utilized:

$$\frac{\partial z}{\partial t} = \frac{SD-SE}{1-P} \tag{4.4}$$

The new compact form of the one-dimensional hydro-morphodynamic model of the previous equations is represented as below:

$$\frac{\partial \boldsymbol{U}}{\partial t} + \frac{\partial \boldsymbol{F}}{\partial x} = S \tag{4.5}$$

Where $\boldsymbol{U}$ is the vector that containing the conserved flow variables

$$\boldsymbol{U} = \begin{bmatrix} h \\ hu \\ hc \end{bmatrix} \tag{4.6}$$

$\boldsymbol{F}$ and $\boldsymbol{G}$ are the flux vectors in x and y directions, respectively.

$$\boldsymbol{F} = \begin{bmatrix} hu \\ hu^2 + 0.5gh^2 \\ huc \end{bmatrix} \tag{4.7}$$

Where $\boldsymbol{S}$ is the source term vector

$$\boldsymbol{S} = \begin{bmatrix} \frac{SE-SD}{1-P} \\ gh(S_{ox} - S_{fx}) - v_t\left(\frac{\partial^2 hu}{\partial x^2}\right) - \frac{(\rho_s-\rho_w)gh^2}{2\rho}\frac{\partial C}{\partial x} - \frac{(\rho_0-\rho)(SE-SD)u}{\rho(1-P)} \\ \frac{1}{h}\frac{\partial}{\partial x}\left(hD_x\frac{\partial C}{\partial x}\right) + SE - SD \end{bmatrix} \tag{4.8}$$

4.5.2 Erosion Rate

The erosion phenomena mechanics of cohesive soil such as mud has been presented by Mehta (1989). The erosion process in cohesive soil starts when the bond forces between the particles are broken. These forces are influenced by a number of biological and chemical factors. The erosion occurs when the flow shear stress of water flowing over the soil surface exceeds the critical shear stress for erosion. The bottom shear stress controls and causes the erosion while sediment bed characteristics dominate the erosion resistance (Amoudry and Souza (2011)).

The erosion rate could be represented by the equation presented in Ariathurai and Arulanandan (1978) using Partheniades' formula (Partheniades (1965)):

$$SE = E\left(\frac{\tau}{\tau_E} - 1\right) for\ \ \tau \geq \tau_E \tag{4.9}$$

$$SE = 0\ for\ \ \tau < \tau_E \tag{4.10}$$

Where the coefficient E is the erodibility of the bed or erosion rate in some literature, τ is the flow shear stress, τ_E is the critical shear stress for erosion.

Li and Amos (2001) discussed how the prediction basis for the critical shear stress of the cohesive sediment is unknown. For that reason, more measurements must be executed for different mud types and for specific sites. The value of the critical shear stress for erosion depends on the degree of consolidation, mineralogy and any benthic biological activities. However, despite this measure being a source of error during modelling, the researchers still prefer to get the value from the previous literature or by using a calibrated value in cohesive sediment transport modelling (Bailey and Hamilton (1997); Altunkaynak and Wang (2010)).

The flow shear stress is an important parameter in the study of dynamics of sediments in the water stream. It is assumed to be proportional to the square of the horizontal velocity based on the equations of Lopes *et al.* (2006) that are employed in the model to calculate the bottom shear stress (flow shear stress) as below :

$$\tau_x = \rho g \frac{u\,(u^2+v^2)^{\frac{1}{2}}}{{C_z}^2}$$

$$\tau_y = \rho g \frac{v\,(u^2+v^2)^{\frac{1}{2}}}{{C_z}^2}$$

Where τ_x and τ_y are the bottom shear stress in the x and y direction, C_z is the Chezy coefficient:

$$C_z = \frac{\sqrt[6]{h}}{n}$$

Where n is the Manning roughness coefficient.

Another formulation that could be used is the following proposed by Parchure and Mehta (1985) based on the principle of floc erosion rate.

$$SE = E_f \exp(a(\tau - \tau_E)^b) \quad (4.11)$$

E_f , is the floc erosion rate.

Despite the wide use of formulae for calculating the erosion rate, SE, none take into account all the physical process of the erosion. They have been employed to predict the erosion of individual particle or flocs. However, those formulae ignore the mass erosion that is represented by the local failure of the bed from lumps of eroded sediment (Winterwerp and Van Kesteren (2004)).

4.5.2.1 Erosion Coefficient E (Erodibility)

This parameter has very significant influence on the erosion rate of cohesive sediment transport model, as discussed later. This parameter depends on the physio-chemical properties of the bottom sediment layer (Liu *et al.* (2002)). Some authors argue that it also depends on the salinity (Hayter and Mehta (1986)). However, no formulations that relate the erodibility in this case with salinity parameters have been introduced yet. Zhu (2006) during his experimental work, introduced a new formula to calculate the erodibility based on the available soil properties as below:

$$E = \frac{K[(s-1)gD_{50}]^{0.5}}{c(s-1)^{3.0}} \quad (4.12)$$

Where K is a non-dimensional coefficient with a value of $K = 0.642$. s is the soil relative density that calculated by $s = {\rho_s}/{\rho_w}$. D_{50} is the median particle diameter in m and c is the cohesion of the soil in N/m^2. However, the author argued that there are more soil erodibility-influential factors that influence the erosion which should be studied later. Figure (4-2) shows a graphical representation of the equation that was presented by Zhu (2006).

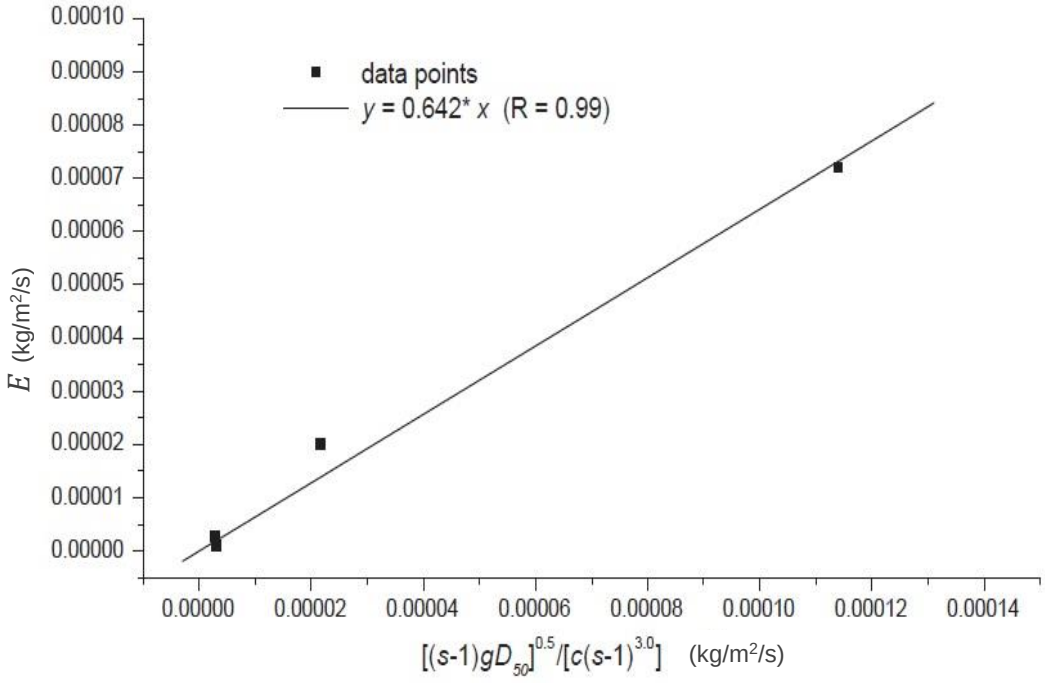

Figure 4-2: The calibrated E and equation (Zhu (2006))

Many researchers have suggested calibrated values for E (Chapalain *et al.* (1994); Amos *et al.* (1992); Parchure and Mehta (1985)). The magnitude of E varies from 0.0005 (Kg/m^{2}s) to 0.005 (Kg/m^{2}s) based on Altunkaynak and Wang (2010). While it is often taken as 5×10^{-5} (Kg/m^{2}s) based on Mulder and Udink (1991). For different situations e.g. most lagoon and estuaries, the typical values of E is 2×10^{-5} (Kg/m^{2}s) (Lopes *et al.* (2006); Dyer (1986)) which is used in the present model.

Table (4-1) shows some different values of the erodibility that was presented by Parchure and Mehta (1985).

Table 4-1: Erodibility Values by (Zhu (2006); Parchure and Mehta (1985))

Researcher	Material	E(Kg/m^2/s)
Parchure and Mehta (1985)	Kaolinite in tap water	8.3×10^{-7}
	Kaolinite in salt water	2.3×10^{-6}
	Lake mud in salt water	5.3×10^{-6}
	Bay mud (Partheniades (1965))	6.7×10^{-8}
	Lake mud (Lee (1979))	7.0×10^{-7}
	Estuarial mud (Thorn and Parsons (1977))	7.0×10^{-7}
	Estuarial mud (Thorn and Parsons (1979)	3.1×10^{-4}
	Kaolinite(Dixit (1982))	1.0×10^{-4}

4.5.2.2 Critical Shear Stress of Erosion

The critical shear stress represents the minimum value of the flow shear stress at which the entrainment occurs, in other words, the erosion occurs when the water flow shear stress exceeds the critical shear stress of erosion. It is a function of the degree of bed compaction measured by the dry density of the bottom layer (Liu *et al.* (2002)). A simple formula was presented by Delo (1988) to calculate the critical shear stress of erosion for cohesive bed.

$$\tau_E = A_1(\rho_d)^{E_1}$$

Where, ρ_d is the dry density of the bed sediments, A_1 and E_1 are the coefficients that depend on the mud type .

Figure (4-3) shows a relationship between the critical shear stress of erosion and the sediment dry density as determined by Liu *et al.* (2002).

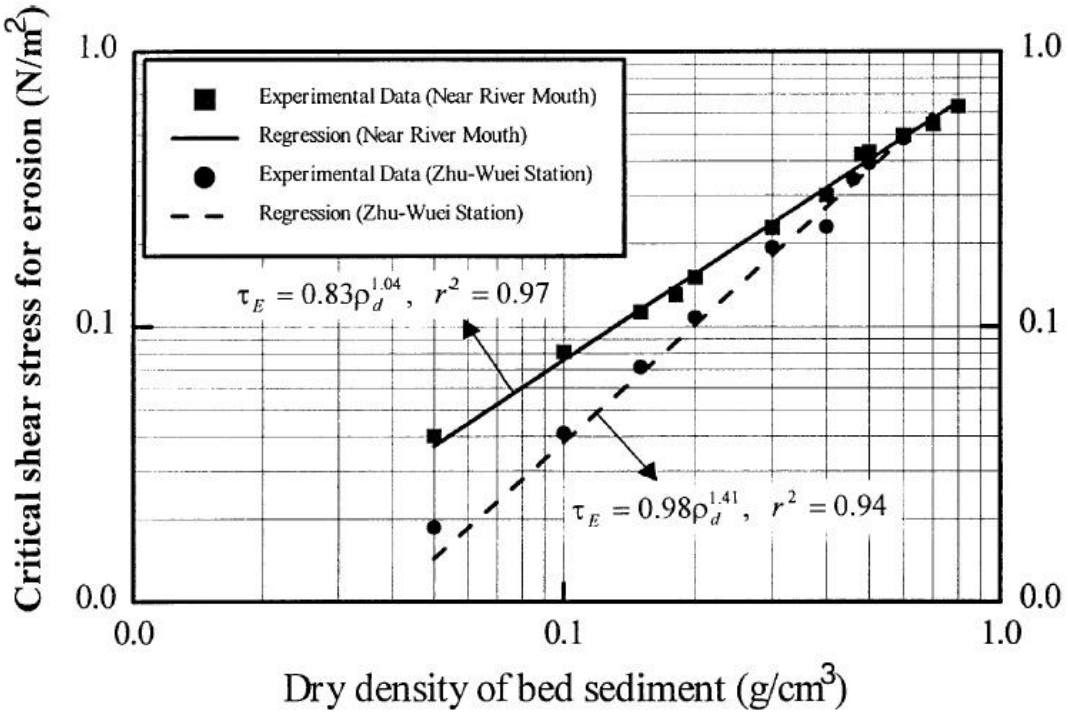

Figure 4-3: Relationship between critical shear stress for erosion and sediment dry density (Liu *et al.* (2002))

This figure is plotted, based on experiments conducted on samples of bed sediments that were collected from the site of the Tanshui estuary, to show the relationship between the critical shear stress and the dry density. From this experiment data near the river mouth and the Zhu-Wuei station, Liu *et al.* (2002) derived two formulae by linear regression to calculate the critical shear stress of erosion. The formulae are $\tau_E = 0.83{\rho_d}^{1.04}$ and $\tau_E = 0.98{\rho_d}^{1.14}$.

The increase of the bed sediment consolidation, and the physio-chemical effects produce a rise in the critical shear stress of erosion (Winterwerp and Van Kesteren (2004)) and decrease the bed porosity (Amoudry and Souza (2011)). Successively, they limit the extent of erosion. This is an essential difference between the cohesive sediment bed and the non-cohesive sediment bed.

4.5.3 Deposition Rate

The deposition process occurs when the sediment particles reach the channel bed and settle there. It was stated by Winterwerp and Van Kesteren (2004) that

erosion and deposition interact in three different regimes: the erosional state, in which the erosion is the only process that occurs when the flow shear stress τ is larger than the critical shear stress of erosion τ_E; the equilibrium state in which neither deposition nor erosion occurs, $(\tau_D < \tau < \tau_E)$, and the depositional state in which only deposition exists and where the critical shear stress of the deposition is larger than the flow shear stress.

The following formula, used to calculate deposition, was suggested by Krone (1962), then adopted and modified by Odd and Owen (1972)

$$SD = W_s\, C_b\, P_d \tag{4.13}$$

Where, W_s is the settling velocity of the sediment particles, C_b is the sediment concentration at bottom layer, this bottom layer concentration is close to the depth averaged concentration C (Lopes *et al.* (2006)), and P_d is the probability of deposition which varies from 0 to 1. The probability of deposition is calculated by

$$P_d = 1 - \left(\frac{\tau}{\tau_D}\right) for\ \ \tau \leq \tau_D \tag{4.14}$$

$$P_d = 0\ for\ \ \tau > \tau_D \tag{4.15}$$

τ_D , is the critical shear stress of the deposition which is measured by N/m^2

4.5.3.1 Critical Shear Stress of Deposition

The critical shear stress of deposition τ_D represent the maximum value of the flow shear stress at which the deposition occurs. More specifically, it is the particle threshold to deposit on the bed (Lopes *et al.* (2001)).

The deposition occurs when the flow shear stress is less than the critical shear stress for deposition $\tau < \tau_D$. It depends on the flocs size. It is difficult to find the in situ values for the critical shear stress for deposition due to the difficulties of taking the measurements close to the bed. This parameter is obtained by the process of calibration and validation to find the best fitted value within the simulation (Lopes *et al.* (2001); Clarke and Elliott (1998)).

Previous work assumed that a constant value or τ_D was considered a reasonable approximation (Cancino and Neves (1999a); Cancino and Neves

(1999b)). For most lagoons and estuaries, the typical value of τ_D is 0.1N/m^2 (Lopes *et al.* (2006); Dyer (1986)).

4.5.3.2 Settling Velocity

In non-cohesive sediments the particles are settling individually rather than in flocs which is the case of the cohesive sediments. Figure (4-4) presents a simple idea about the structure of the flocs and the bond forces that bond the fine cohesive particles.

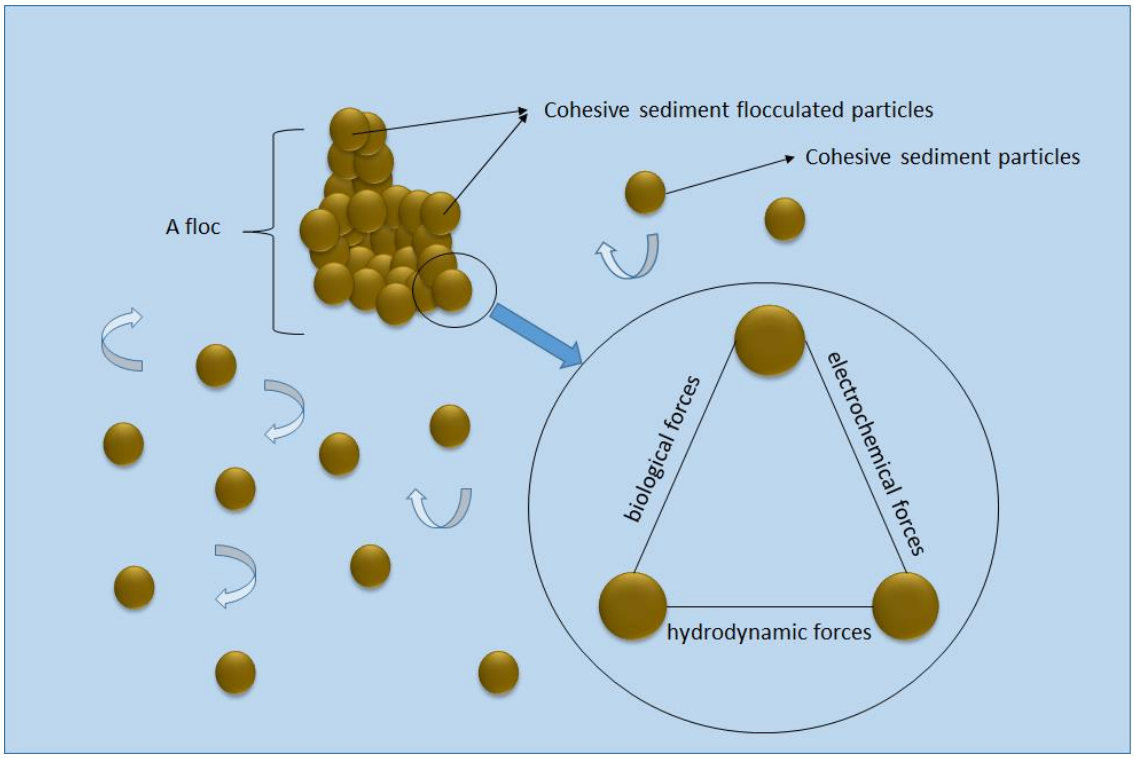

Figure 4-4: A floc and bonding forces between cohesive sediment particles in a water flow

The floc is a group of fine sediment particles that are linked together by biological, hydrodynamic, and electrochemical forces. It is formed by a process called flocculation, which is the forming and breaking up processes that occurs on a group of cohesive sediment particles. The flocculation process characterises cohesive sediments and depends on different factors that are the physio-chemical properties of the sediment and the water, and some physical process such as the turbulence (Winterwerp (1998)). From above, flocculation produces different floc sizes which have an influence on the settling velocity, The settling velocity W_s, is an important parameter that influences the

entrainment of the sediments. It depends on the gravitational force and the vertical shear due to settling movement (Liu *et al.* (2002)) and the flocculation effects (Winterwerp (1998)). The gravitational forces depends on the individual particle's density that forms the flocs, and on the porosity of the flocs that are occupied by water.

The settling velocity is affected by the concentration of the sediments C. In other words, the particles settled as flocs and the settling velocity is calculated based on equation (4.16) when $C<C_{HS}$. While the hindered affect is regarded the concentration C is exceed C_{HS} which is 20kg/m^3 and the settling velocity is calculated based on the equation (4.17) (Nicholson and O'Connor (1986)).

$$W_s = K_1 C^m \; for \; C < C_{HS} \tag{4.16}$$

$$W_s = K_1[1.0 - K_2(C - C_{HS})]^{m_1} \quad for \; C > C_{HS} \tag{4.17}$$

Where k_1 (m^4/kg s) and k_2 (m^3/kg) are constants that depend on the mineralogy of the sediments, and the exponent m and m_1 depend on particle size and shape (Franz *et al.* (2014)). Mehta (1986) suggested a range of m values from 1 to 2. Nicholson and O'Connor (1986) suggested the values of K_1 =0.006, K_2=0.01, m =1 and m_1=5. Another value for $m_1$is suggested for fine particles, that is 4.65, by Dyer (1986).

Figure (4-5), was presented by Teisson (1991) to demonstrate the relationship between the settling velocity and the particle diameter for both isolated and flocculated particles. It shows that the particle diameters less than 64 μm have a range of settling velocity for different particles forms. In the case of single or isolated particles, it was found that the relationship is linearly increasing. While for the flocculated particles, it is clear that the settling velocity varies from 0.3 mm/s for the particles around 1 μm and increases nonlinearly to reach around 5 mm/s for particles sizes 64 μm. Figure (4-5) gives a clear picture of the settling velocity- particle diameter relationship for cohesive sediment but it does not take into account the influence of the floc size on the settling velocity.

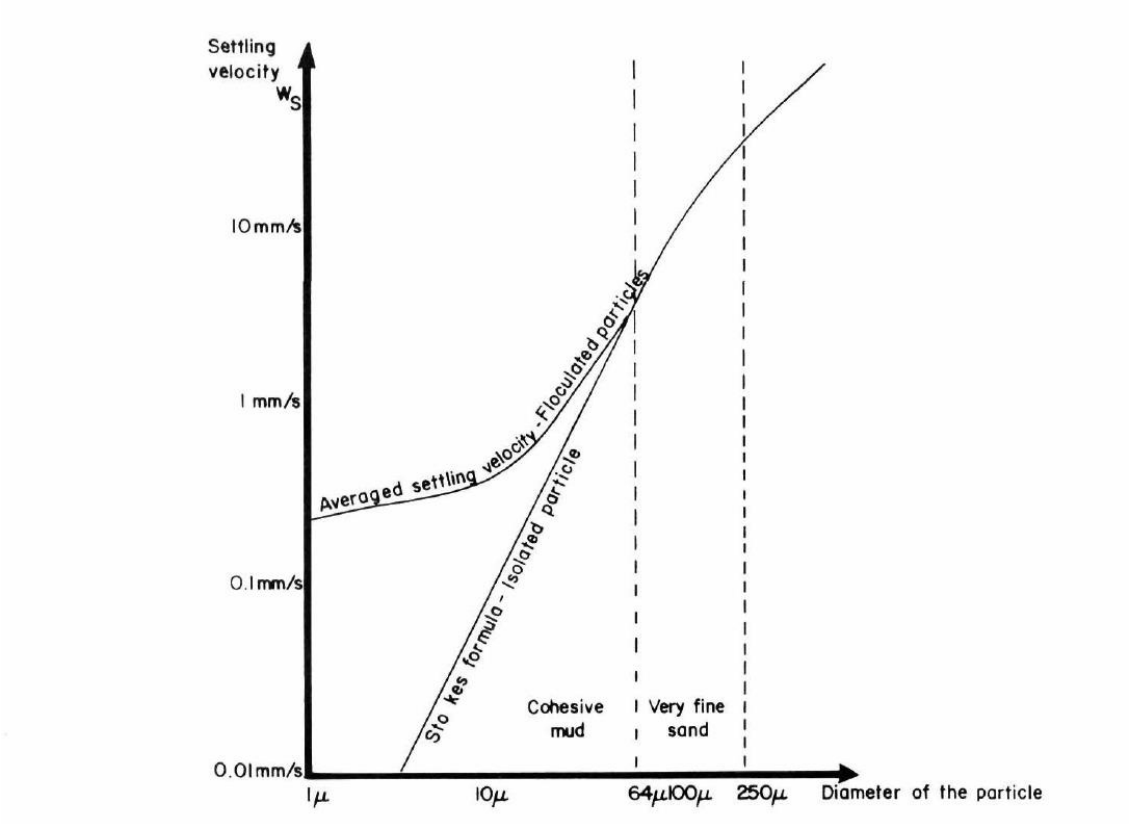

Figure 4-5: Settling velocities of isolated or flocculated particles (Teisson (1991))

4.5.4 Numerical solution

The compact form of the equations system is represented in Equation (4.18)

$$\frac{\partial \boldsymbol{U}}{\partial t} + \frac{\partial \boldsymbol{F}}{\partial x} = S \tag{4.18}$$

Where $\boldsymbol{U}$, $\boldsymbol{F}$, and $\boldsymbol{S}$ are presented in Section (4.5.1).

The equation can be discretised using finite volume method at rectangular mesh, and is presented in a new form as demonstrated by Equation (4.19) below:

$$\boldsymbol{U}_i^{t+1} = \boldsymbol{U}_i^t - \frac{\Delta t}{\Delta x}\left(\boldsymbol{F}_{i+\frac{1}{2}} - \boldsymbol{F}_{i-\frac{1}{2}}\right) + \Delta t \boldsymbol{S}^t \tag{4.19}$$

Where $\boldsymbol{F}_{i\mp\frac{1}{2},}$ is the numerical flux value at the cell interfaces in x direction.

Figure (4-6) shows thee neighbour cells in the finite volume method in one dimension.

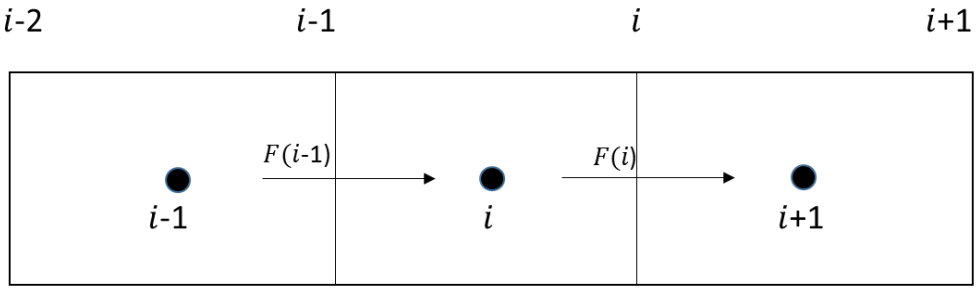

Figure 4-6: One-dimensional finite volume mesh

In the finite volume method, the fluxes are calculated at the cell interfaces. This is a kind of Riemann problem allowing for discontinuity at the interfaces. To overcome this problem, a wide range of numerical schemes including both exact Riemann solvers and approximate Riemann solvers, have been introduced (Toro (2001)). In this research, a first order accuracy Godunov type approximate Riemann solver, HLL (Harten-Lax-van Leer), is utilized to solve the system in Equation (4.19).

The HLL numerical flux, in Equation (4.20) is derived by applying the integral form of the conservation lows in appropriate control volume, is calculated as below:

$$F_{i+\frac{1}{2}} = \begin{cases} F_l & if\ S_l \geq 0 \\ F_R & if\ S_R \leq 0 \\ F^{hll} & S_L \leq 0 \leq S_R \end{cases} \tag{4.20}$$

$$F^{hll} = \frac{S_R F_L - S_L F_R + S_R S_L (U_R - U_L)}{S_R - S_L} \tag{4.21}$$

Where F_l and F_{R} are the conservative variable vectors at the left and right sides of each cell interface. F^{hll} is calculated as in Equation (4.21) . S_L, and S_R are the wave speeds. The above parameters are calculated as below:

$$S_l = \begin{cases} \min\left(u_i - \sqrt{gh_i}, u^* - \sqrt{gh^*}\right) & if\ \ h_i > 0 \\ u_{i+1} - 2\sqrt{gh_{i+1}} & if\ h_i = 0 \end{cases} \tag{4.22}$$

$$S_R = \begin{cases} \min\left(u_{i+1} + \sqrt{gh_i}, u^* - \sqrt{gh^*}\right) & if\ \ h_i > 0 \\ u_{i+1} + 2\sqrt{gh_{i+1}} & if\ h_i = 0 \end{cases} \tag{4.23}$$

Where

$$u^* = \frac{1}{2}(u_i + u_{i+1}) + \sqrt{gh_i} - \sqrt{gh_{i+1}}; \quad (4.24)$$

$$\sqrt{gh^*} = \frac{1}{2}\left(\sqrt{gh^*} + \sqrt{gh^*}\right) + \frac{1}{4}(u_i - u_{i+1}) \quad (4.25)$$

In this work the C++ programing language was used to implement the model. Figure (4-7) demonstrates the computational procedure that is utilized at each time step for the this model implementation which include:

1) Input of the initial conditions that include the calibrated critical shear stress of erosion, critical shear stress of deposition, hydraulic and sediment information, including water depth, bed elevation, flow velocity, sediment concentration.
2) Calculation of the settling velocity and the flow shear stress for the present time step from the information in Step 1.
3) Comparison of the flow shear stress with the critical shear stress for erosion and the critical shear stress for deposition. If the flow shear stress:
   i. $\tau > \tau_E$ then calculate the erosion SE.
   ii. $\tau < \tau_D$ then calculate the deposition SD.
   iii. $\tau_D < \tau < \tau_E$ then no sediment transport.
4) Taking a step in time with the solution of the governing equations system, based on the information from previous steps and update of the values of the hydraulic and sediment which include water depth, bed elevation, flow velocity, sediment concertation.
5) If time of simulation $t < \mathrm{Tmax}$, return to Step 2 and repeat Step 2 to 4.
6) If time of simulation $t \geq \mathrm{Tmax}$ then stop.

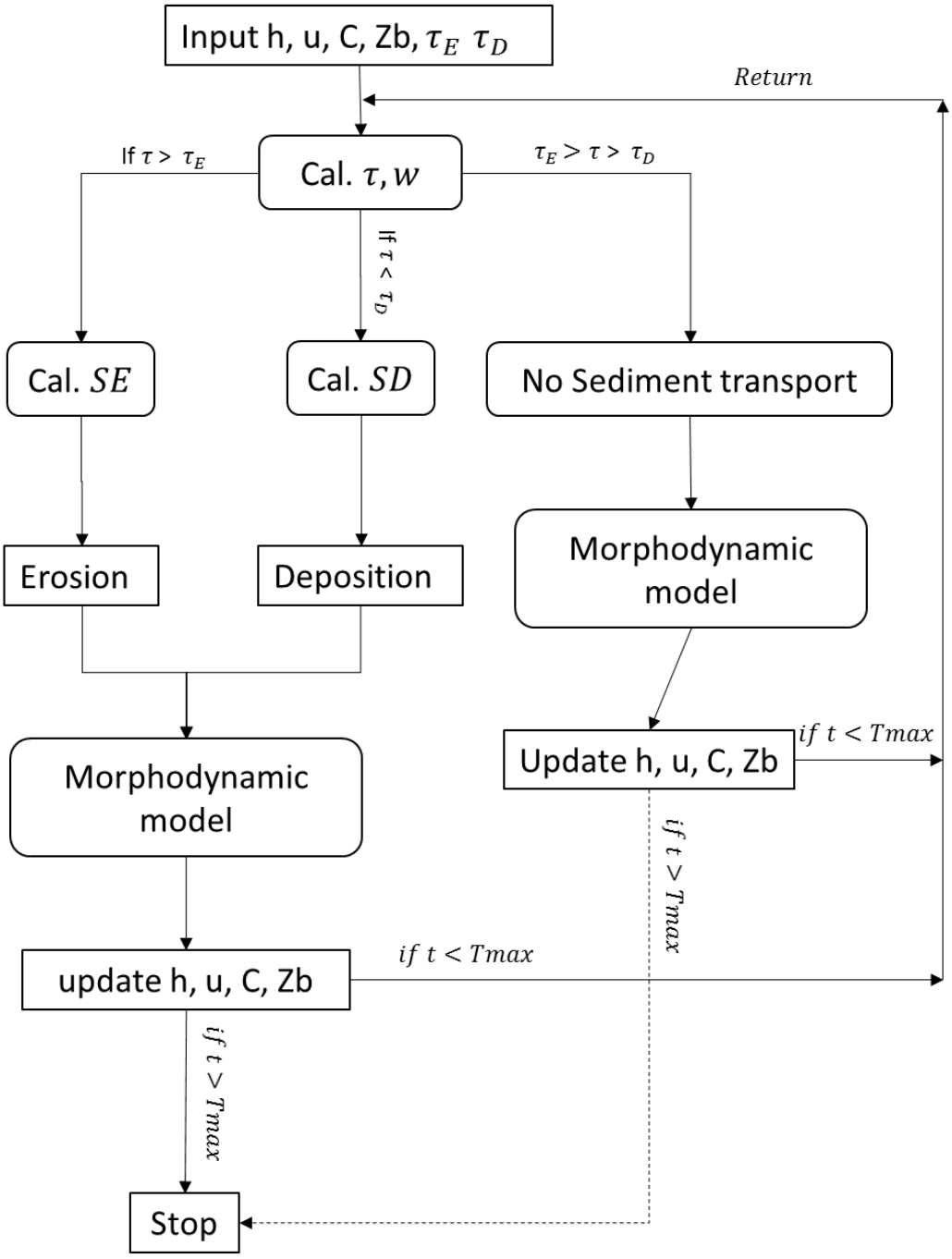

Figure 4-7: The Framework of the computational processing

4.6 Comparison between the model with cohesive sediment and the model with non-cohesive sediment

In this section, the constructed one-dimensional model with cohesive sediment transport is tested against a numerical model with non-cohesive sediment transport model as a benchmark test. The numerical model presented in Chapter 3 is employed as a bench mark model. The objective of this test is to obtain a first impression about the how reasonable the model behaviour is compared to the previous model when the different (i.e. cohesive) bed material is employed.

To perform the test, the numerical results are also compared to the experimental dam break case that had been performed in Taipei University (Capart and Young (1998)).

In the numerical model with the cohesive sediment transport, a rectangular mesh with a grid size of 0.005m is employed. The chosen cell size formed 500 cells that represent the whole channel length. A tolerance of water depth of 0.0005m is utilized to handle the wet-dry bed problems. The value of 0.025 is used to represent the Manning roughness of the bed. The sediment porosity is given as 0.28. The calibrated bed erodibility value is taken as 0.0002 (Kg/m^2s).The simulation was performed for 0.505 s.

Figures (4-8), (4-9), and (4-10) show the comparison between the water level and bed level between the two numerical models at time 0.303 sec, 0.404 sec, and 0.505 sec respectively. It can be seen that the erosion process for the model with cohesive bed is slower and progressed slowly. The reason for that is, for the cohesive bed, the sediment particles are attached together by different biological and electrochemical forces that prevented the individual particle from being detached far from bed in case of low flow shear stresses. As a result, the hydraulic jump formed is small and advanced to the upstream direction with a slower progress than the non-cohesive. While the wave front of the water flow advanced smoothly with high velocity to the downstream direction with lower water level compared to the other model. Whereas the result of the numerical model with non-cohesive sediment transport model

shows high erosion process of the bed at the dam break location. The erosion process scours a hole which is progressively increased in depth and width with time evolution. This fast process forms a hydraulic jump which moves to the upstream progressively. As a result, the water level after the hydraulic jump is higher than the case of the model with cohesive sediment, with a slower time arrival of the wave front .

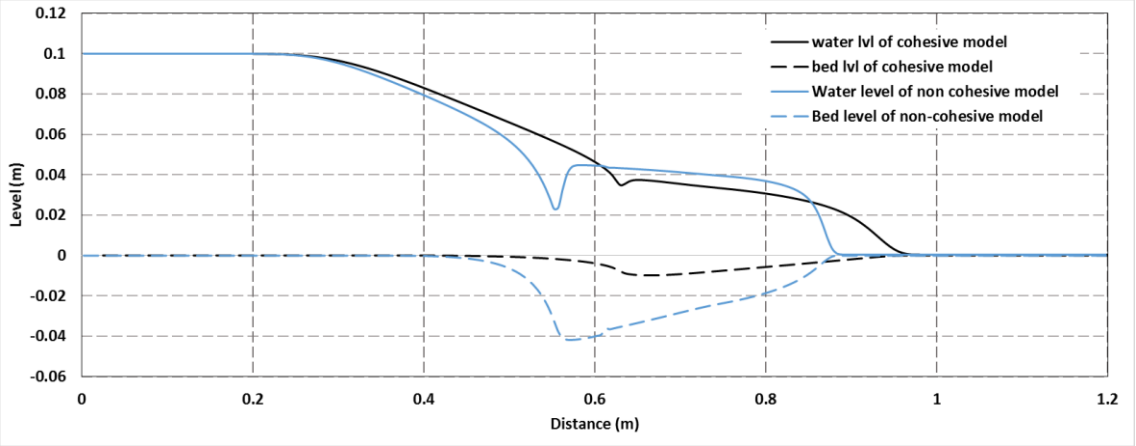

Figure 4-8: Comparison Between Cohesive and Non-cohesive Dam-Break for work at 0.303s

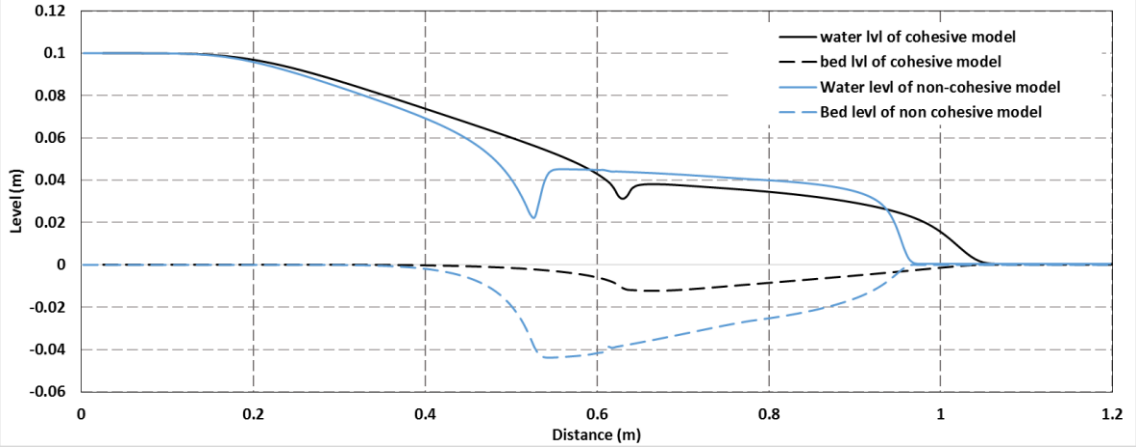

Figure 4-9: Comparison Between Cohesive and Non-cohesive Dam-Break for work at 0.404s

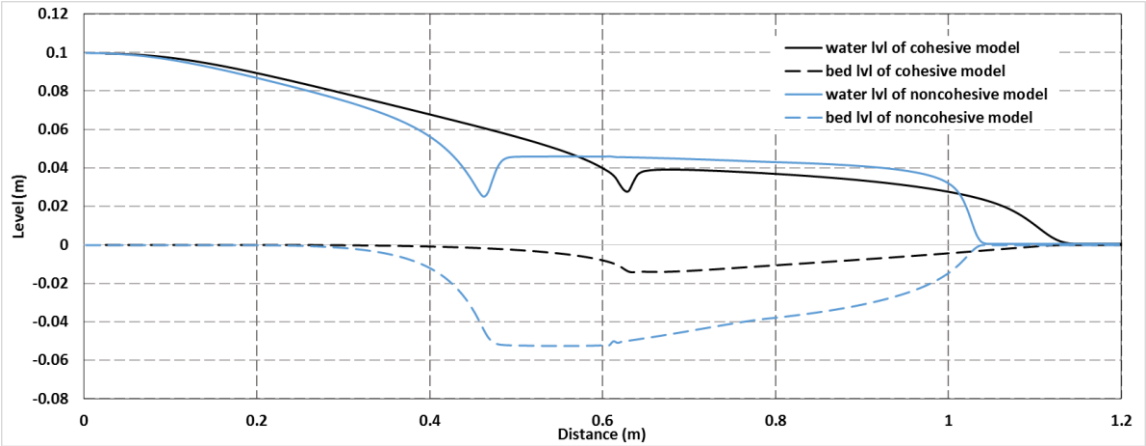

Figure 4-10: Comparison Between Cohesive and Non-cohesive Dam-Break for work at 0.505s

From comparison in the figures and the explanation above, the behaviour of the new-cohesive sediment numerical model is consistent with this physical situation. Additional more complex tests are describes in the next section to help validate and give confidence in this cohesive model.

4.7 Validation of The Hydro-Morphodynamic Model with Cohesive Sediment Transport Model.

It is very important to test the model capability to simulate real water flow cases on a movable cohesive bed. The presented model is tested against laboratory experiments that was carried out at the fluid Mechanics Laboratory of Delft University of Technology 2005 by Zhu (2006). In these experiments, two flumes were built to test dike erosion. One of the flume is used as a storage basin while the second one is the testing flume where the dike is constructed inside. The testing flume set up is 35.5m length, 0.8m width and 0.85m depth. The tests focused on the first three stages of the experiment, in which the breach develops mainly vertically with only very little widening. At the middle of the flume, a wooden wall was placed to narrow the dike's length section to be 40cm instead of 0.8cm. Another wooden wall was placed vertically next to the first one to prevent the water flow from the upstream to the downstream from that side as shown in Figure (4-11).

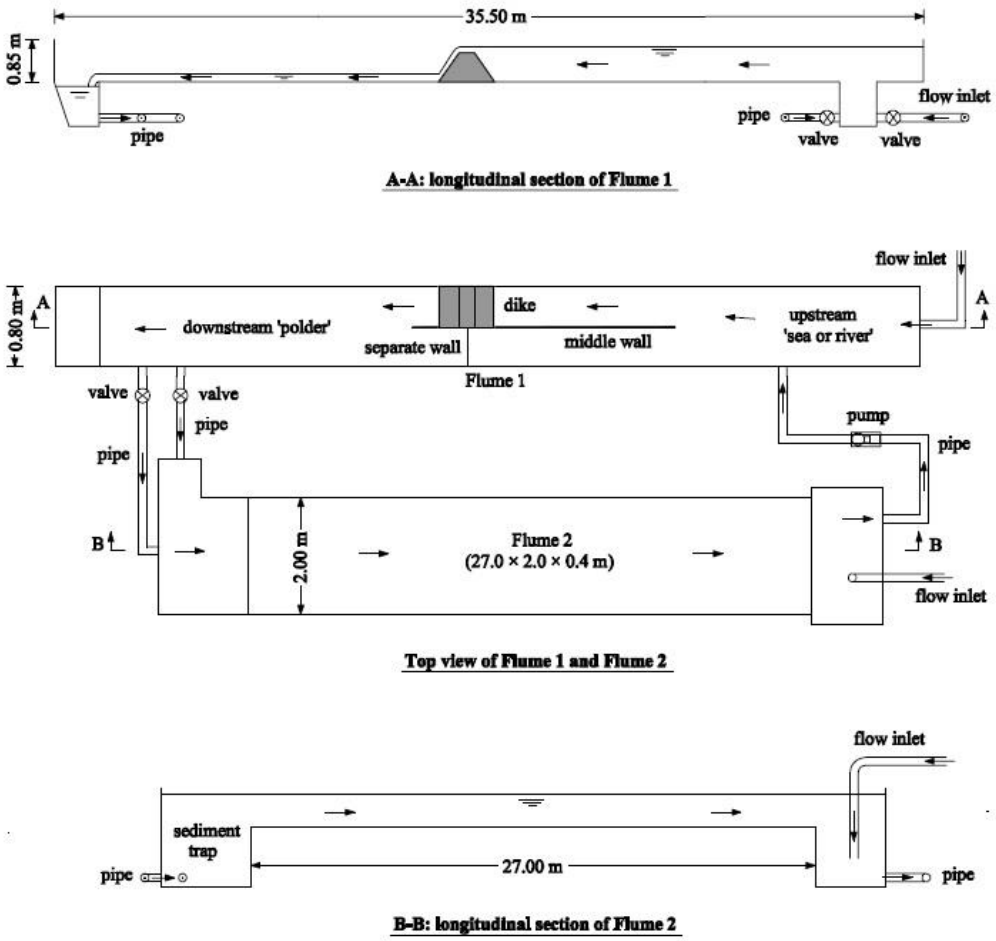

Figure 4-11: A simple sketch for the experimental setup (Zhu (2006))

In this research, the numerical model is tested against one experiment, Test 2, that have been carried out by Zhu (2006). The dike dimensions and of DUT laboratory series of experiments is shown in the following table.

Table 4-2: Dike Dimensions

Dike Dimensions	Value
Dike height	0.75 m
Dike crest length	0.4 m
Dike crest length width	0.6 m
Dike upstream slope	1:2:0
Dike downstream slope	1:2:0

The dike is constructed using sand-silt-clay mixtures. In Test T2, the clay was prepared artificially by using different soil products and mix them together. the properties of the soil that was employed in the experiment is shown as in the table below:

Table 4-3: Experiment parameters value

Item		Value
Dike materials' properties	n	0.025
	τ_E(N/m^2)	5
	τ_D(N/m^2)	Unknown
	E(Kgm-^{2}s^{-1})	2.7 x 10^{-6}
	ρ_0(Kg/m^3)	1936
	Void ratio	0.61
Dike foundation's properties.	Non-erodible foundation	

The porosity of the soil is calculated based on the void ratio by employing the formula $p = \frac{void\ ratio}{1+void\ ratio}$. In this experiment the porosity $P = 0.38$. The soil layers were compacted by using a hand-operated compaction roller. The water inflow discharge that supplied the dike on the upstream side was varied by controlling upstream water level. This was adjusted to supply a stable 0.83m water level during the experiment duration (Zhu (2016)).

For the numerical simulation, the validation was performed for 8400s. The channel length was simplified to be 5.5m long. A uniform mesh is employed with a grid size of 0.05m to form 112 cells to represent the specific domain. A small water depth equal to 0.0005m is utilized to handle the wet/dry problem of the bed. Figures (4-12), (4-13), (4-14), and (4-15) show comparisons between the experiment measurements and the numerical simulation the vertical dam breaching after 1200s, 3600s, 6000s, and 8400s, respectively.

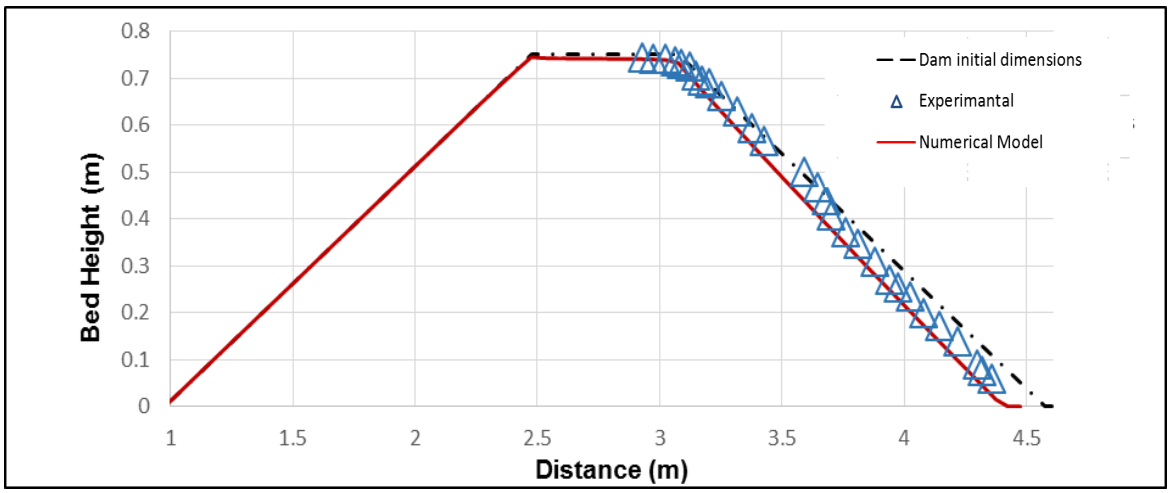

Figure 4-12: Dam erosion at time 1200s

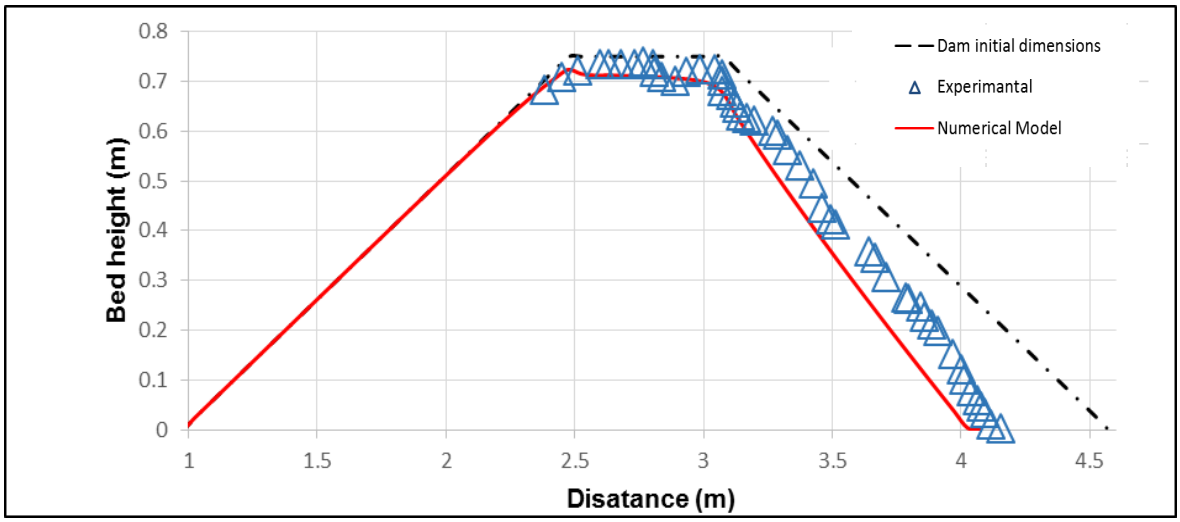

Figure 4-13: Dam erosion at time 3600s

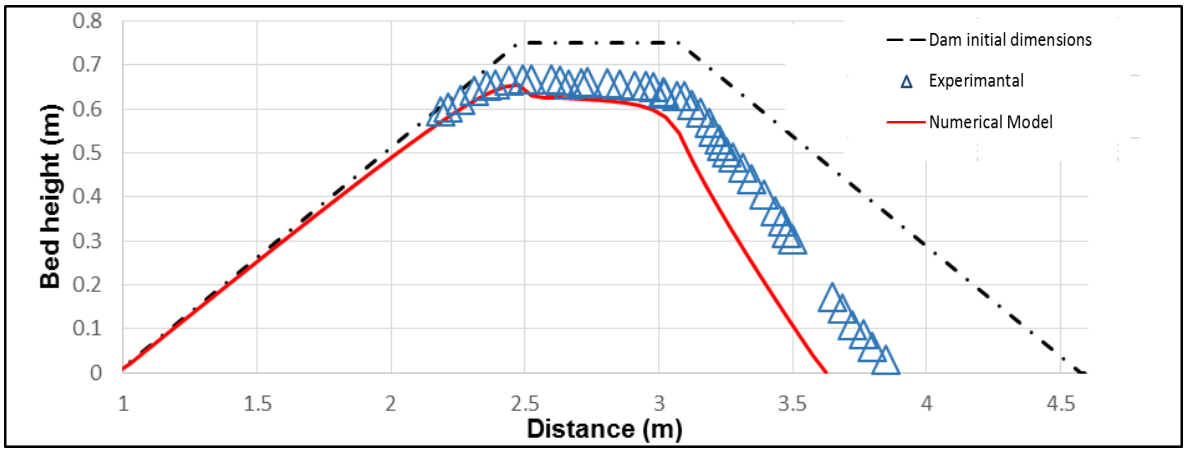

Figure 4-14: Dam erosion at time 6000s

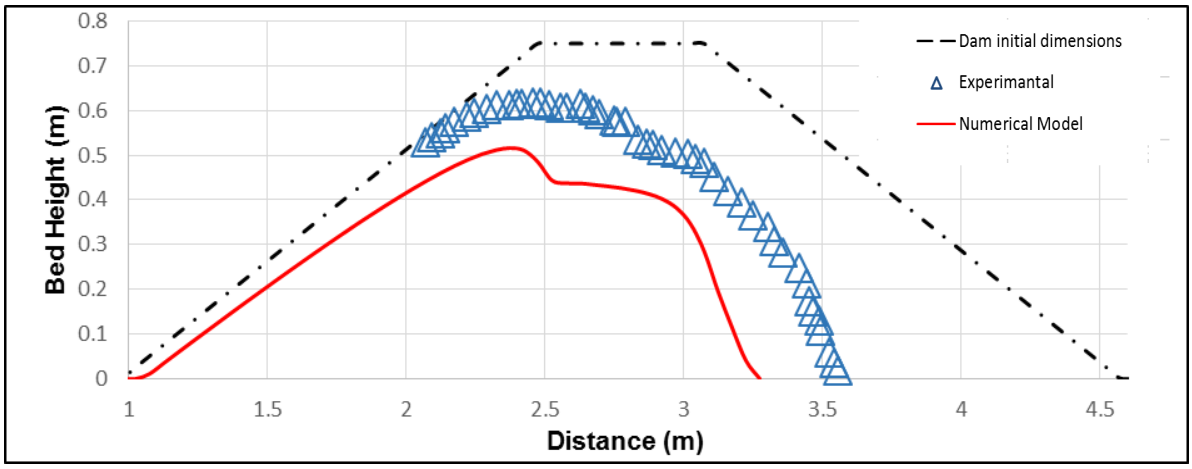

Figure 4-15: Dam erosion at time 8400s

It can be seen that the bed change for the simulation has the same tendency as that for the bed change for the experiment. The numerical model seems to predict the erosion process faster than the experimental case. This difference is anticipated and related to: first, the simplicity of the presented numerical model; second, the recorded data of the experiment where it is difficult to control the water level at the inflow water discharge to get a stable water level at the upstream of the dam. To get better understanding of the parameters that influence the numerical model, it is necessary to undertake additional simulation on such parameters as shown in the next sections.

Generally, the bed change in the figures above, shows a good agreement between the numerical results and the experiment results. It shows that the model is capable of simulating dam breaching cases and capable of predicting the erosion process effectively.

4.8 Comparison of Different Entrainment Flux Formulae

Work has been done specifically by a variety of scientist and engineers to understand the erosion mechanism of the cohesive bed. Four formulae have been presented by different researchers (Partheniades (1965); Parchure and Mehta (1985); Ockenden *et al.* (1989); Izumi and Parker (2000)) to study the erosion process in cohesive sediment particles. Table (4-4) shows the four formulae and the parameters that each formula is depend on.

Table 4-4: Erosion Formulae

Author	formulae	parameters
Parchure and Mehta (1985)	$SE = E.e^{\propto\sqrt{\tau-\tau_E}}$	$E, \propto, \tau_E$
Ockenden et al. (1989)	$SE = E(\tau - \tau_E)$	E, τ_E
Izumi and Parker (2000)	$SE = E(\frac{\sqrt{u^2+v^2}}{u_c} - 1)^\gamma$	E, γ
Partheniades (1965)	$SE = E\,(\frac{\tau}{\tau_E} - 1)$	E, τ_E

Note: SE erosion rate

τ = shear flow stress (N/m^2)

τ_E=critical shear stress for erosion (N/m^2)

E= erodibility (Kg/m^{2}s)

$\propto$= erosion coefficient (m/N$^{0.5}$)

γ= an exponent

It is very important to investigate the performance of these formulae to get better understanding about how these formulae influence the sediment transport model and the simulation accuracy within a full channel model. In this section the four different formulae are included separately in the sediment transport channel flow model and the morphological model to simulate the water flow over cohesive movable bed. The results of the simulations are compared against each other and against an experimental study. The experimental work that was carried out in Delft University of Technology 2005 by Zhu (2006) is employed.

For the numerical simulation, the flume was simplified to be 5.5m long. The rectangular mesh with a size of dx=0.05m that generated 112 cells for the simplified domain is used. The Manning roughness was taken as 0.025 following. The critical shear stress for erosion τ_E is 5 N/m^2. The bed density is 1936 kg/m^3 with porosity equal to 0.38. the erodibility of the bed is employed as 27x10^{-6} kg/m^2/s. All these parameters were selected following Zhu (2006). The simulations were run for 8400 seconds. The Figures (4-16), (4-17), (4-18), and (4-19) show the comparison of the bed change evolution for each formula with time after 1200s, 3600s, 6000s, and 8400s, respectively.

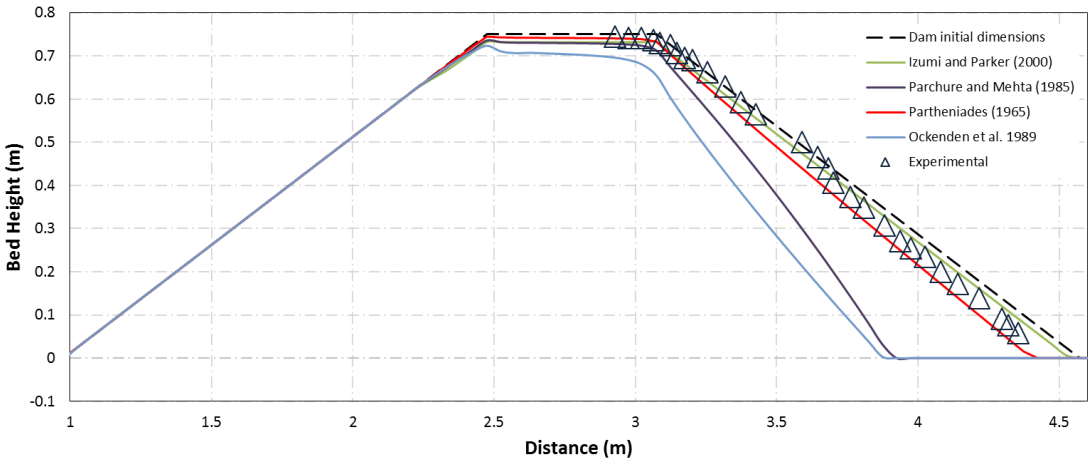

Figure 4-16 : Erosion evolution by different entrainment formulae at t=1200s

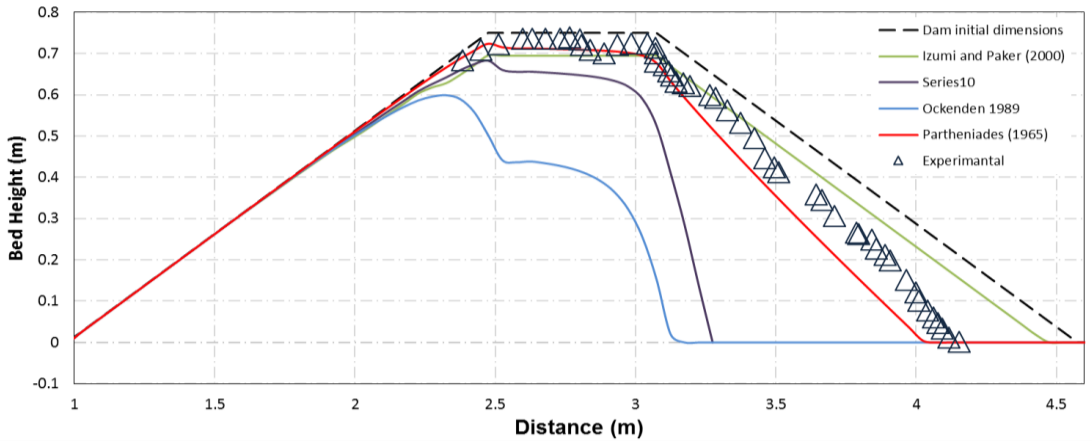

Figure 4-17: Erosion evolution by different entrainment formulae at t=3600s

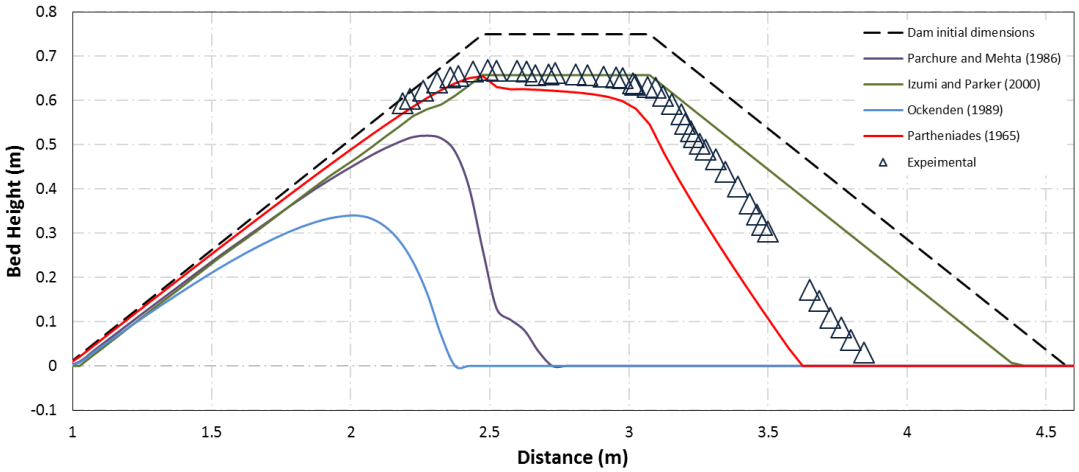

Figure 4-18: Erosion evolution by different entrainment formulae at t=6000s

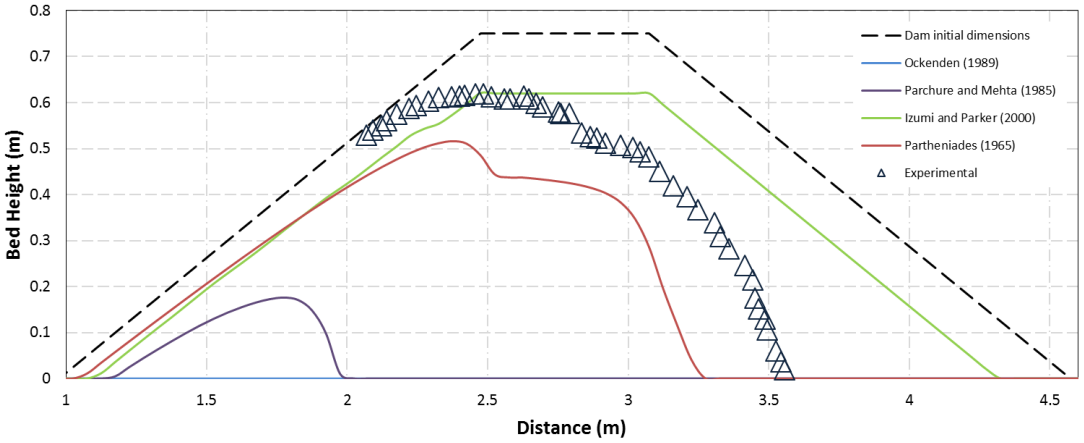

Figure 4-19: Erosion evolution by different entrainment formulae at t=8400s

From the figures above it can be noted that the four formulae show different behaviour of the numerical model result. The formula that had been presented by Ockenden *et al.* (1989) shows significant erosion. This formula has overestimated the erosion - as demonstrated by that fact that the dam body has washed away at t=8400s – far earlier than in the experiment. On the other hand, the formula that is presented by Parchure and Mehta (1985) result in effectively a higher resistance to erosion by the flow. It can be seen that the numerical model shows that a fast erosion process occurred during the time evolution, but the dam is not eroded completely at t=8400s. However, the erosion process, that was predicted by this model, is also an over estimation. The model that of Izumi and Parker (2000) displays unique behaviour. It shows that a slight erosion process occurs, with a good agreement with the measurement appearing at the early stage of the simulation for t=1200s and t=3600s but with different morphological change. During the time evolution, the model shows less agreement with the measurement where the erosion process continues to be under estimated.

The numerical results that are obtained based on Partheniades (1965) formula, Figures (4-16) to (4-19), show the best agreement with the measurements at both the early and late stages of the erosion evolution. The numerical curve shows the same tendency of that in experimental work. In general, the Partheniades (1965) formula shows that it is compatible with the presented

numerical, and it shows a good capability to predict the erosion process that occurs in the real experiment. It is also seen that the numerical results of Izumi and Parker (2000) formula, Figures (4-16) to (4-19), are good but less accurate in compression to that of Partheniades (1965) formula. It shows very high resistance for erosion. On the other hand, the formulae that presented by Ockenden *et al.* (1989) and Parchure and Mehta (1985), Figures (4-16) to (4-19), show a weak capability to predict the erosion process and produce overestimated result.

4.9 Sensitivity Test of the Model to Manning Roughness, Gamma, and Alpha

In this section, an important study of different parameters that influence the erosion process is performed. Studies of this kind are very important to get better understanding about the sensitivity to the parameter of the numerical model. The parameters that are to be examined in this study are, γ that is involved in the formula due to Izumi and Parker (2000), α that is involved in the Parchure and Mehta (1985) formula, and Manning roughness n. (A study involving more parameters will be presented and investigated in the next chapter). To perform the tests, the experimental setup that was carried out in Delft University of Technology 2005 by Zhu (2006) is utilised.

For the numerical simulation, all the information that are presented in Section (4.8) are adopted. The tests were run for 1200 seconds.

The first group of sensitivity tests is performed to study γ. It is a dimensionless exponent. It is a function of soil type and conditions and determined empirically Izumi and Parker (2000). Empirical investigations for γ values found that it ranges between 0.5 – 4 (Ariathurai and Arulanandan (1978); Sheng and Lick (1979); Teisson *et al.* (1993); Howard (1994); Johansen *et al.* (1994); Izumi and Parker (2000)). In the present study, the values 0.5, 1.0, 1.25, and 1.5, for γ, are employed. Figure (4-20) demonstrates the influence of different values of γ on the numerical solution.

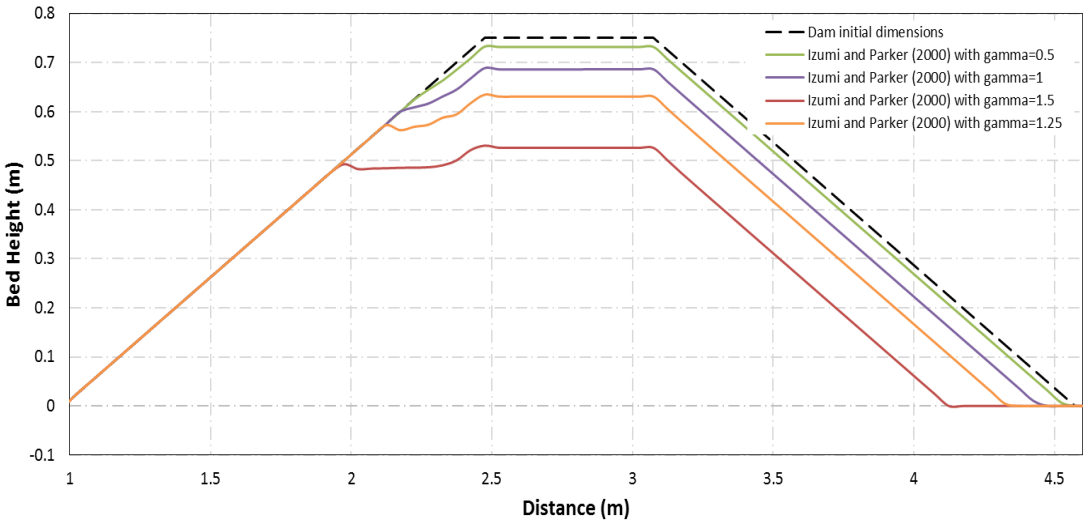

Figure 4-20: The influence of the parameter Gamma γ on the entrainment formula of Izumi and Parker (2000)

From the figure above, the model is clearly sensitive to the parameter γ within the range chose. It is found that the increase of γ value results in an increase in the erosion process and vice versa. Despite the fact that model is sensitive to the γ value, it is relatively easy to calibrate this value and choose a suitable value that produces numerical results in agreement with experimental measurements.

The second group of the tests performed to study the influence of α value that is involved in Parchure and Mehta (1985) formula. The α is the erosion coefficient. It depends on the type of sediment and fluid Parchure and Mehta (1985).The value of erosion coefficient that presented in previous experimental works were found to vary significantly based on the literature, as mentioned by the previous authors, this is because of :

1. Bed forming procedures, in laboratory work, and also the sediment type.
2. The differences of the temperature.
3. The influence of the equipment on the stochastic nature of the bed shear stress τ_b.
4. The effect of sediment high concentration on the bed shear stress τ.

5. Non appropriate estimation of the bed shear stress τ value.

In their work, Parchure and Mehta (1985), they employed a small range of different values of the erosion coefficient and considered it to vary only in the range of (13.6- 18.4m/$N^{0.5}$). While, it is employed as a calibrated factor in some literature Lumborg and Pejrup (2005). They used the value 6.5m/$N^{0.5}$ as a calibrated value, however this value caused instability in the model in current research.

To study the influence of the erosion coefficient on the erosion rate of the formula of Parchure and Mehta (1985), in the presented numerical model, the values of 0.5, 0.6, 0.75, 1 of α were utilized. These values doesn't produce instability in the present model and they are compatible with the flow shear stress of the experiment circumstances. Figure (4-21) demonstrates the results of this study.

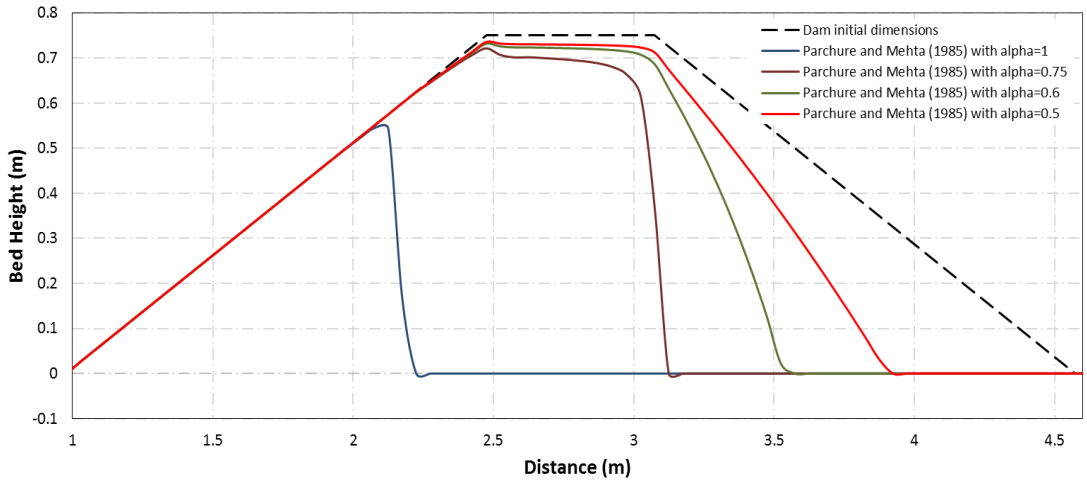

Figure 4-21: The influence of the parameter Alpha α on the entrainment formula of Parchure and Mehta (1985)

From Figure (4-21) above, it can be seen that the numerical model is very sensitive to the value of α. A small change of α value produces a huge difference of two curves for same time duration of the test. The increasing of α results a non-linear increase in the erosion processes in the numerical solution. This high sensitivity of the model to the α values complicates the calibration process to choose a suitable value that capable of giving numerical results consistent with experiments.

The last group of tests is carried out to study the impact of the Manning roughness n on the numerical solution for the presented numerical model. The formula that had been presented by Partheniades (1965) is employed in this group of tests to simulate the erosion process. The Manning roughness n values of 0.022, 0.023, and 0.025 were utilised in the tests where these values are close to that used in the experiment of Zhu (2006). Figure (4-22) demonstrates the impact of different roughness on the numerical solution.

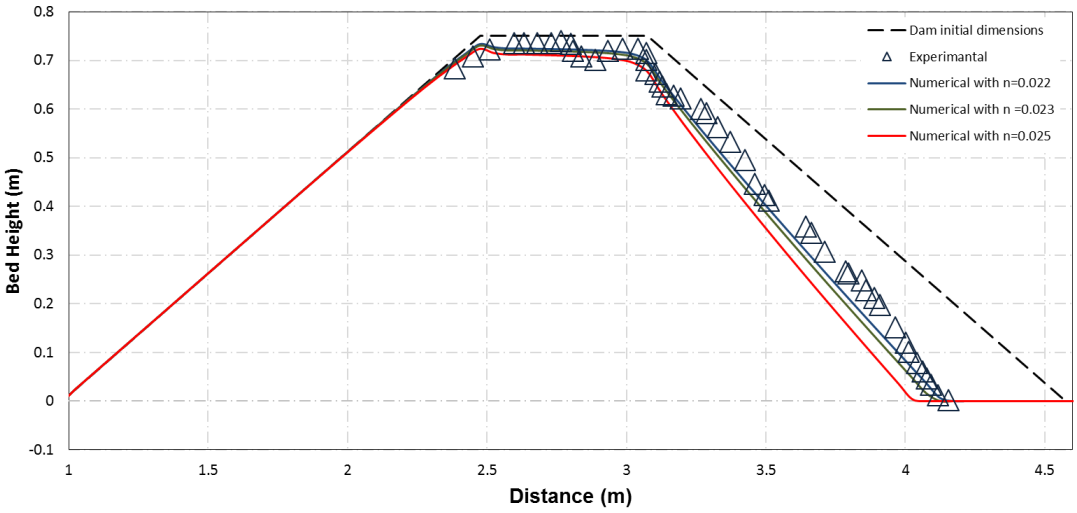

Figure 4-22: The influence of the Manning roughness on erosion process on the numerical solution after t=3600s

From Figure (4-22) above, it is clearly seen that the Manning roughness n has a significant impact on the numerical result of the presented model. The increase of Manning roughness value will increase the erosion process and vice versa. It clearly seen that the value 0.022 for n gives results for the simulation more consistent with experimental than the values 0.023 and 0.025. For the numerical solution purposes, it is easy to choose a suitable value for Manning roughness n that is compatible with the numerical model and give better simulation result.

4.10 Summary

In this chapter, a simple one-dimensional hydro-morphodynamic model has been presented. This model is built based on shallow water equations that are coupled with a cohesive sediment transport model. These models were combined with a bed evolution model. The hydro-morphodynamic model is presented to deal with water flow over cohesive movable bed. The source terms was treated by employing simple techniques. The first order accurate HLL finite volume method is utilized to solve the governing equations.

The advection-diffusion equation is employed to represent the sediment transport model where the suspension is the dominant transport mechanism for the fine sediment particles. In this situation the bed-load sediment transport model is ignored and not simulated.

The model is tested against experimental data. The laboratory experiment that was carried out at the fluid Mechanics Laboratory of Delft University of Technology 2005 by Zhu (2006) is utilized for this purpose. The validation test shows a good agreement between the numerical result and the measurements.

An important study was performed by utilizing four different erosion formulae that had been presented previously by different researchers, to investigate the influence of these formulae on the numerical solution of the present model. It is found that the formula presented by Partheniades (1965) gives the results most consistent with the experimental study.

More investigations were performed in this research to investigate the impact of several parameters i.e. γ, α, and the Manning roughness n on the numerical solutions. It is found that the model is sensitive to all of these parameters. However, the numerical model shows that it has very high sensitivity to α, which make it difficult to choose an accurate or appropriate value to achieve results similar to experimental measures.

To sum up, the scheme presented shows that the model has the capability to simulate and predict the water flow over a movable bed that consists of fine cohesive particles.

Chapter 5 Two Dimensional Hydro-Morphodynamic Model With Cohesive Bed Materials.

In this chapter, the model that was presented in Chapter 4 is extended to a two dimensional model to deal with geometry change, the effect of the second dimension, y, and flow cases that include water flow over movable beds which consist of fine cohesive sediments. A parametric study is performed to obtain better understanding about the impact of the parameters on the model. Finally, the two models that deal with water flow on cohesive bed and non-cohesive bed are unified to form one model that is capable of dealing with the two cases.

5.1 Introduction

In reality, flow occurs in three dimensions, where, the three components of the velocity u, v, and w and the bed or channel geometry have an important impact on the whole water flow. Furthermore, they have a significant influence on the bed change, scouring, sediment diffusivity, and sediment concentration. In other words, the real flow cases have a complexity that makes it very difficult to be represented in only one-dimensional model. Therefore, the one-dimensional model is in many circumstances not appropriate to represent all these complicated cases and scenarios. Thus, it is important to build a two-dimensional numerical model that deals with water flow over a movable bed that consists of cohesive sediment particles. Such models can provide more accurate results and better understanding about the flow hydrodynamics, sediment transport, and morphological change processes for these cases.

Based on that point of view, some of following substantial questions need clear answers:

1- How do the two-dimensional HMD-C model results differ from the two-dimensional HMD-NC model?
2- How do different parameters influence the numerical solution of the HMD-C model?
3- Which parameters have a major influence on the numerical simulation result?

5.2 Construction of HMD-C

In this section, the two-dimensional hydro-morphodynamic model with the cohesive sediment transport model is introduced.

5.2.1 Governing Equations

To introduce a numerical model of the water flow over movable bed that consist of cohesive sediments, the shallow water Equations (4.1) and (4.2) that were introduced in Chapter 4, are utilised. These equations are extended to include the y dimension terms (Fagherazzi and Sun (2003); Cao *et al.* (2004); Simpson and Castelltort (2006)).

The SWEs, consist of the mass and momentum conservation equations for water-sediment mixture, are presented as below:

$$\frac{\partial h}{\partial t} + \frac{\partial hu}{\partial x} + \frac{\partial hv}{\partial y} = \frac{-\partial z}{\partial t} \tag{5.1}$$

$$\frac{\partial hu}{\partial t} + \frac{\partial}{\partial x}\left(hu^2 + \frac{1}{2}gh^2\right) + \frac{\partial huv}{\partial y} = gh\left(S_{ox} - S_{fx}\right) + v_t\left(\frac{\partial^2 hu}{\partial x^2} + \frac{\partial^2 hu}{\partial x \partial y}\right) - \frac{(\rho_s - \rho_w)gh^2}{2\rho}\frac{\partial C}{\partial x} - \frac{(\rho_0 - \rho)(SE - SD)u}{\rho(1-P)} \tag{5.2}$$

$$\frac{\partial hv}{\partial t} + \frac{\partial huv}{\partial x} + \frac{\partial}{\partial y}\left(hv^2 + \frac{1}{2}gh^2\right) = gh\left(S_{oy} - S_{fy}\right) + v_t\left(\frac{\partial^2 hv}{\partial x \partial y} + \frac{\partial^2 hv}{\partial y^2}\right) - \frac{(\rho_s - \rho_w)gh^2}{2\rho}\frac{\partial C}{\partial y} - \frac{(\rho_0 - \rho)(SE - SD)v}{\rho(1-P)} \tag{5.3}$$

The sediment transport model is represented by employing the advection-diffusion equation in two-dimensions. It is represented in Equation (5.4) .

$$\frac{\partial hC}{\partial t} + \frac{\partial huC}{\partial x} + \frac{\partial hvC}{\partial y} = \frac{1}{h}\frac{\partial}{\partial x}\left(hD_x\frac{\partial C}{\partial x}\right) + \frac{1}{h}\frac{\partial}{\partial y}\left(hD_y\frac{\partial C}{\partial y}\right) + \sum_{i=1}^{n}\frac{S_i}{h} \tag{5.4}$$

To represent the bed morphological changes in the presented model, Equation (4.4) that was presented in Chapter 4 is utilised and below for clarity:

$$\frac{\partial z}{\partial t} = \frac{SD - SE}{1 - P}$$

5.3 Numerical Solution

The new two dimensional compact form of the HMD-C model of Equations (5.1), (5.2), (5.3), and (5.4) is introduced as below:

$$\frac{\partial \boldsymbol{U}}{\partial t}+\frac{\partial \boldsymbol{F}}{\partial x}+\frac{\partial \boldsymbol{G}}{\partial y}=S \tag{5.5}$$

Where $\boldsymbol{U}$ is the vector that containing the conserved flow variables

$$\boldsymbol{U}=\begin{bmatrix} h \\ hu \\ hv \\ hc \end{bmatrix} \tag{5.6}$$

$\boldsymbol{F}$ and $\boldsymbol{G}$ are the flux vectors in x and y directions, respectively. They are introduced as in Equations (5.7) and (5.8).

$$\boldsymbol{F}=\begin{bmatrix} hu \\ hu^2+0.5gh^2 \\ huv \\ huc \end{bmatrix} \tag{5.7}$$

$$\boldsymbol{G}=\begin{bmatrix} hv \\ hvu \\ hv^2+0.5gh^2 \\ hvc \end{bmatrix} \tag{5.8}$$

$\boldsymbol{S}$, is the source term vector of the system. It is represented as below:

$$\boldsymbol{S}=\begin{bmatrix} -\frac{SE-SD}{1-P} \\ gh\left(S_{ox}-S_{fx}\right)+v_t\left(\frac{\partial^2 hu}{\partial x^2}+\frac{\partial^2 hu}{\partial x\partial y}\right)-\frac{(\rho_s-\rho_w)gh^2}{2\rho}\frac{\partial C}{\partial x}-\frac{(\rho_0-\rho)(E-D)u}{\rho(1-P)} \\ gh\left(S_{oy}-S_{fy}\right)+v_t\left(\frac{\partial^2 hv}{\partial x\partial y}+\frac{\partial^2 hv}{\partial y^2}\right)-\frac{(\rho_s-\rho_w)gh^2}{2\rho}\frac{\partial C}{\partial y}-\frac{(\rho_0-\rho)(E-D)v}{\rho(1-P)} \\ \frac{1}{h}\frac{\partial}{\partial x}\left(hD_x\frac{\partial C}{\partial x}\right)+\frac{1}{h}\frac{\partial}{\partial y}\left(hD_y\frac{\partial C}{\partial y}\right)+SE-SD \end{bmatrix} \tag{5.9}$$

Where v_t is the turbulent viscosity coefficient or eddy coefficient, $v_t=\theta u_* h$, where θ is an empirical coefficient, and $0.0<\theta<1.0$.

To solve the compact form of Equation (5.5), it can be discretised by using the finite volume method at uniform rectangular mesh as discussed in Chapter 3, Figure (3-1).

The discretised equation is now written as below:

$$\boldsymbol{U}_{i,j}^{t+1} = \boldsymbol{U}_{i,j}^{t} - \frac{\Delta \mathrm{t}}{\Delta x}\left(\boldsymbol{F}_{i+\frac{1}{2},j} - \boldsymbol{F}_{i-\frac{1}{2},j}\right) - \frac{\Delta t}{\Delta y}\left(\boldsymbol{G}_{i,j+\frac{1}{2}} - \boldsymbol{G}_{i,j-\frac{1}{2}}\right) + \Delta t \boldsymbol{S}^{t} \quad (5.10)$$

Where $\boldsymbol{F}_{i\mp\frac{1}{2},j}$ and $\boldsymbol{G}_{i,j\mp\frac{1}{2}}$ represent the numerical flux value at the cell interfaces in x and y directions respectively.

In this equation, the numerical fluxes are calculated at the cell interfaces. Special attention is needed to avoid the problem that appears as a discontinuity at the interfaces. In this research, the 1st order accurate Godunov type approximate Riemann solver HLL (Harten-Lax-van Leer) is employed to solve the system in Equation (5.10) Toro (2001). Details of this solver were presented in Chapter 4.

5.4 Testing of the Two-Dimensional Model

Most laboratory and numerical work has investigated water flow on a movable bed with non-cohesive bed materials. It is rare to find a laboratory experiment that deals with cases of cohesive bed materials. Such cases are very important to validate the numerical models. Therefore, the researcher examined the new model using a different approach.

In this section, the new HMD-C model is tested and compared against the HMD-NC model that was presented in Chapter 3. To perform such this comparison test, the laboratory experiment that was performed at the Université Catholique de Louvain (Goutiere *et al.* (2011)), is employed.

As mentioned earlier (but repeated for clarity), the experiment was performed in 6m long flume. The flume had two different widths that are 0.25m from the beginning of the channel to 4m length and 0.5m for the residual length. The dam was located at the centre of the flume. The upstream filled with 0.25m height water level, while the downstream considered as a dry bed. The channel bed was filled with a 0.1m height uniform sand layer. The sand median diameter was 1.72mm, with specific density of s = 2.63, and 39% of porosity. The experimental setup is presented in Figure (3-20) Chapter 3.

For simulation, the channel domain is represented as a grid with dimensions of 120 x 60 structured rectangular cells with dx = 0.05m and dy = 0.025m respectively. A closed boundary at the upstream of the flume is assumed, while the boundary at the end of the downstream was assumed as an open boundary with free outflow. The Manning coefficient n = 0.023. The simulation was performed for 50s and the numerical result was compared with the result of the HMD-NC model at 4.2m, 4.3m, and 4.5m as shown in the figures below.

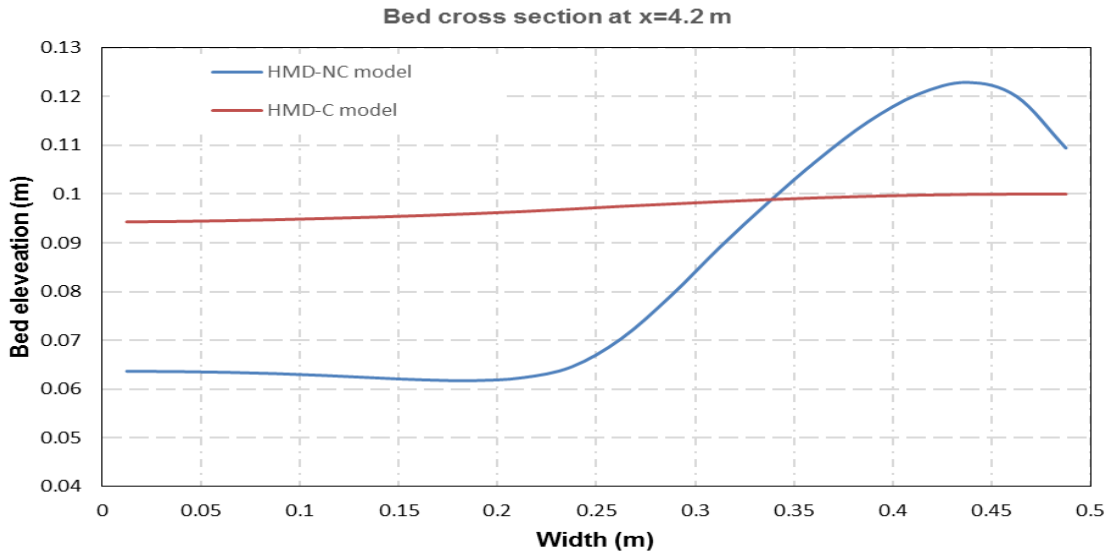

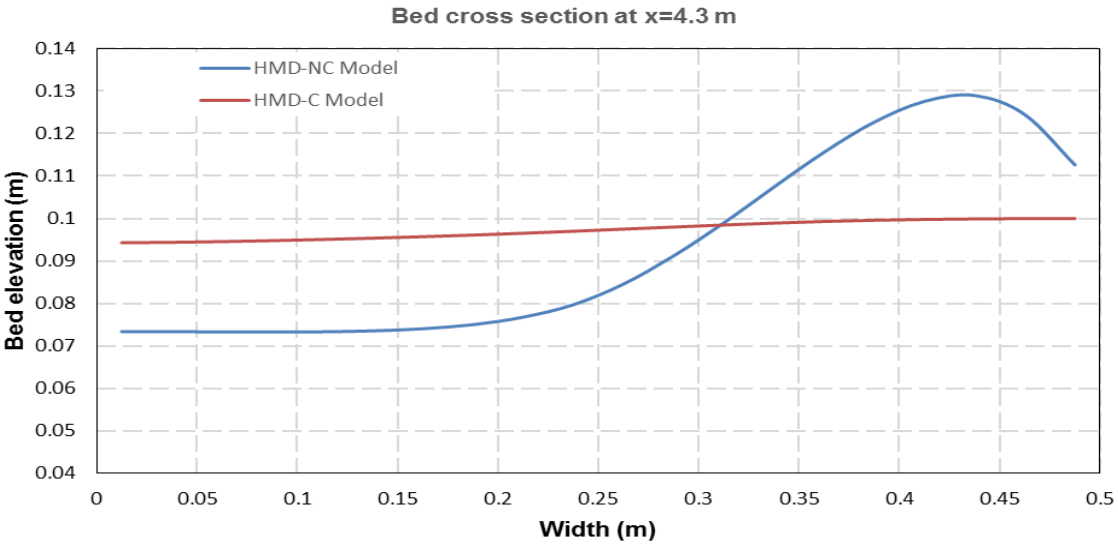

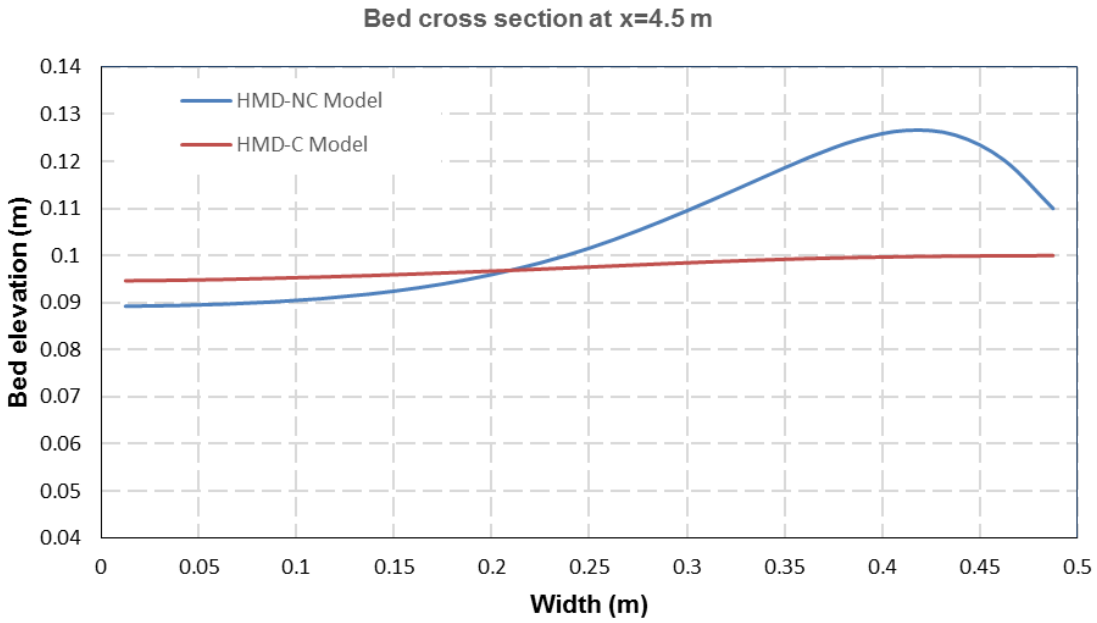

Figure 5-1: Bed Level Comparison Between The HMD-C

The spatial simulation of the bed evolution is tested. A comparison of cross sections for the bed of the channel between the HMD-C model and the HMD-NC model is performed. This comparison is monitored at distance x = 4.2m, x = 4.3m and x = 4.5m as shown in Figure (5-1). The main feature in the HMD-C result are the erosion, where the scour hole occurs at the beginning of the widening close to the wall. It is clearly seen that the scour hole depth, that is plotted from the results of the HMD-C model, is much smaller compared to that produced by the HMD-NC model. The difference in the erosion depth between the two models decreases as shown at x=4.5m, the reason for that decrease is that the non-cohesive bed material shows lower erodibility following the widening because the higher flow shear stress occurs at closer distance from the widening. The reason of the smaller erosion depth in the HMD-C model is attributed to the high resistance to the erosion in cohesive bed case. It can be seen that no deposition occurred in Figure (5-1) for the HMD-C result, which is attributed to the high flow shear stress that exceeded the value of the critical shear stress of deposition, while the mound is formed for the HMD-NC model.

Figure (5-2) demonstrates the three-dimensional bed level comparison between the numerical result of the HMD-C and HMD-NC models.

A)

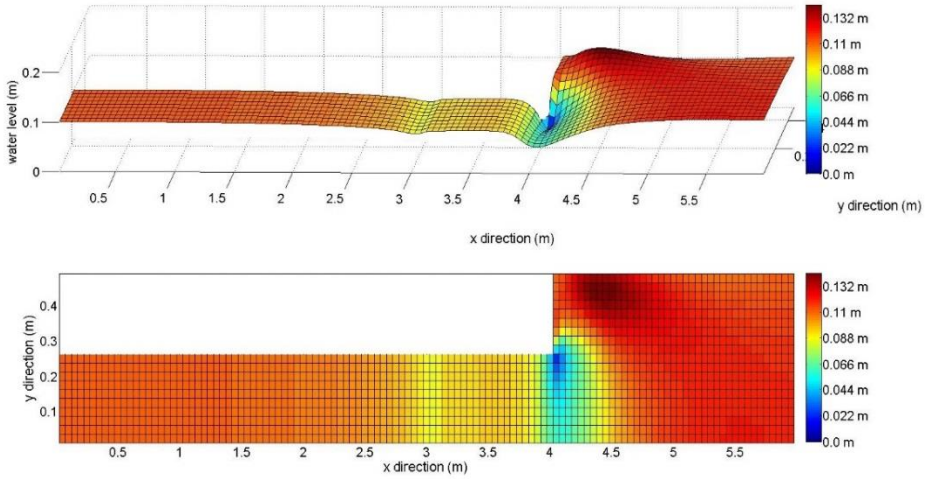

B)

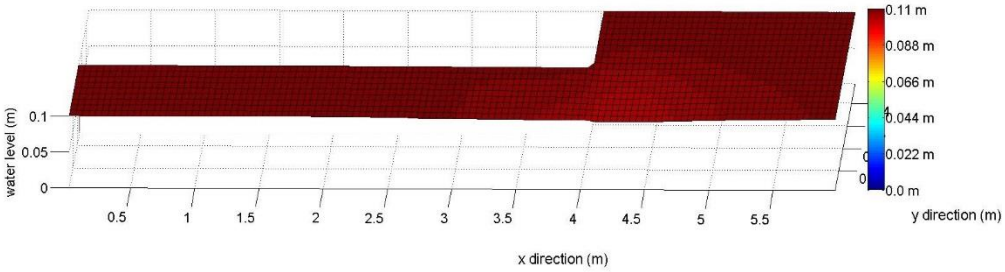

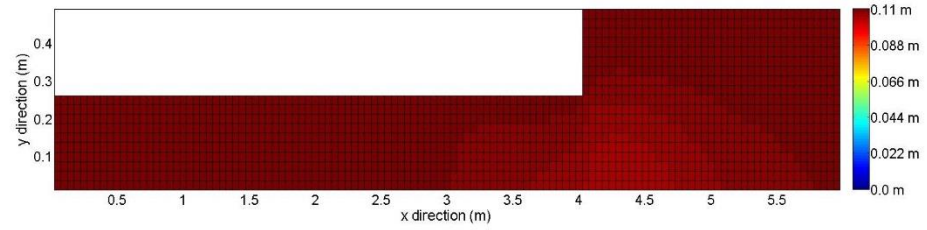

Figure 5-2: 3D Bed Level Comparison Between The Numerical Result Of (a) The HMD-C and (b) HMD-NC Models After t=50 sec

From the Figures A, and B above, the difference between the bed levels of the two simulations is very significant. In Figure 5-2(a), it is clearly seen that there are two locations that were severely eroded. These two locations are located at x =3m where the dam is located, and x = 4m where the widening is located. The erosion at the widening corner is the highest in magnitude because of the

high flow shear stress at that location. The deposition process can be noticed as a significant phenomenon which is results in the hump. This hump is formed by the sand particles that are accumulated and settled at a specific location by the gravity. At this location, the flow shear stress is low and it is not capable of eroding the settled particles again. The hump is located at the far corner of the wide channel and continues to the middle of the channel closer to the wall.

Figure 5-2(b) represents the water flow over a movable bed that consists of cohesive materials which is simulated using the HMD-C model. The results are quite different compared to those of the case of the HMD-NC model. In general, the erodibility of the bed E is very low. The erosion magnitude at the dam location, where x = 3m, is very low and it is difficult to be seen in the 3D figure. The severe erosion process occurs at x =4m at the right side wall of the widening and is spread around the maximum erosion point. It is noteworthy that no deposition can be seen in the figure as all the particles are suspended and carried away.

To sum up, the previous Figures (5-1, and 5-2), show a significant differences in the results for the HMD-C and HMD-NC models whether in the bed erodibility, or the location and rate of deposition and erosion. Higher bed resistance to the erosion is seen in the HMD-C model with no deposition for the sediment particles which are not the same for the HMD-NC mode.

5.5 Parametric Study

In this section, an important investigation is performed to study the influence of different parameters on the numerical model result. These different parameters may have direct or indirect influence on the numerical model. To perform this investigation, a series of dam break tests were carried out under constant initial conditions. To perform these tests, the dam break case in the widening channel presented above is employed. The parameters that had been studied in this chapter are, the bed erodibility, critical shear stress for erosion, critical shear stress for deposition, porosity, and settling velocity.

For the numerical simulation purposes and for the all tests, the flume of the experiment is divided into 7200 structured cells with a mesh size 120 x 60 cell. The cell size is dx=0.05m and dy=0.025m. The Manning coefficient n=0.023. Each test was executed for 50s. The numerical result of each group of tests was compared with the result of the HMD-NC model at x =4.2m, 4.3m, and 4.5m.

5.5.1 Erodibility

This parameter is expected to be have a high influence on the erosion process. To study the influence of this parameter, three values of erodibility were employed in the test, that are 0.0001 (kg/m^{2}s), 0.0003 (kg/m^{2}s), and 0.0006 (kg/m^{2}s). These values were chosen based on the calibrated values that had been presented in literature. Figure (5-3) shows the comparison of the influence of different erodibility values on the erosion process at three sections at x= 4.2m, 4.3m, and 4.5m.

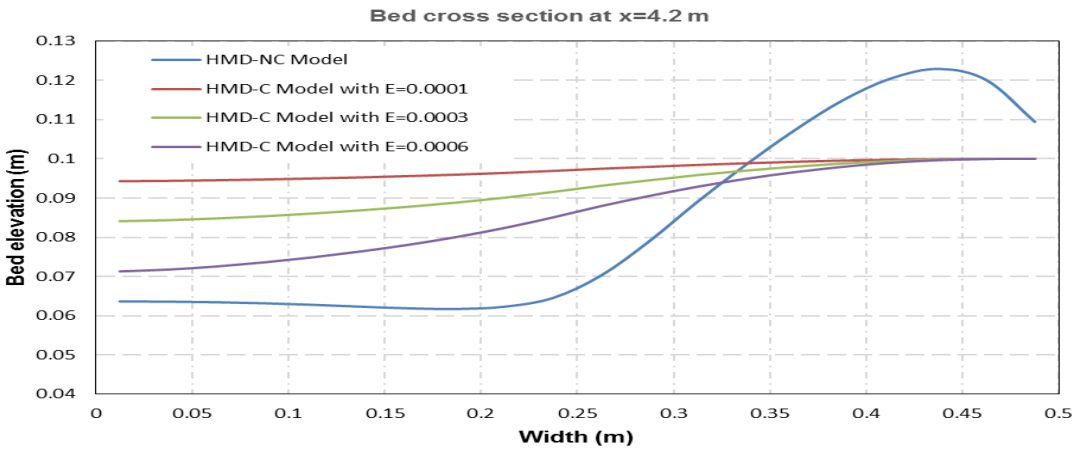

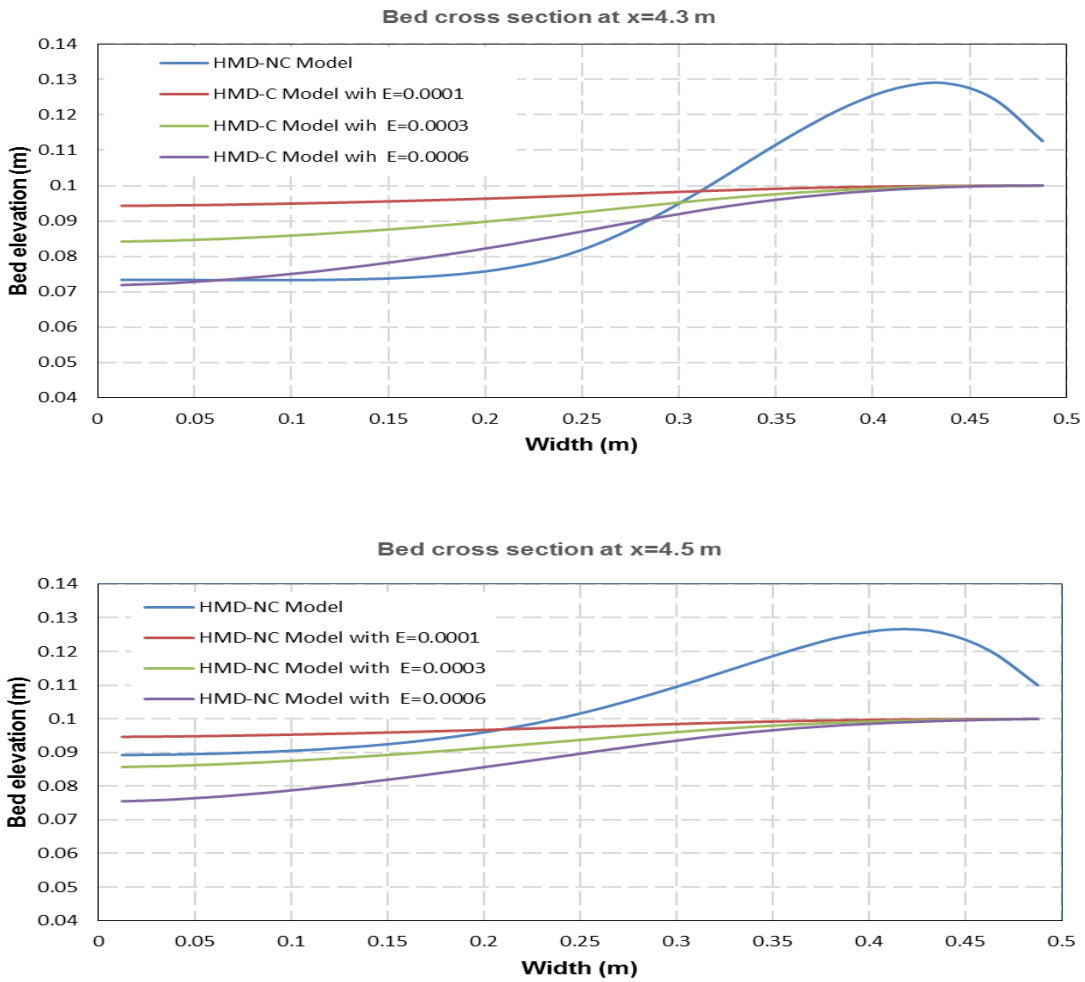

Figure 5-3: Erodibility influence on the HMD-C Model Numerical Result at sections 4.2m, 4.3m, and 4.5m.

It can be seen that the HMD-C model is very sensitive to the erodibility value. The increasing of E value results more erosion and scouring on the cohesive bed and vice versa. It can be seen that the increasing of the E value (to unrealistic values) may easily produce in-accurate results for the erosion process. The reason for this is, that the high value of E may show high erosion process produces a high scoured depth that exceeds the scoured depth for the non-cohesive bed as shown in Figure (5-3). Wary of this the researcher used smaller values of E as presented in Chapter 4 Section (4.5.2.1).

Figure (5-4) shows a three-dimensional comparison for the bed evolution after 50s simulation.

A)

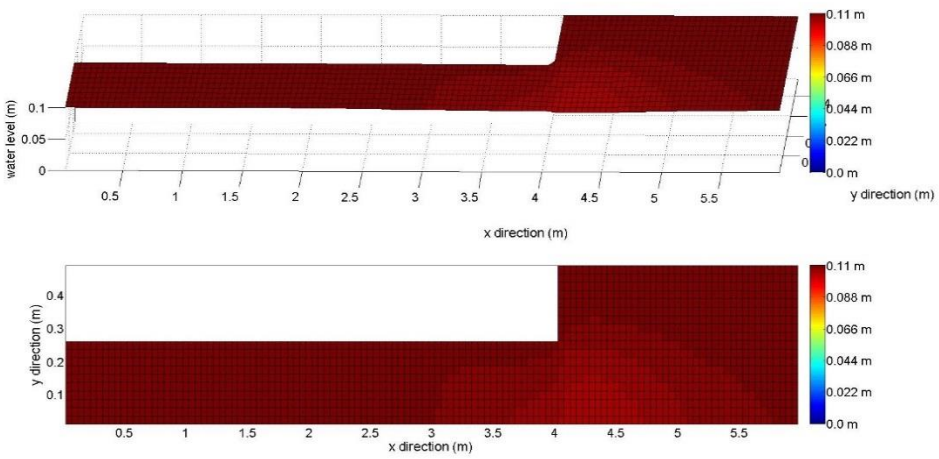
water level (m)
0.1
0.05
0
0.5
1
1.5
2
2.5
3
3.5
4
4.5
5
5.5
x direction (m)
y direction (m)
0.11 m
0.088 m
0.066 m
0.044 m
0.022 m
0.0 m
y direction (m)
0.4
0.3
0.2
0.1
x direction (m)

B)

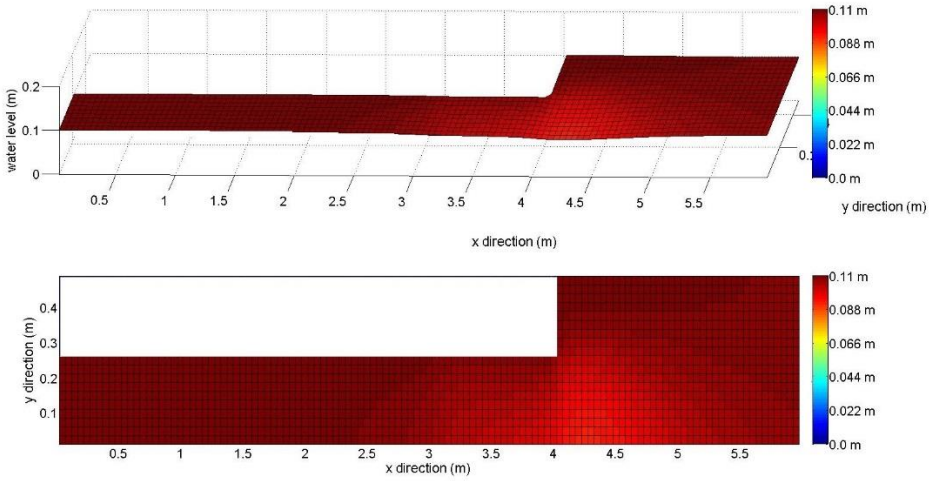
water level (m)
0.2
0.1
0
0.5
1
1.5
2
2.5
3
3.5
4
4.5
5
5.5
x direction (m)
y direction (m)
0.11 m
0.088 m
0.066 m
0.044 m
0.022 m
0.0 m
y direction (m)
0.4
0.3
0.2
0.1
x direction (m)

C)

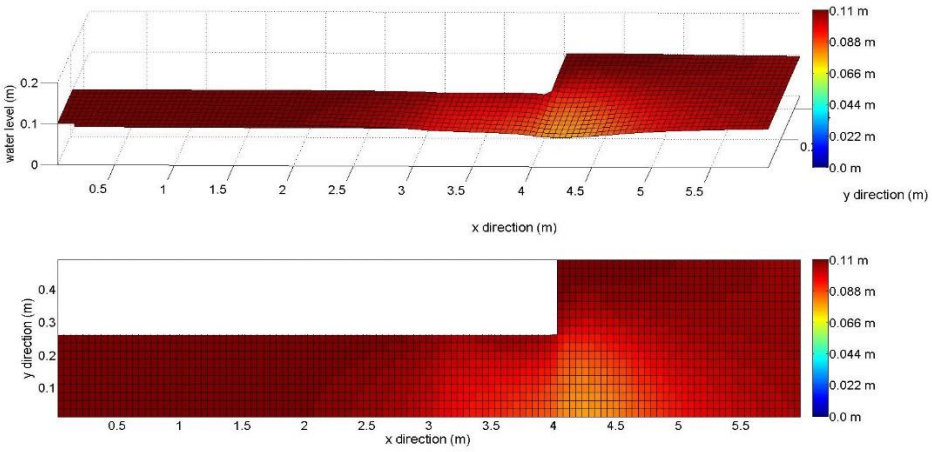

Figure 5-4: 3D For Bed Elevation To Show The Erodibility Influence On The Numerical Result of The HMD-C Model.

It is clear that the bed with lower erodibility E=0.0001 (kg/m^{2}s), as shown in Figure 5-4(a), has the lower scouring depth. While the bed that has higher erodibility E= 0.0003 (kg/m^{2}s), as shown in Figure 5-4 (b), has higher scouring depth. Figure 5-4(c) have the higher value of erodibility which is E=0.0006 (kg/m^{2}s). In this figure, the high score depth is clearly seen compared to the Figure 5-4(a).

From above, it is found that the erodibility has a great influence on the erosion process for the cohesive bed where high erodibility produce high scour depth. And the model is very sensitive to the E values. Special attention is required during the calibration of the E value to obtain accurate results for the simulations.

5.5.2 Critical shear stress for erosion

This parameter is directly involved in the equation of the erosion rate. In carrying out the study, three values of the critical shear stress for erosion were involved. The values are 0.9 N/m^2, 1.3 N/m^2, and 1.1 N/m^2. These calibrated values were chosen to make sure that the erosion occurs at low flow shear stresses. Figure (5-5) shows the influence by presenting a comparison of the results from different values critical shear stress for erosion on the erosion process at three sections at x= 4.2m, 4.3 m, and 4.5m.

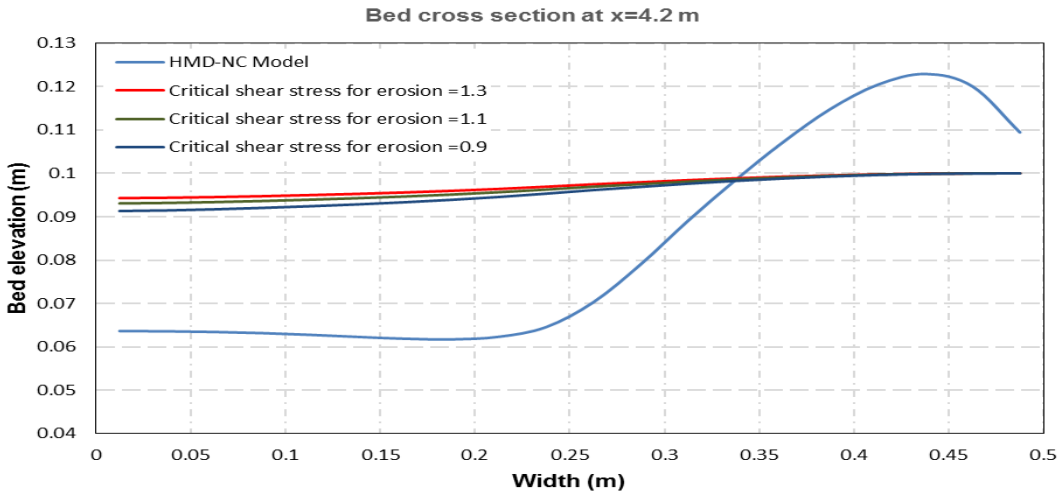
Bed cross section at x=4.2 m
HMD-NC Model
Critical shear stress for erosion =1.3
Critical shear stress for erosion =1.1
Critical shear stress for erosion =0.9
Bed elevation (m)
Width (m)
0.13
0.12
0.11
0.1
0.09
0.08
0.07
0.06
0.05
0.04
0
0.05
0.1
0.15
0.2
0.25
0.3
0.35
0.4
0.45
0.5

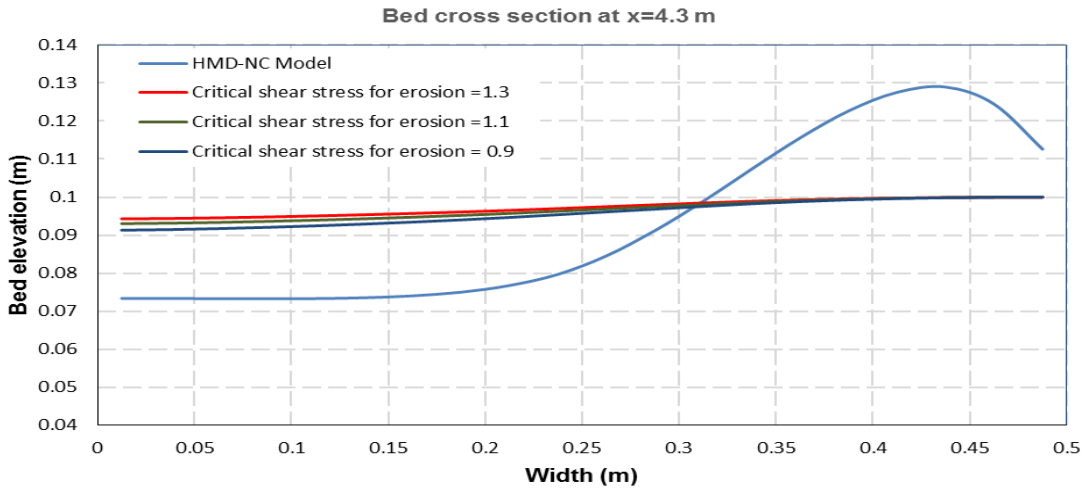
Bed cross section at x=4.3 m
HMD-NC Model
Critical shear stress for erosion =1.3
Critical shear stress for erosion =1.1
Critical shear stress for erosion = 0.9
Bed elevation (m)
Width (m)
0.14
0.13
0.12
0.11
0.1
0.09
0.08
0.07
0.06
0.05
0.04
0
0.05
0.1
0.15
0.2
0.25
0.3
0.35
0.4
0.45
0.5

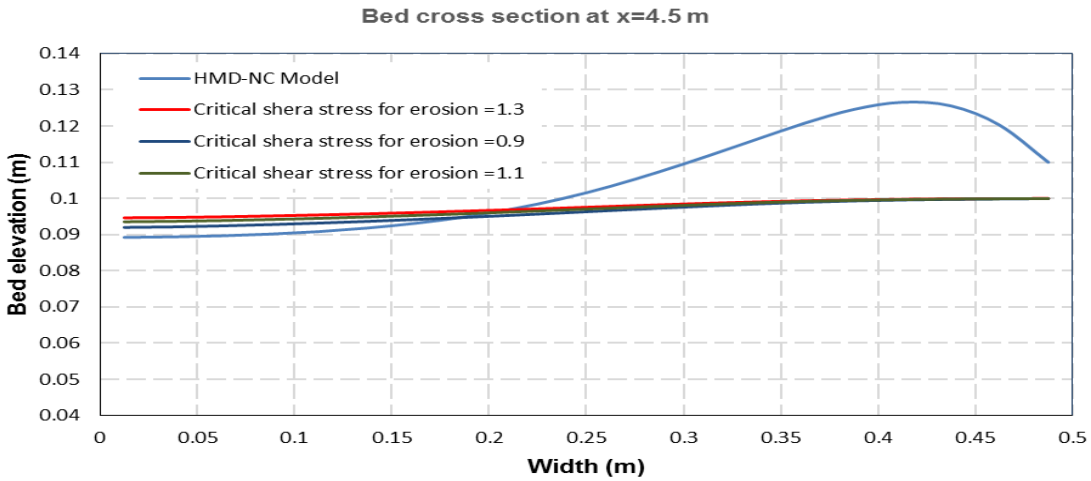

Figure 5-5: The Influence Critical Shear Stress for Erosion on the HMD-C Model Numerical Result at sections 4.2m, 4.3m, and 4.5m.

From Figure (5-5) above, it can be seen that the HMD-C model is sensitive to the values of critical shear stress for erosion. The increase of the τ_E will delay the onset of the erosion process, because the τ_E represents the critical value of the inception motion of the cohesive particles to be eroded by the water flow. In addition to that, increasing of the τ_E value will decrease the erosion rate. The reason for this is that the residual flow shear stress that exceed the τ_E, which are necessary to erode the cohesive particle, will decrease. This leads to a decrease of the erosion rate, see Equation (4.9). It can be seen that the numerical model results with smaller values of the $\tau_E = 0.9$ N/m^2 produce high erosion rate with higher scour depth, while smaller erosion rate is found with higher value of $\tau_E = 1.3$ N/m^2.

From the above, it can be seen that the numerical model is sensitive to the critical shear stress for erosion τ_E. The value of τ_E needs a special attention when it is chosen. A higher value of τ_E is compatible with a lower value of bed erodibility E and it should be chosen based on the degree of bed compaction that is measured by the dry density of the bottom layer (Liu *et al.* (2002)).

5.5.3 Settling Velocity

Settling velocity is a very important parameter that has a high impact on the numerical models with non-cohesive soil. There is a lack of understanding its influence on the numerical models with cohesive bed materials. The settling velocity parameter is included in the deposition rate formula where it influences the deposition rate, see Equation (4.13).

To perform this study, three different values are used during the simulation tests. The values are 0.0003 m/s, 0.0015 m/s, and 0.003 m/s. These calibrated values were chosen based on Figure (4-5) in Chapter 4. Figure (5-6) shows the impact of the different values of settling velocity on the numerical result at three sections, at x= 4.2m, 4.3m, and 4.5m.

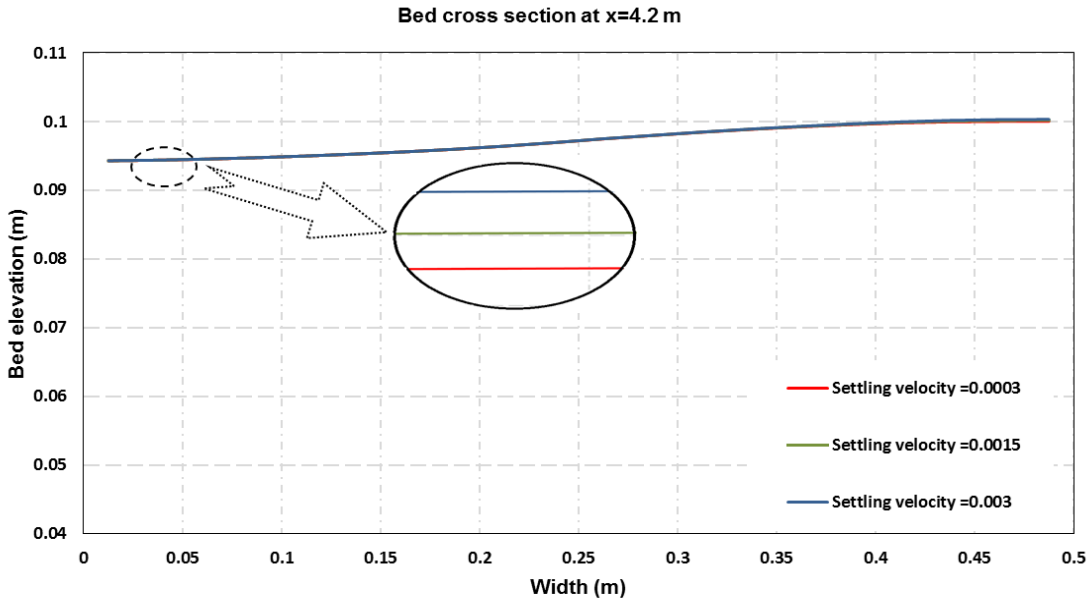

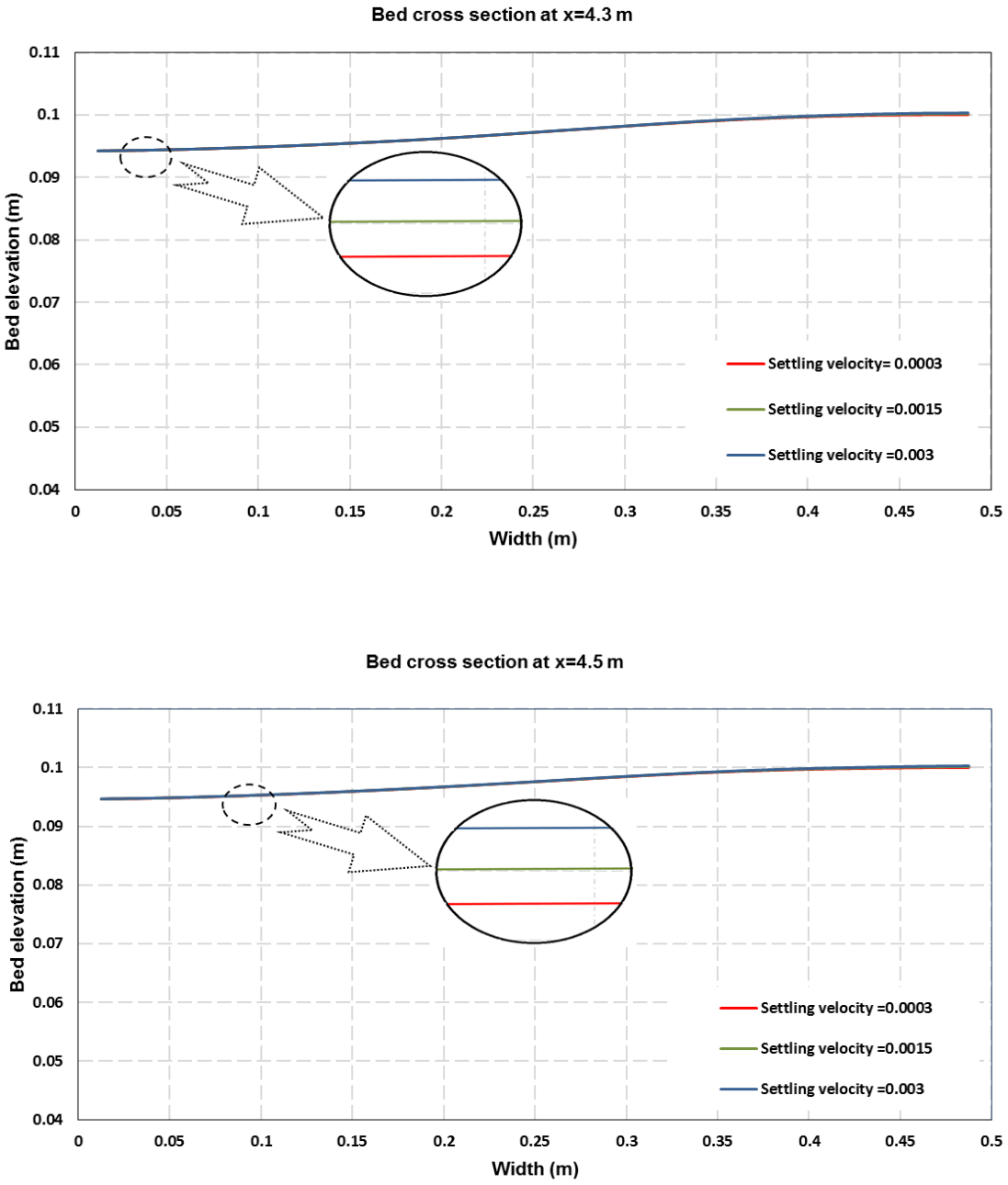

Figure 5-6: The Influence of the settling velocity on the HMD-C Model Numerical Result at sections 4.2m, 4.3m, and 4.5m.

Figure (5-6) demonstrates a very low sensitivity of the numerical model to the sediment particles settling velocity w. The increasing of the settling velocity decreases the erosion depth. The reason for this is, that the settling velocity has a direct influence on the deposition rate according to Equation (4.13). This means that the deposition rate will increase because of the increasing of the

particles that settle at the bed. It was found that the difference percentage in the result of the numerical model between the higher value of $w = 0.003$ m/s (red curve), and the smallest value of $w = 0.0003$ m/s (blue curve), is (0.068%).

To sum up, the settling velocity has almost no influence on the erosion rate but has a slight influence on the deposition process and this leads to slight influence on the numerical result.

5.5.4 Porosity

Porosity is the soil property that represent the percent of void space in a soil volume (Terzaghi *et al.* (1996)). It indicates how water moves through the soil sample by infiltration (Mukhlisin *et al.* (2006)). Soil with high porosity has bigger spaces between particles and this allow the water to infiltrate between the particles that form this soil (Bryan (1976)). Physically, it has an influence on the soil particles and allows for them to be detached from the soil-water interface. Fine particles soil with low porosity may show higher resistance to being eroded by water flow (Papamichos and Vardoulakis (2005)). To investigate the influence of the porosity on the numerical model solution, four values for porosity are employed. These values are 0.36, 0.38, 0.39, 0.40.

Figure (5-7) demonstrates the influence of different values of porosity on the numerical model result at three locations of the channel at x = 4.2m, 4.3m, and 4.5m.

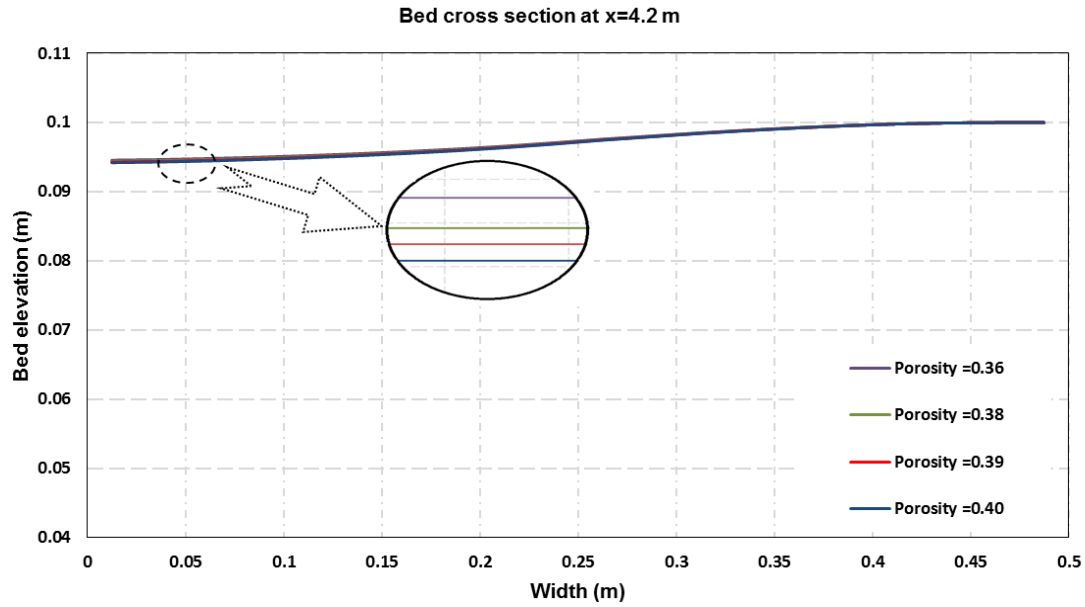
Bed cross section at x=4.2 m
Bed elevation (m)
0.11
0.1
0.09
0.08
0.07
0.06
0.05
0.04
0
0.05
0.1
0.15
0.2
0.25
0.3
0.35
0.4
0.45
0.5
Width (m)
Porosity =0.36
Porosity =0.38
Porosity =0.39
Porosity =0.40

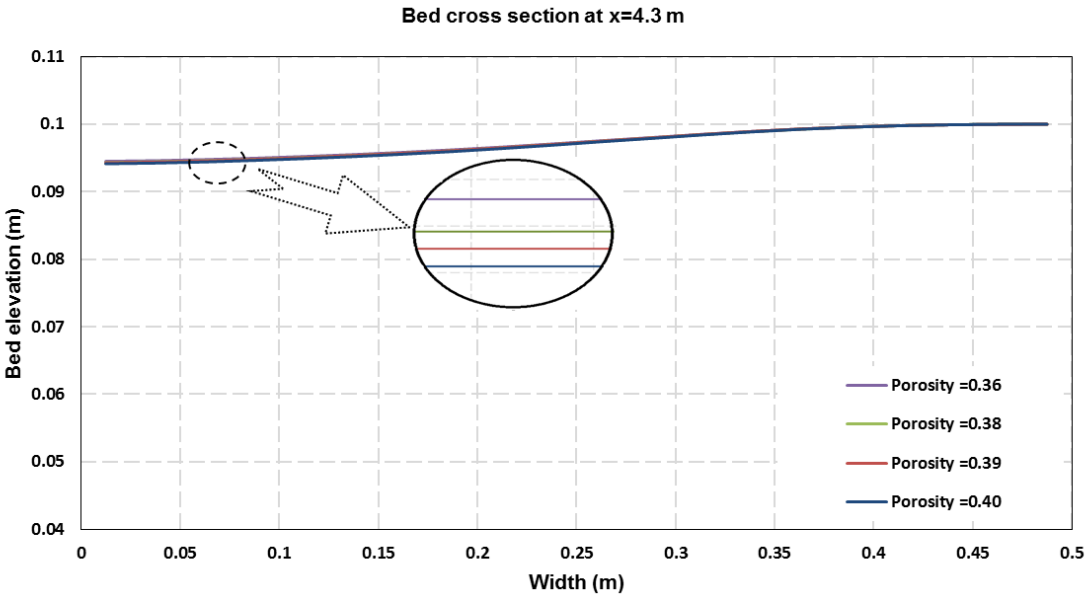
Bed cross section at x=4.3 m
Bed elevation (m)
0.11
0.1
0.09
0.08
0.07
0.06
0.05
0.04
0
0.05
0.1
0.15
0.2
0.25
0.3
0.35
0.4
0.45
0.5
Width (m)
Porosity =0.36
Porosity =0.38
Porosity =0.39
Porosity =0.40

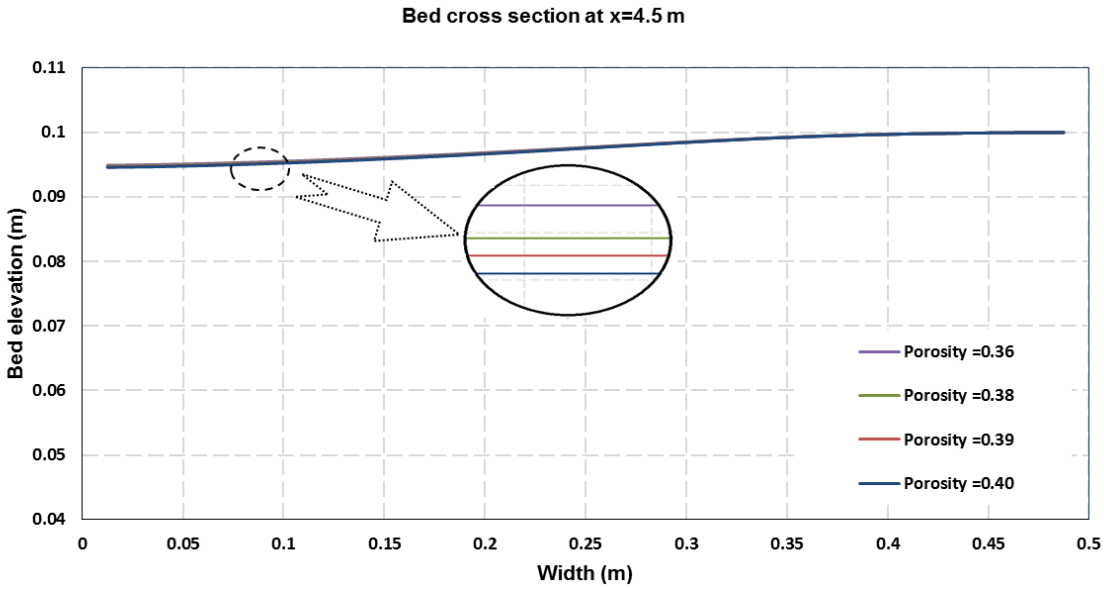

Figure 5-7: The Influence of the Bed Porosity on the HMD-C Model Numerical Result at sections 4.2m, 4.3m, and 4.5m.

Clearly, the numerical model has a very low sensitivity to the bed porosity P, which can be seen from the figures above. It is noticed that the increase of the porosity will increase the erosion depth. Because the decrease of the porosity means decrease in the voids between the particles and this leads to a difficulty for the water to infiltrate into these voids which results a minimizing of the particles that are detached by flow shear stress. Physically, the decrease of the porosity will increase the critical shear of erosion and will decrease the bed erodibility (Buls *et al.* (2017)), as shown in Figures (5-8) and (5-9) respectively. Numerically, the porosity influences the morphological model according to Equation (5.6).

It is noticeable that the different percentage in the result of the numerical model between the higher value of $P = 0.36$ (purple curve), and the smallest value of $P = 0.4$ (blue curve), is found to be (0.159 %).

From above, the numerical model shows very slight sensitivity to the bed porosity variation.

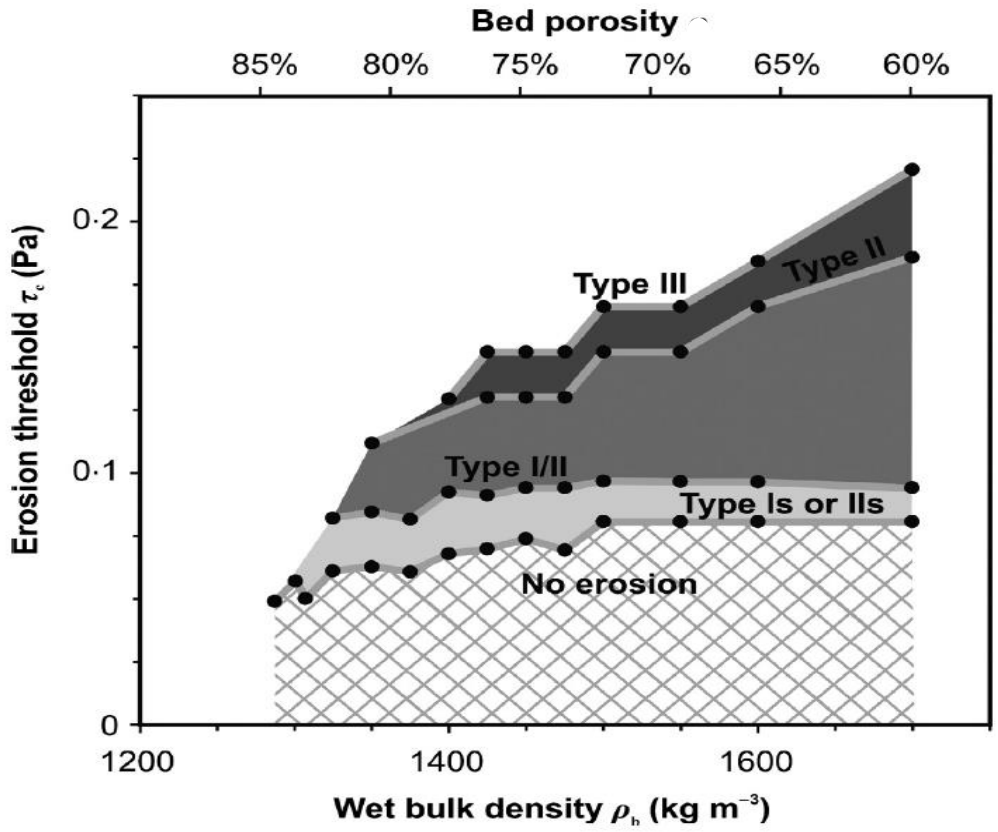

Figure 5-8: The Influence of the Bed Porosity on the Critical Shear Stress of Erosion (Buls *et al.* (2017))

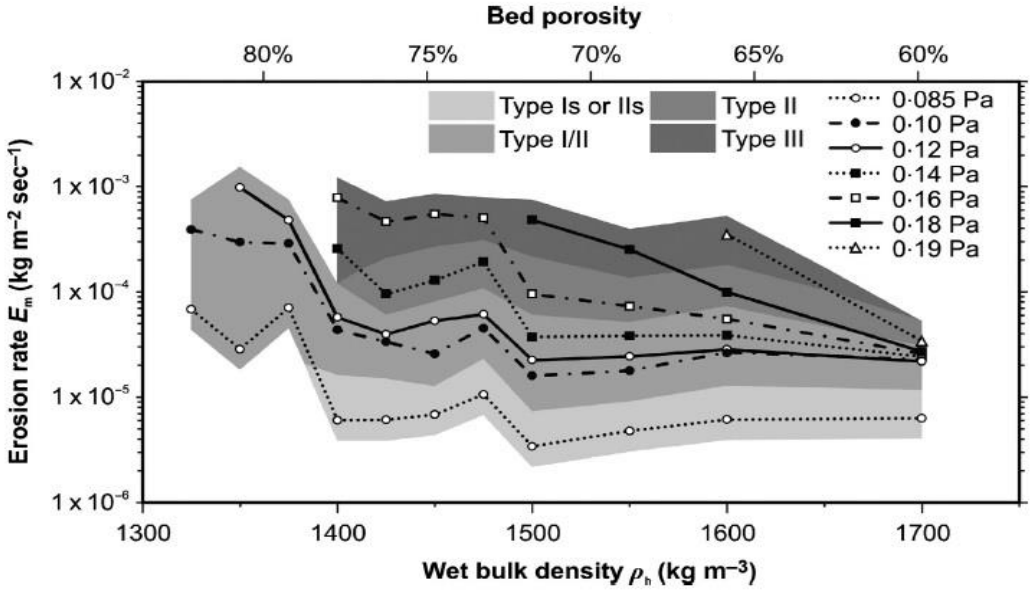

Figure 5-9: The Influence of the Bed Porosity on the Bed Erodibility (Buls *et al.* (2017))

5.5.5 Critical shear stress for deposition

This parameter is involved directly to the deposition formula, see Equations (4.13), (4.14), and (4.15). The increase of the flow shear stress may prevents the particle from being deposited. Therefore, small increase for the critical shear stress of deposition may have no influence on the numerical results. To study the influence of this parameter on the presented model, four values of the critical shear stress of deposition were chosen. These values are 4 N/m^2, 5 N/m^2, 6 N/m^2, and 10 N/m^2. These high values were chosen to increase the deposition rate for low flow shear stresses. This can ease the studying of the influence of this parameter on the numerical results.

Figure (5-10) demonstrate the comparison of the influence of different values of critical shear stress for deposition numerical model result at three sections at x= 4.2m, 4.3m, and 4.5m.

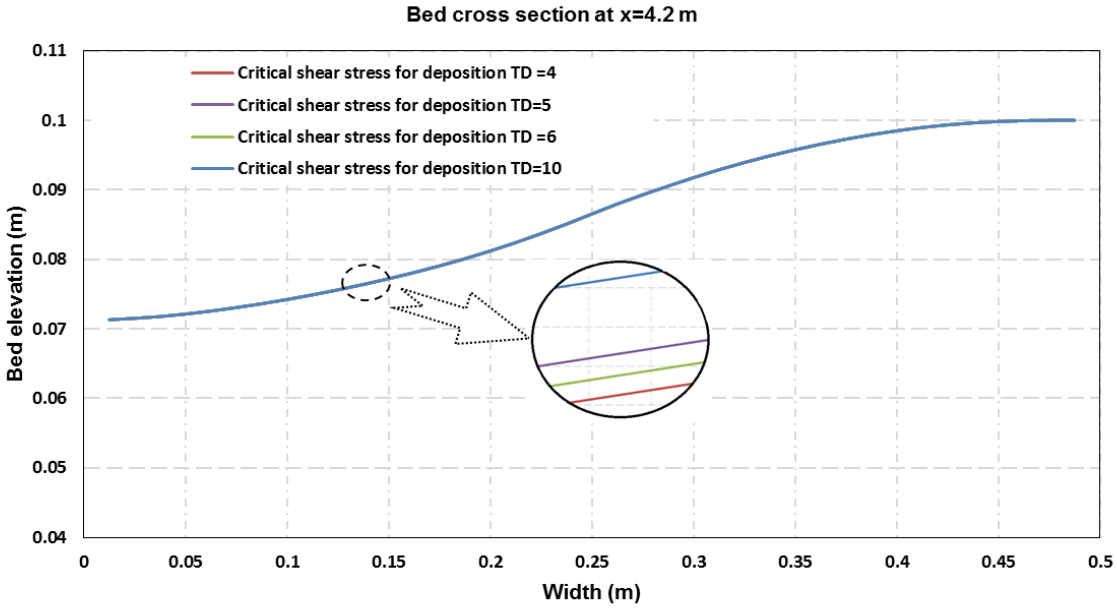

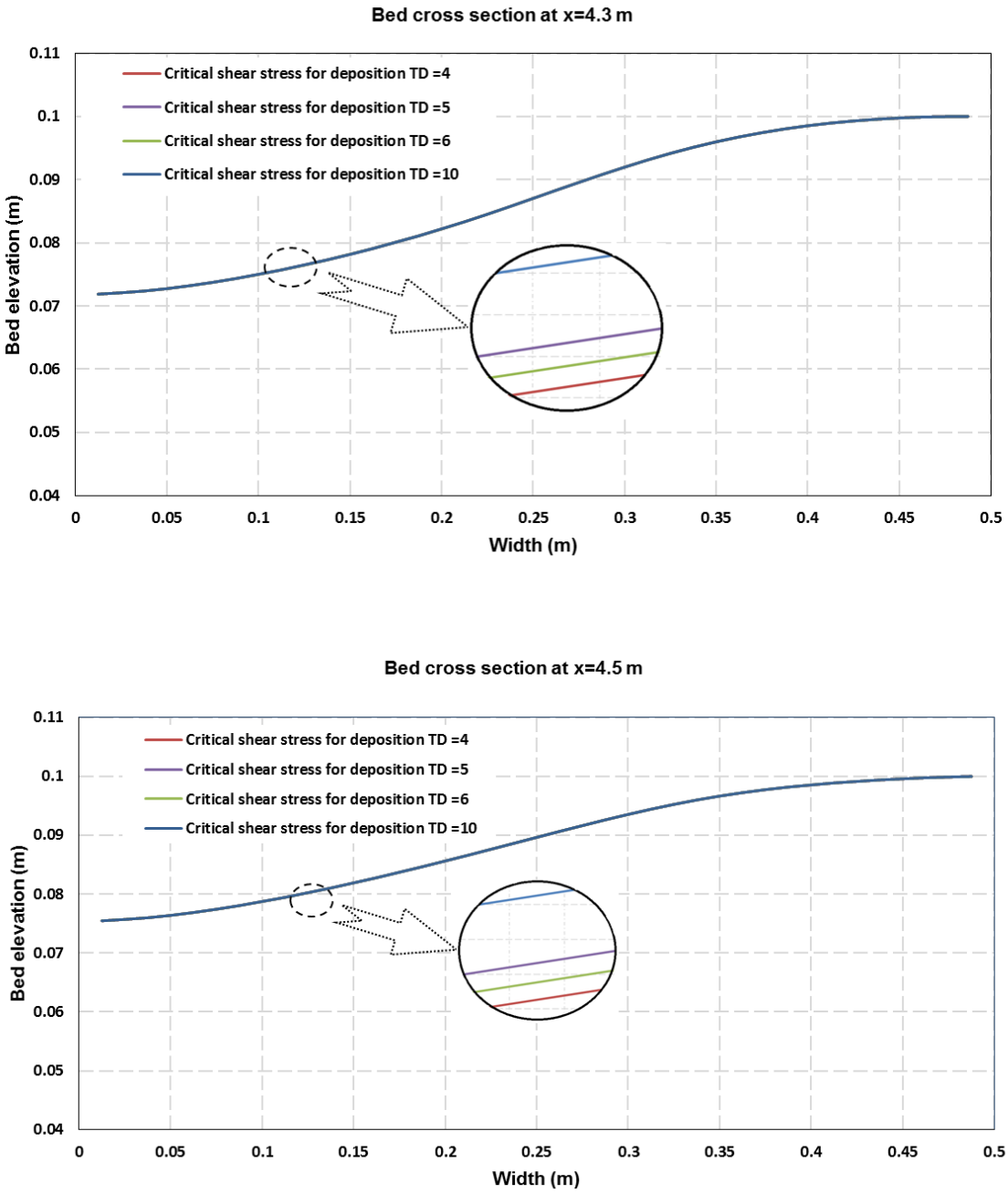

Figure 5-10: The Influence of the Critical Shear Stress for Deposition on the HMD-C Model Numerical Result at sections 4.2 m, 4.3 m, and 4.5m.

It is clear from Figure (5-10) above that the numerical model is insensitive to the value of the critical shear stress of deposition τ_D. Because the deposition process occurs for a small range of flow shear stresses, which are less than the critical shear stress for deposition τ_D. In other words, the water flow has very low velocities. While in this simulation, the applied flow shear stress exceeds the τ_D during the tests in which the erosion process is the dominant. It can be

seen that the difference percentage of numerical results between the higher value of $\tau_D = 10$ N/m^2 (blue curve), and the smallest value of $\tau_D = 4$ N/m^2 (red curve), is only (0.00348%) which is a very small percentage.

From above, the numerical model shows no significant sensitivity to the critical shear stress of deposition τ_D. In other words, the deposition process (formula) can be neglected for water flow cases with high flow shear stresses.

5.5.6 Outcome of the Parametric Study

In the previous section, a series of simulations were executed to investigate a group of parameters that are expected to influence the numerical result of the presented model. These investigations are necessary to get better understanding about their impact on the simulation. The parameters that were investigated are the erodibility E, the porosity P, settling velocity w, the critical shear stress for erosion τ_E, and the critical shear stress for deposition τ_D.

It is found that the erodibility has the highest impact on the numerical result, while the critical shear stress of deposition has the lowest impact on the result. Special attention is required when choosing or calibrating the erodibility value. A small increase or decrease in the calibrated value of erodibility may produce an overestimated erosion process for the simulated case because of the high sensitivity of the numerical model to this value. Conversely, the numerical model shows very low sensitivity to the critical shear stress for deposition which could be neglected in the cases of high flow shear stresses. It is found that there is only (0.00348%) difference of the bed level for two different values of difference τ_D despite using very high values of τ_D to investigate its influence.

The numerical model shows a significant sensitivity to the critical shear stress of erosion τ_E. This parameter represents the critical value of the inception motion of the eroded cohesive particle. Small values of τ_E may produce high erosion depth, while higher values produce smaller erosion depth.

The numerical model shows very low sensitivity for the settling velocity and the porosity. Where these parameter can influence the morphological change.

5.6 Unified of HMD-C and HMD-NC Models

The presented and tested models in Chapters 3, 4, and 5 were unified in a final form to introduce the hydro-morphodynamic with cohesive and non-cohesive sediment transport model (HMD-C-NC). This new model is capable of dealing with the water flow over movable beds that consist of either non-cohesive soil or cohesive soil. The model chooses a suitable calculation procedure to reproduce the simulating case based on the size of sediment particles. In the case of a bed that has sediment particles with size $d50 > 63\mu m$, the model will deal with the bed as a non-cohesive bed and the HMD-NC Model will be activated, while for sediment particles with size $d50 < 63\ \mu m$, the soil of the bed will be considered as a cohesive soil and the HMD-C model will be activated.

Figure (5-11) shows the framework of the computational procedure that is employed at each time step for the HMD-C-NC model.

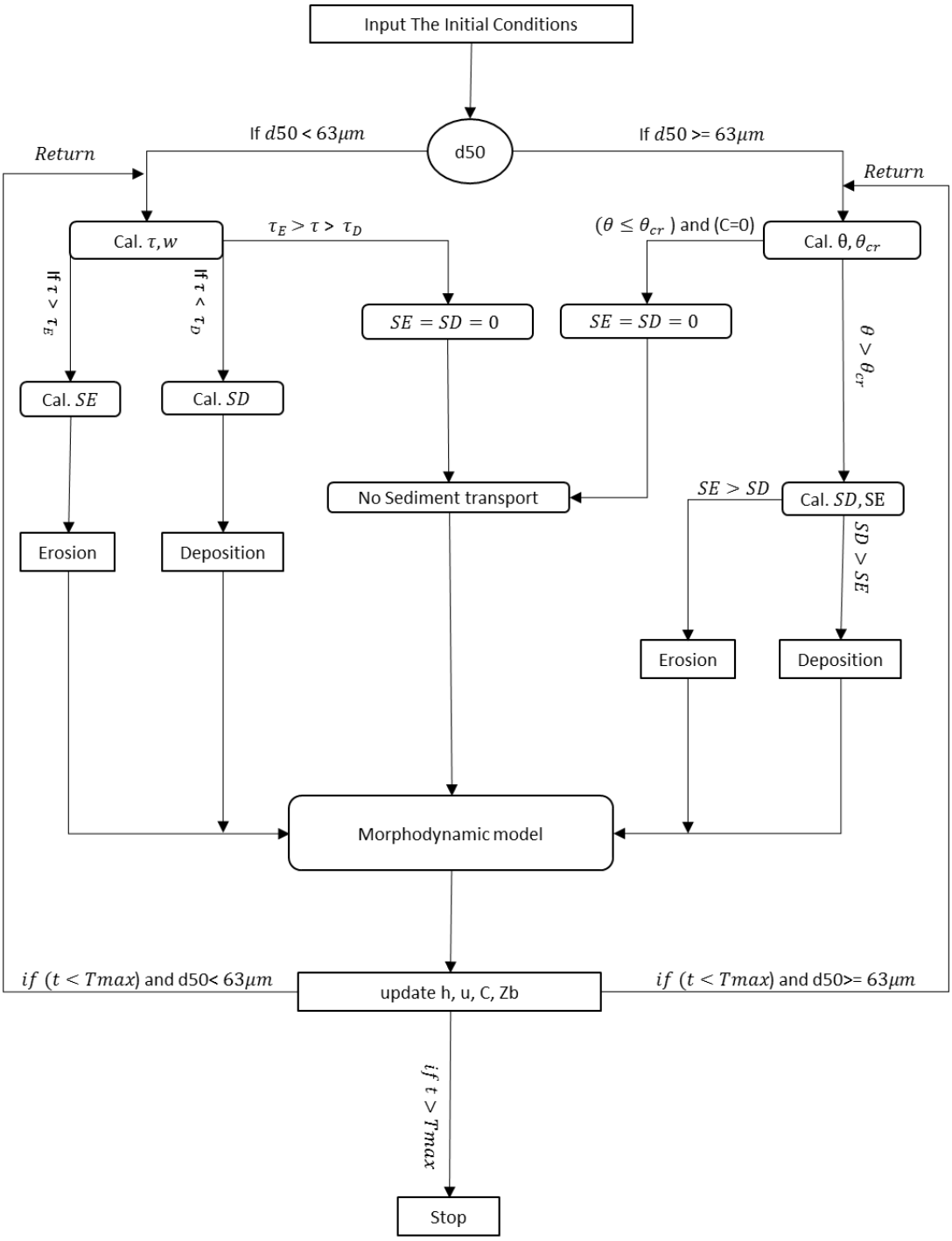

Figure 5-11: The Framework of the Computational Processing

In flowchart above, the computational procedure that is take place at each time step for the presented model includes:

1. Input the calibrated critical shear stress of erosion, critical shear stress of deposition and the initial conditions that include the hydraulic and sediment

information, including water depth, bed elevation, flow velocity, sediment concertation.

2. Check the mean particle size to where, if $d50$ >= or < than 63μm.
3. If the $d50$ < 63μm then calculate the settling velocity and the flow shear stress for the present time step from the information in Step 1.
4. Compare the calculated flow shear stress with the given critical shear stress for erosion and the critical shear stress for deposition. If the flow shear stress:

    i. $\tau > \tau_E$ then calculate the erosion SE.
    ii. $\tau < \tau_D$ then calculate the deposition SD.
    iii. $\tau_D < \tau < \tau_E$ then no sediment transport.

5. If the $d50$ >= 63μm, then calculate the shields parameter θ and the critical shields parameter θ_{cr} for the present time step from the information in Step 1.
6. Compare the calculated shields parameter θ with the critical Shields parameter θ_{cr}. If:

    i. $\theta > \theta_{cr}$ then calculate the erosion SE and the deposition SD.
    ii. ($\theta \leq \theta_{cr}$) and (C=0) then $SE = SD = 0$ and no sediment transport accrues.
    iii. ($\theta \leq \theta_{cr}$) and (C≠0) calculate SD, $SE = 0$.

7. Solve the governing equations system of the model for a step in time, based on the information mentioned in previous steps and update the values of the hydraulic and sediment which include water depth, bed elevation, flow velocity, sediment concertation.
8. If time of simulation $(t < Tmax)$ and $d50 < 63\mu m$ return to Step 3 and repeat Step 2 to 4 then 7.
9. If time of simulation $(t < Tmax)$ and $d50 \geq 63\mu m$ return to Step 5 and repeat Step 5 to 7.
10. If time of simulation $t \geq Tmax$ then stop.

5.7 Summary

In this chapter the researcher extended the one-dimensional HMD-C model to two-dimensional HMD-C model. It combines three models which are; the hydraulic model, sediment transport model and bed evolution model. The hydraulic model governing equations are derived from Navier–Stokes equations by averaging the depth to produce the two-dimensional shallow water equations. This model is linked to the suspended model which is represented by the two-dimensional advection-diffusion model, and to the bed evolution model. The system is discretised using a finite volume method and solved using one order accuracy HLL approximate Riemann solver.

Due to the lack of the experimental works that test the water flow over a movable cohesive bed, the researcher used different approach to test the model. He utilised an experiment of dam-break water flow over a movable non-cohesive bed as a benchmark or a guide to compare the new model result with non-cohesive model result and see whether the results are reasonable or not. The laboratory experiment that was performed at the Université Catholique de Louvain (Goutiere *et al.* (2011)), is utilized for this purpose. The comparison study shows reasonable and logical result where the new model, HMD-C shows less erodibility compared with the HMD-NC model.

Important investigations have been performed in the latter part of the chapter to study the influence of different parameters on the numerical model to understand the model sensitivity for these parameters. The parameters that were included in this study are the bed erodibility, the critical shear stress for erosion, the critical shear stress for deposition, the settling velocity, and the porosity. It is found that the erodibility has the largest impact on the model result. The model shows less sensitivity when different values of the critical shear stress for erosion are employed in the model. In contrast, the model has very low sensitivity to the critical shear stress for deposition, bed porosity, and the settling velocity.

As a final stage, the two-dimensional HMD-C model is unified with the two-dimensional HMD-NC model that was presented in the previous chapters to

form the final version of the HMD-C-NC model that is capable of dealing with water flow over movable beds which are constructed either of cohesive or non-cohesive soil. This combined model examine flow and sedimentation cases and chooses the formulae that are related to it based on the size of sediment particles. Where bed that has sediment particles with size $d50 > 63\mu m$, will be treated as a non-cohesive bed, while sediment particles with size $d50 < 63\mu m$, will be considered as a cohesive bed.

To sum up, the model shows a reasonable capability to simulate and predict the water flow over movable cohesive bed and better understanding about the model sensitivity for different parameters is found in this chapter.

Chapter 6 Conclusions and Future Work

6.1 Introduction

In this chapter, a brief discussion about the findings and conclusions that have been obtained are presented. Furthermore, a recommendation is made by the researcher that the model presented in this study is utilised for future river hydro-morphological studies and research. This can lead to better understanding about the water flow over movable beds that consist of different types of material.

The main contributions of the work presented in this thesis are the introduction of a new numerical hydro-morphodynamic model based on the shallow water theory with the incorporation of a movable bed model which incorporates physics of both cohesive or non-cohesive bed material movement. This is a first step towards filling the gap that exists in the modelling community – that most models hydro-morphodynamic models focus on one sediment type, and most of those only on non-cohesive beds.

The construction methodology and solving method of the presented hydro-morphodynamic model are explained extensively. The new model has been evaluated and tested against wide range of experiments and previous work.

In the next sections, the summary of each element of the model are discussed separately.

6.2 One and Two-Dimensional Hydrodynamic Models

Robust one and two-dimensional hydrodynamic models have been constructed. (The sediment transport and the morphological changes were not included at this stage). The robustness of the models is due to their applicability to both steady and unsteady flow problem over complex irregular topography (Song *et al.* (2011); Guan (2014)). The models were constructed on structured grid based on the traditional shallow water equations. Simple techniques where utilised to treat the source terms. The upwind technique is applied at the cell centre to discretised the bed slope. A first order accurate HLL approximate

Riemann solver combined with a finite volume method is utilised to solve the governing equations explicitly. The models were validated and using experimental measurements previously published in the open literature. The numerical results for the one-dimensional and two-dimensional models show a good agreement with measurements.

It is found that the proposed numerical models are robust, the presented schemes are straight-forward and simple to implement and they are applicable to predict flow over irregular topography for the fixed bed cases.

6.3 Hydro-morphodynamic Model with Non-Cohesive Sediment Transport Model (HMD-NC Model)

A one-dimensional hydro-morphodynamic model was presented to simulate water flow over movable bed that consists of non-cohesive materials (such as sand). This model is a combination of three elements: the hydrodynamics, the sediment transport, and the bed evolution. This model is built based on shallow water theory for fluids flow with further terms included to account for the other elements. The terms include the morphological evolution process, streamwise variable concentration, and the momentum transfer that results from the sediment exchange between water column and the erodible bed boundary. The governing equations was explicitly solved by using a first order accurate HLL solver combined with a finite volume method on structured rectangular mesh. The combined model was tested and validated with experimental measurement available in published literature.

The initial one-dimensional model was extended to two-dimensions to include the influence of the geometry and the bed topography in both the x and y directions. More tests and validation with experimental measurements were executed.

The numerical results of the presented models showed a good agreement in comparison to the experimental measurements. It is found that the model is capable of reproducing the flow over irregular topography for the movable bed when different modes of sediment transport occurred. Where the utilised

sediment transport model is capable of predicting the total sediment transport that includes the suspended sediment transport as well as bed load transport.

6.4 One-Dimensional Hydro-morphodynamic Model with Cohesive Sediment Transport Model (HMD-C Model)

This new model is the core of the research presented in this thesis . A new hydro-morphodynamic model is introduced that can simulate water flow over movable bed which consist of cohesive materials such as clay. The model is constructed based on shallow water equations that are coupled with sediment transport model and combined with the bed evolution model. A second order turbulent viscosity term, which represents the diffusive turbulent momentum transfer associated with Reynold stresses is added to the shallow water equations as an additional term. The advection diffusion equation is employed to represent the suspended sediment transport model where the suspension is the mechanism that dominates the transport of the fine sediment. A first order accurate HLL finite volume method is utilized to solve the governing equations.

The model is validated against previously published measurements from an experimental dam break case. The simulation results of this model shows a good agreement with the measurements. The HMD-C Model is tested against the HMD-NC Model where the same physical situation was applied to both tests. The comparison demonstrates that the behaviour of the HMD-C Model is consistent with this physical situation. In this model the bed load transport is ignored because the suspended sediment transport is the dominant mechanism of the sediment transport for fine sediment particles.

The presented numerical model is robust. It can be applied to simulate water flow over a movable complex irregular topography that consists of cohesive materials. This model shows the ability to simulate extreme water flow cases such as dam breaching processes and to simulate the temporal and spatial changes appropriately.

6.5 Two-Dimensional Hydro-morphodynamic Model with Cohesive Sediment Transport Model (HMD-C Model)

The new novel HMD-C model is extended to introduce the two-dimensional HMD-C model. This upgrading takes into account the influence of the geometry and the bed topography in the x and y directions. Thus, the model becomes more realistic and can produce results with higher accuracy. The first order accurate HLL approximate Riemann solver finite volume method is utilized to solve the governing equations.

To validate the new model a different validation approach was employed because of the shortage of the experimental works that examines water flow over movable cohesive beds. A physical experiment of water flow over a movable non-cohesive bed was employed as a benchmark or a guide to validate and compare the new model result with non-cohesive model results. The comparison shows a reasonable result where the new model, HMD-C shows less erodibility compared with the HMD-NC model with a different tendency. This difference in the behaviour of the two models is considered reasonable.

6.6 The Parametric Study

An important study was performed in this research by employing the new HMD-C model in it to study different erosion formulae and the parameters that these require to investigate their impact on the numerical results and to get better understanding of fine sediment transport simulations.

For the erosion formulae, it is found that the numerical results show different level of sensitivity and performance. It is noticed that the Partheniades erosion formula (Partheniades (1965)) for erosion gives the most consistent results in comparison with the measurements.

For the parameter sensitivity tests, the different parameters included were: the bed erodibility, Manning roughness, the critical shear stress for erosion, the critical shear stress for deposition, the settling velocity, and the porosity. Some parameters shows large impact on the numerical result such as erodibility,

Manning roughness, and the critical shear stress for erosion. While the other parameters show very low influence on the numerical result such as the critical shear stress for deposition, bed porosity, and the settling velocity.

6.7 Research Achievements

From to the sections above, this research is performed and good contribution is added to the knowledge based on the following achievements:

- Introduction of a novel Hydro-morphodynamic model (HMD-C Model) which designed to simulate water flow over cohesive movable beds.
- Production of a novel unified model (HMD-C-NC Model), that is capable of simulating water flow over movable bed that consist of cohesive and non- cohesive materials based on the particle diameter.
- A unique investigation to compare a group of entrainment formulae to give a better understanding about the erosion process mechanism models and optimum formula that reproduces more accurate results.
- The study of the influence of different parameters on the numerical models to understanding better the water flow and sediment transport predictions of these models.

6.8 Future Work and Recommendations

6.8.1 Apply The Presented Model on Large Scale Cases

One of the topics that concerns the engineers are fluvial management and flood prediction. It is well known that river morphodynamic influences channel mobility, floodplain evolution and associated habitat development. On the other hand, flooding is a natural hazard that can directly cause damages to people's life, their property, and infrastructure. It is characterized by the high destructive energy that produces high sediment erosion processes that can cause turbidity, nutrient, and contaminant problems. These processes take place covering wide areas with complex topography. Numerical modelling for such areas is attractive because it is money-saving and convenient to implement. However,

the presented model is validated and tested against small scale cases and have not applied for large scale cases. It is recommended to employ the presented numerical model in rivers and flood simulations with large scale domains.

6.8.2 Develop a Bank Erosion Model

In reality, there are many complicated fluvial processes occurring in the flood events. These processes have a significant influence on the water flow, sediment transport processes, stream geomorphology, and river ecosystems. One of these processes is bank failure or bank erosion. This kind of failure is a combination of basal erosion, which occurs because of the fluvial entrainment effects at the bank toe, and mass failure, where the remaining bank falls because of the instability. Different mechanisms characterise the bank failure are: planar, curved, rotational and cantilever failures. The most important factor that influence the failure mechanism is the soil characteristics (cohesive or non-cohesive). However, the presented model does not take into account such phenomenon. Developing a bank failure model capable of dealing with different kinds of soil, and incorporating it in the presented model is required. This will enhance the efficiency of the model to reproduce high accuracy and realistic results in fluvial modelling and make it applicable to wider range of river simulation cases.

6.8.3 Develop the Meshing Technique

In the numerical modelling, it is very important to represent the domain or the geometry with a suitable grid system. This grid system can influence the accuracy of the numerical result. Different systems have been implemented to generate the grid mesh. This includes structured grids and unstructured grids. In this research, a simple rectangular structured meshing grid system is utilised to produce the numerical model. This type of grids is easy to generate and computationally time-saving. However, it is difficult to implement them to represent complex geometries accurately. Despite the fact that unstructured grids are complicated to generate mesh and computationally time-consuming, it can be utilised to represent the domain and complex geometries appropriately.

In further research, it would be worth investigating the use of adaptive quadtree grids to simulating flood flows and flow in rivers as they travel over natural terrain. This technique can produce simulations efficiently with high resolution with less cost than for the same solver on a uniform grid. Furthermore, the generation of quadtree grids is automatic and fast, and they are easy to adapt during the progression of the computation progress.

References:

Alcrudo, F. and P. Garcia- Navarro. 1993. A high- resolution Godunov- type scheme in finite volumes for the 2D shallow- water equations. *International Journal for Numerical Methods in Fluids,* **16**(6), pp.489-505.

Alho, P., A. J. Russell, J. L. Carrivick and J. Käyhkö. 2005. Reconstruction of the largest Holocene jökulhlaup within Jökulsá á Fjöllum, NE Iceland. *Quaternary Science Reviews,* **24**(22), pp.2319-2334.

Aliparast, M. 2009. Two-dimensional finite volume method for dam-break flow simulation. *International Journal of Sediment Research,* **24**(1), pp.99-107.

Altunkaynak, A. and K.-H. Wang. 2010. Triple diagram models for prediction of suspended solid concentration in Lake Okeechobee, Florida. *Journal of hydrology,* **387**(3), pp.165-175.

Amos, C. L., G. Daborn, H. Christian, A. Atkinson and A. Robertson. 1992. In situ erosion measurements on fine-grained sediments from the Bay of Fundy. *Marine Geology,* **108**(2), pp.175-196.

Amoudry, L. O. and A. J. Souza. 2011. Deterministic coastal morphological and sediment transport modeling: A review and discussion. *Reviews of Geophysics,* **49**(2).

Anastasiou, K. and C. Chan. 1997. Solution of the 2D shallow water equations using the finite volume method on unstructured triangular meshes. *International Journal for Numerical Methods in Fluids,* **24**(11), pp.1225-1245.

Ariathurai, R. and K. Arulanandan. 1978. Erosion rates of cohesive soils. *Journal of the hydraulics division,* **104**(2), pp.279-283.

Audusse, E., F. Bouchut, M.-O. Bristeau, R. Klein and B. T. Perthame. 2004. A fast and stable well-balanced scheme with hydrostatic reconstruction for shallow water flows. *SIAM Journal on Scientific Computing,* **25**(6), pp.2050-2065.

Audusse, E. and M.-O. Bristeau. 2005. A well-balanced positivity preserving "second-order" scheme for shallow water flows on unstructured meshes. *Journal of Computational Physics,* **206**(1), pp.311-333.

Bailey, M. C. and D. P. Hamilton. 1997. Wind induced sediment resuspension: a lake-wide model. *Ecological Modelling,* **99**(2-3), pp.217-228.

Begnudelli, L. and B. F. Sanders. 2006. Unstructured grid finite-volume algorithm for shallow-water flow and scalar transport with wetting and drying. *Journal of hydraulic engineering,* **132**(4), pp.371-384.

Benkhaldoun, F., I. Elmahi and M. Seaı. 2007. Well-balanced finite volume schemes for pollutant transport by shallow water equations on unstructured meshes. *Journal of computational physics,* **226**(1), pp.180-203.

Bermúdez, A., A. Dervieux, J.-A. Desideri and M. E. Vázquez. 1998. Upwind schemes for the two-dimensional shallow water equations with variable depth using unstructured meshes. *Computer methods in applied mechanics and engineering,* **155**(1-2), pp.49-72.

Bermudez, A. and M. E. Vazquez. 1994. Upwind methods for hyperbolic conservation laws with source terms. *Computers & Fluids,* **23**(8), pp.1049-1071.

Black, K., T. Tolhurst, D. Paterson and S. Hagerthey. 2002. Working with natural cohesive sediments. *Journal of Hydraulic Engineering,* **128**(1), pp.2-8.

Bryan, R. B. 1976. Considerations on soil erodibility indices and sheetwash. *Catena,* **3**(1), pp.99-111.

Buls, T., K. Anderskouv, P. L. Friend, C. E. Thompson and L. Stemmerik. 2017. Physical behaviour of Cretaceous calcareous nannofossil ooze: Insight from flume studies of disaggregated chalk. *Sedimentology,* **64**(2), pp.478-507.

Caleffi, V., A. Valiani and A. Bernini. 2007. High-order balanced CWENO scheme for movable bed shallow water equations. *Advances in water resources,* **30**(4), pp.730-741.

Cancino, L. and R. Neves. 1999a. Hydrodynamic and sediment suspension modelling in estuarine systems: Part I: Description of the numerical models. *Journal of Marine Systems,* **22**(2), pp.105-116.

Cancino, L. and R. Neves. 1999b. Hydrodynamic and sediment suspension modelling in estuarine systems: Part II: Application to the Western Scheldt and Gironde estuaries. *Journal of Marine Systems,* **22**(2), pp.117-131.

Cao, Z., G. Pender, S. Wallis and P. Carling. 2004. Computational dam-break hydraulics over erodible sediment bed. *Journal of hydraulic engineering,* **130**(7), pp.689-703.

Capart, H. and D. Young. 1998. Formation of a jump by the dam-break wave over a granular bed. *Journal of Fluid Mechanics,* **372**, pp.165-187.

Carrivick, J. L., V. Manville, A. Graettinger and S. J. Cronin. 2010. Coupled fluid dynamics-sediment transport modelling of a Crater Lake break-out lahar: Mt. Ruapehu, New Zealand. *Journal of hydrology,* **388**(3), pp.399-413.

Carrivick, J. L. and E. L. Rushmer. 2006. Understanding high-magnitude outburst floods. *Geology Today,* **22**(2), pp.60-65.

Chapalain, G., Y. P. Sheng and A. T. Temperville. 1994. About the specification of erosion flux for soft stratified cohesive sediments. *Mathematical geology,* **26**(6), pp.651-676.

Chen, C., H. Huang, R. C. Beardsley, H. Liu, Q. Xu and G. Cowles. 2007. A finite volume numerical approach for coastal ocean circulation studies: Comparisons with finite difference models. *Journal of Geophysical Research: Oceans,* **112**(C3).

Chen, C., H. Liu and R. C. Beardsley. 2003. An unstructured grid, finite-volume, three-dimensional, primitive equations ocean model: application to coastal ocean and estuaries. *Journal of atmospheric and oceanic technology,* **20**(1), pp.159-186.

Chinnarasri, C., T. Tingsanchali, S. Weesakul and S. Wongwises. 2003. Flow patterns and damage of dike overtopping. *International Journal of Sediment Research,* **18**(4), pp.301-309.

Chow, V. 1959. *Open channel hydraulics.* McGraw-Hill Book Company, Inc; New York.

Clarke, S. and A. Elliott. 1998. Modelling suspended sediment concentrations in the Firth of Forth. *Estuarine, Coastal and Shelf Science,* **47**(3), pp.235-250.

Cole, P. and G. V. Miles. 1983. Two-dimensional model of mud transport. *Journal of Hydraulic Engineering,* **109**(1), pp.1-12.

Dai, F., C. F. Lee, J. Deng and L. Tham. 2005. The 1786 earthquake-triggered landslide dam and subsequent dam-break flood on the Dadu River, southwestern China. *Geomorphology,* **65**(3), pp.205-221.

Delo, E. 1988. *Estuarine muds manual*. HR Wallingford.

Dyer, K. R. 1986. *Coastal and estuarine sediment dynamics.* John Wiley & Sons, Inc.

Einstein, H. A. 1950. *The bed-load function for sediment transportation in open channel flows.* US Department of Agriculture Washington DC.

Emelen, S. V., Y. Zech and S. Soares-Frazão. 2014. Impact of sediment transport formulations on breaching modelling. *Journal of Hydraulic Research,* (ahead-of-print), pp.1-13.

Fagherazzi, S. and T. Sun. 2003. Numerical simulations of transportational cyclic steps. *Computers & Geosciences,* **29**(9), pp.1143-1154.

Feliciano Cestero, J. A., J. Imran and M. H. Chaudhry. 2014. Experimental Investigation of the Effects of Soil Properties on Levee Breach by Overtopping. *Journal of Hydraulic Engineering*.

Fiedler, F. R. and J. A. Ramirez. 2000. A numerical method for simulating discontinuous shallow flow over an infiltrating surface. *International journal for numerical methods in fluids,* **32**(2), pp.219-239.

Fraccarollo, L. and H. Capart. 2002. Riemann wave description of erosional dam-break flows. *Journal of Fluid Mechanics,* **461**, pp.183-228.

Franz, G., L. Pinto, I. Ascione, M. Mateus, R. Fernandes, P. Leitao and R. Neves. 2014. Modelling of cohesive sediment dynamics in tidal estuarine systems: Case study of Tagus estuary, Portugal. *Estuarine, Coastal and Shelf Science,* **151**, pp.34-44.

Fundamentals of Environmental Measurements. 2014. Basheer Al-Hadeethi. [Online]. [Accessed 24 March 2017]. Available from: http://www.fondriest.com/environmental-measurements/parameters/hydrology/sediment-transport-deposition/

Gallardo, J. M., C. Parés and M. Castro. 2007. On a well-balanced high-order finite volume scheme for shallow water equations with topography and dry areas. *Journal of Computational Physics,* **227**(1), pp.574-601.

Garcia-Navarro, P., F. Alcrudo and J. Saviron. 1992. 1-D open-channel flow simulation using TVD-McCormack scheme. *Journal of Hydraulic Engineering,* **118**(10), pp.1359-1372.

Garcia-Navarro, P. and M. E. Vazquez-Cendon. 2000. On numerical treatment of the source terms in the shallow water equations. *Computers & Fluids,* **29**(8), pp.951-979.

Gilvear, D. J. 1999. Fluvial geomorphology and river engineering: future roles utilizing a fluvial hydrosystems framework. *Geomorphology,* **31**(1), pp.229-245.

Goutiere, L., S. Soares-Frazao and Y. Zech. 2011. Dam-break flow on mobile bed in abruptly widening channel: experimental data. *Journal of Hydraulic Research,* **49**(3), pp.367-371.

Guan, M. 2014. *Geomorphic impacts of rapid sediment-laden flows through computational modelling.* University of Leeds.

Guan, M., N. Wright and P. Sleigh. 2012. Applicability of entrainment formulas to modelling of geomorphic outburst flows. *In: Proceedings of the 10th International Conference on Hydroinformatics (2012)*: Leeds.

Guan, M., N. Wright and P. Sleigh. 2013. A robust 2D shallow water model for solving flow over complex topography using homogenous flux method. *International Journal for Numerical Methods in Fluids,* **73**(3), pp.225-249.

Guan, M., N. G. Wright and P. Andrew Sleigh. 2015a. Multimode morphodynamic model for sediment-laden flows and geomorphic impacts. *Journal of Hydraulic Engineering,* **141**(6), p04015006.

Guan, M., N. G. Wright and P. A. Sleigh. 2014. 2D Process-Based Morphodynamic Model for Flooding by Noncohesive Dyke Breach. *Journal of Hydraulic Engineering,* **140**(7), p04014022.

Guan, M., N. G. Wright, P. A. Sleigh and J. L. Carrivick. 2015b. Assessment of hydro-morphodynamic modelling and geomorphological impacts of a sediment-charged jökulhlaup, at Sólheimajökull, Iceland. *Journal of Hydrology,* **530**, pp.336-349.

Hayter, E. and A. Mehta. 1986. Modelling cohesive sediment transport in estuarial waters. *Applied Mathematical Modelling,* **10**(4), pp.294-303.

Hou, J., Q. Liang, F. Simons and R. Hinkelmann. 2013. A stable 2D unstructured shallow flow model for simulations of wetting and drying over rough terrains. *Computers & Fluids,* **82**, pp.132-147.

Howard, A. D. 1994. A detachment-limited model of drainage basin evolution. *Water resources research,* **30**(7), pp.2261-2285.

Hubbard, M. E. and P. Garcia-Navarro. 2000. Flux difference splitting and the balancing of source terms and flux gradients. *Journal of Computational Physics,* **165**(1), pp.89-125.

Izumi, N. and G. Parker. 2000. Linear stability analysis of channel inception: downstream-driven theory. *Journal of Fluid Mechanics,* **419**, pp.239-262.

Johansen, C., T. Larsen and O. Petersen. 1994. Experiments on erosion of mud from the Danish Wadden Sea. *In: Experiments on Erosion of Mud from the Danish Wadden Sea*.

Kawahara, M. and T. Umetsu. 1986. Finite element method for moving boundary problems in river flow. *International Journal for Numerical Methods in Fluids,* **6**(6), pp.365-386.

Krámer, T. and J. Józsa. 2007. Solution-adaptivity in modelling complex shallow flows. *Computers & Fluids,* **36**(3), pp.562-577.

Krone, R. B. 1962. Flume studies of the transport of sediment in estuarial shoaling processes.

Kurganov, A. and D. Levy. 2002. Central-upwind schemes for the Saint-Venant system. *ESAIM: Mathematical Modelling and Numerical Analysis,* **36**(3), pp.397-425.

Lax, P. and B. Wendroff. 1960. Systems of conservation laws. *Communications on Pure and Applied mathematics,* **13**(2), pp.217-237.

Lee, S. H. and N. G. Wright. 2010. Simple and efficient solution of the shallow water equations with source terms. *International Journal for Numerical Methods in Fluids,* **63**(3), pp.313-340.

Leonard, B. P. 1979. A stable and accurate convective modelling procedure based on quadratic upstream interpolation. *Computer methods in applied mechanics and engineering,* **19**(1), pp.59-98.

Leopardi, A. 2001. *Modelli bidimensionali di corpi idrici naturali*. thesis, University of Napoli “Federico II”.

Leveque, R. J. 1998. Balancing source terms and flux gradients in high-resolution Godunov methods: the quasi-steady wave-propagation algorithm. *Journal of computational physics,* **146**(1), pp.346-365.

Li, M. Z. and C. L. Amos. 2001. SEDTRANS96: the upgraded and better calibrated sediment-transport model for continental shelves. *Computers & Geosciences,* **27**(6), pp.619-645.

Liang, Q., A. Borthwick and G. Stelling. 2004. Simulation of dam-and dyke-break hydrodynamics on dynamically adaptive quadtree grids. *International journal for numerical methods in fluids,* **46**(2), pp.127-162.

Liang, Q. and A. G. Borthwick. 2009. Adaptive quadtree simulation of shallow flows with wet–dry fronts over complex topography. *Computers & Fluids,* **38**(2), pp.221-234.

Liang, Q. and F. Marche. 2009. Numerical resolution of well-balanced shallow water equations with complex source terms. *Advances in water resources,* **32**(6), pp.873-884.

Liu, W.-C., M.-H. Hsu and A. Y. Kuo. 2002. Modelling of hydrodynamics and cohesive sediment transport in Tanshui River estuarine system, Taiwan. *Marine Pollution Bulletin,* **44**(10), pp.1076-1088.

Lopes, J., J. Dias and I. Dekeyser. 2001. Influence of tides and river inputs on suspended sediment transport in the Ria de Aveiro lagoon, Portugal. *Physics and Chemistry of the Earth, Part B: Hydrology, Oceans and Atmosphere,* **26**(9), pp.729-734.

Lopes, J. F., J. M. Dias and I. Dekeyser. 2006. Numerical modelling of cohesive sediments transport in the Ria de Aveiro lagoon, Portugal. *Journal of Hydrology,* **319**(1), pp.176-198.

Lowe, S. A. 2003. Omission of critical Reynolds number for open channel flows in many textbooks. *Journal of professional issues in engineering education and practice,* **129**(1), pp.58-59.

Lumborg, U. 2004. Cohesive sediment transport modelling—application to the Lister Dyb tidal area in the Danish Wadden Sea. *Journal of Coastal Research*, pp.114-123.

Lumborg, U. and M. Pejrup. 2005. Modelling of cohesive sediment transport in a tidal lagoon—an annual budget. *Marine Geology,* **218**(1), pp.1-16.

Lumborg, U. and A. Windelin. 2003. Hydrography and cohesive sediment modelling: application to the Rømø Dyb tidal area. *Journal of Marine Systems,* **38**(3), pp.287-303.

Luo, Y., L. Chen, M. Xu and J. Huang. 2014. Breaking mode of cohesive homogeneous earth-rock-fill dam by overtopping flow. *Natural Hazards*, pp.1-14.

Mehta, A. J. 1984. *Estuarine Cohesive Sediment Dynamics: Proceedings of a Workshop on Cohesive Sediment Dynamics with Special Reference to Physical Processes in Estuaries, Tampa, Florida, November 12–14, 1984.* Springer Science & Business Media.

Mehta, A. J. 1986. Characterization of cohesive sediment properties and transport processes in estuaries. *Estuarine cohesive sediment dynamics.* Springer, pp.290-325.

Mehta, A. J. 1989. On estuarine cohesive sediment suspension behavior. *Journal of Geophysical Research: Oceans,* **94**(C10), pp.14303-14314.
Mingham, C. and D. Causon. 1998. High-resolution finite-volume method for shallow water flows. *Journal of Hydraulic Engineering,* **124**(6), pp.605-614.
Morris, M., M. Hassan and K. Vaskinn. 2007. Breach formation: Field test and laboratory experiments. *Journal of Hydraulic Research,* **45**(sup1), pp.9-17.
Morris, M. W. 2011. *Breaching of earth embankments and dams*. thesis, Open University.
Mukhlisin, M., K. I. Kosugi, Y. Satofuka and T. Mizuyama. 2006. Effects of soil porosity on slope stability and debris flow runout at a weathered granitic hillslope. *Vadose Zone Journal,* **5**(1), pp.283-295.
Mulder, H. P. and C. Udink. 1991. Modelling of cohesive sediment transport. A case study: the western Scheldt estuary. *Coastal Engineering 1990.* pp.3012-3023.
Nicholson, J. and B. A. O'connor. 1986. Cohesive sediment transport model. *Journal of Hydraulic Engineering,* **112**(7), pp.621-640.
Ockenden, M., R. Jones and I. Hale. 1989. Grangemouth mud properties. *Technical Report SR197.* Hydraulics Research Ltd Wallingford.
Odd, N. and M. Owen. 1972. SUMMARY OF PAPER 7517. A TWO-LAYER MODEL OF MUD TRANSPORT IN THE THAMES ESTUARY. *Proceedings of the Institution of Civil Engineers,* **51**(4), p714.
Ongley, E., B. Krishnappan, G. Droppo, S. Rao and R. Maguire. 1992. Cohesive sediment transport: emerging issues for toxic chemical management. *Hydrobiologia,* **235**(1), pp.177-187.
Pandoe, W. W. and B. L. Edge. 2004. Cohesive sediment transport in the 3D-hydrodynamic-baroclinic circulation model: study case for idealized tidal inlet. *Ocean Engineering,* **31**(17), pp.2227-2252.
Papamichos, E. and I. Vardoulakis. 2005. Sand erosion with a porosity diffusion law. *Computers and Geotechnics,* **32**(1), pp.47-58.
Parchure, T. M. and A. J. Mehta. 1985. Erosion of soft cohesive sediment deposits. *Journal of Hydraulic Engineering,* **111**(10), pp.1308-1326.
Partheniades, E. 1965. Erosion and deposition of cohesive soils. *Journal of the Hydraulics Division,* **91**(1), pp.105-139.
Perthame, B. and C. Simeoni. 2001. A kinetic scheme for the Saint-Venant system¶ with a source term. *Calcolo,* **38**(4), pp.201-231.
Pickert, G., V. Weitbrecht and A. Bieberstein. 2011. Breaching of overtopped river embankments controlled by apparent cohesion. *Journal of Hydraulic Research,* **49**(2), pp.143-156.
Pontillo, M., L. Schmocker, M. Greco and W. H. Hager. 2010. 1D numerical evaluation of dike erosion due to overtopping. *Journal of Hydraulic Research,* **48**(5), pp.573-582.
Rogers, B., M. Fujihara and A. G. Borthwick. 2001. Adaptive Q-tree Godunov-type scheme for shallow water equations. *International Journal for Numerical Methods in Fluids,* **35**(3), pp.247-280.
Rogers, B. D., A. G. Borthwick and P. H. Taylor. 2003. Mathematical balancing of flux gradient and source terms prior to using Roe's approximate Riemann solver. *Journal of Computational Physics,* **192**(2), pp.422-451.

Rozov, A. L. 2003. Modeling of washout of dams. *Journal of Hydraulic Research,* **41**(6), pp.565-577.
Sanders, B. F. 2008. Integration of a shallow water model with a local time step. *Journal of Hydraulic Research,* **46**(4), pp.466-475.
Schmocker, L., P.-J. Frank and W. H. Hager. 2014. Overtopping dike-breach: effect of grain size distribution. *Journal of Hydraulic Research,* (ahead-of-print), pp.1-6.
Schmocker, L. and W. H. Hager. 2009. Modelling dike breaching due to overtopping. *Journal of Hydraulic Research,* **47**(5), pp.585-597.
Schmocker, L. and W. H. Hager. 2012. Plane dike-breach due to overtopping: effects of sediment, dike height and discharge. *Journal of Hydraulic Research,* **50**(6), pp.576-586.
Sheng, Y. P. and W. Lick. 1979. The transport and resuspension of sediments in a shallow lake. *Journal of Geophysical Research: Oceans,* **84**(C4), pp.1809-1826.
Simpson, G. and S. Castelltort. 2006. Coupled model of surface water flow, sediment transport and morphological evolution. *Computers & Geosciences,* **32**(10), pp.1600-1614.
Singh, J., M. S. Altinakar and Y. Ding. 2011. Two-dimensional numerical modeling of dam-break flows over natural terrain using a central explicit scheme. *Advances in Water Resources,* **34**(10), pp.1366-1375.
Sleigh, P., P. Gaskell, M. Berzins and N. Wright. 1998. An unstructured finite-volume algorithm for predicting flow in rivers and estuaries. *Computers & Fluids,* **27**(4), pp.479-508.
Soares-Frazão, S. and Y. Zech. 2011. HLLC scheme with novel wave-speed estimators appropriate for two-dimensional shallow-water flow on erodible bed. *International Journal for Numerical Methods in Fluids,* **66**(8), pp.1019-1036.
Song, L., J. Zhou, J. Guo, Q. Zou and Y. Liu. 2011. A robust well-balanced finite volume model for shallow water flows with wetting and drying over irregular terrain. *Advances in Water Resources,* **34**(7), pp.915-932.
Soulsby, R. 1997. *Dynamics of marine sands: a manual for practical applications.* Thomas Telford.
Teisson, C. 1991. Cohesive suspended sediment transport: feasibility and limitations of numerical modeling. *Journal of Hydraulic Research,* **29**(6), pp.755-769.
Teisson, C., M. Ockenden, P. Le Hir, C. Kranenburg and L. Hamm. 1993. Cohesive sediment transport processes. *Coastal Engineering,* **21**(1-3), pp.129-162.
Terzaghi, K., R. B. Peck and G. Mesri. 1996. *Soil mechanics in engineering practice.* John Wiley & Sons.
Toro, E. F. 2001. *Shock-capturing methods for free-surface shallow flows.* John Wiley.
Van Emelen, S., V. Ferbus, T. Spitaels, Y. Zech and S. Soares Frazao. 2013. Experimental investigation of the erosion of a sand dike by overtopping. *In: 35th IAHR world congress*.
Van Emelen, S., C. Swartenbroekx, Y. Zech and S. Soares Frazao. 2011. Numerical modelling of the breaching process in an earthen dike. *In:*

Fifth International Conference on Advanced COmputational Methods in ENgineering (ACOMEN 2011).
Van Rijn, L. 1984a. Sediment Transport, Part II: Suspend load Transport. . *Hydr. Engrg., ,* **ASCE, 1104**(11), pp. pp.1613-1641.
Van Rijn, L. C. 1984b. Sediment transport, part I: bed load transport. *Journal of hydraulic engineering,* **110**(10), pp.1431-1456.
Vázquez-Cendón, M. a. E. 1999. Improved treatment of source terms in upwind schemes for the shallow water equations in channels with irregular geometry. *Journal of Computational Physics,* **148**(2), pp.497-526.
Wang, Z. and D. S. Bowles. 2006. Three-dimensional non-cohesive earthen dam breach model. Part 1: Theory and methodology. *Advances in water resources,* **29**(10), pp.1528-1545.
Winterwerp, J. C. 1998. A simple model for turbulence induced flocculation of cohesive sediment. *Journal of Hydraulic Research,* **36**(3), pp.309-326.
Winterwerp, J. C. and W. G. Van Kesteren. 2004. *Introduction to the physics of cohesive sediment dynamics in the marine environment.* Elsevier.
Wu, Y., R. Falconer and R. Uncles. 1999. Modelling of water flows and cohesive sediment fluxes in the Humber Estuary, UK. *Marine Pollution Bulletin,* **37**(3), pp.182-189.
Yang, X., Q. Zhang, J. Zhang, F. Tan, Y. Wu, N. Zhang, H. Yang and Q. Pang. 2015. An integrated model for three-dimensional cohesive sediment transport in storm event and its application on Lianyungang Harbor, China. *Ocean Dynamics,* **65**(3), pp.395-417.
Yin, H. and C. Li. 2001. Human impact on floods and flood disasters on the Yangtze River. *Geomorphology,* **41**(2), pp.105-109.
Yoon, T. H. and S.-K. Kang. 2004. Finite volume model for two-dimensional shallow water flows on unstructured grids. *Journal of Hydraulic Engineering,* **130**(7), pp.678-688.
Zhang, J., C. Zhou, K. Xu and M. Watanabe. 2002. Flood disaster monitoring and evaluation in China. *Global Environmental Change Part B: Environmental Hazards,* **4**(2), pp.33-43.
Zhang, S. and J. G. Duan. 2011. 1D finite volume model of unsteady flow over mobile bed. *Journal of Hydrology,* **405**(1), pp.57-68.
Zhao, D., H. Shen, G. Tabios Iii, J. Lai and W. Tan. 1994. Finite-volume two-dimensional unsteady-flow model for river basins. *Journal of Hydraulic Engineering,* **120**(7), pp.863-883.
Zhao, G., P. Visser, P. Peeters and J. Vrijling. 2014. Hydrodynamic erosion in cohesive embankment breach. *In: Scour and Erosion: Proceedings of the 7th International Conference on Scour and Erosion, Perth, Australia, 2-4 December 2014*: CRC Press, p.441.
Zhou, J. G., D. M. Causon, D. M. Ingram and C. G. Mingham. 2002. Numerical solutions of the shallow water equations with discontinuous bed topography. *International journal for numerical methods in fluids,* **38**(8), pp.769-788.
Zhou, J. G., D. M. Causon, C. G. Mingham and D. M. Ingram. 2001. The surface gradient method for the treatment of source terms in the shallow-water equations. *Journal of Computational physics,* **168**(1), pp.1-25.

Zhou, J. G., D. M. Causon, C. G. Mingham and D. M. Ingram. 2004. Numerical prediction of dam-break flows in general geometries with complex bed topography. *Journal of hydraulic engineering,* **130**(4), pp.332-340.
Zhu, Y. 2006. *Breach growth in clay-dikes*. thesis, TU Delft, Delft University of Technology.
Zhu, Y. 2016. *Personal communication.* 6 October.
Zoppou, C. and S. Roberts. 2000. Numerical solution of the two-dimensional unsteady dam break. *Applied Mathematical Modelling,* **24**(7), pp.457-475.